AD-A107 566 MONTANA STATE UNIV BOZEMAN DEPT OF CIVIL ENGINEERING--ETC F/G 13/10
MICROBIAL FOULING AND ITS EFFECT ON POWER GENERATION.(U)
SEP 81 W G CHARACKLIS, F L ROE, N ZELVER N00014-80-C-0475

UNCLASSIFIED NL

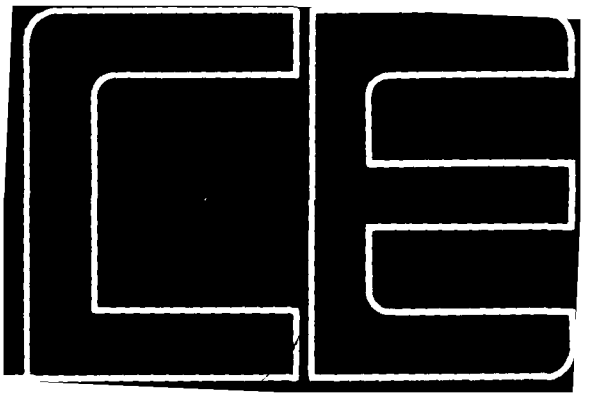

MICROBIAL FOULING
AND ITS EFFECT ON POWER GENERATION

by

W. G. Characklis
F. L. Roe
N. Zelver

First Summary Report
September, 1981

Prepared for M. K. Ellingsworth, Program Monitor
Power Program
The Office of Naval Research
Arlington, Virginia 22217

Under Contract N00014-80-C-0475

Department of Civil Engineering
Montana State University
Bozeman, Montana 58717

SECURITY CLASSIFICATION OF THIS PAGE (When Data Entered)

REPORT DOCUMENTATION PAGE		READ INSTRUCTIONS BEFORE COMPLETING FORM
1. REPORT NUMBER N00014-80-C-0475	2. GOVT ACCESSION NO. AD-A107566	3. RECIPIENT'S CATALOG NUMBER
4. TITLE (and Subtitle) Microbial Fouling and its Effect on Power Generation		5. TYPE OF REPORT & PERIOD COVERED Summary Report May 15, 1980 to May 15, 1981 6. PERFORMING ORG. REPORT NUMBER
7. AUTHOR(s) W. G. Characklis		8. CONTRACT OR GRANT NUMBER(s) N00014-80-C-0475
9. PERFORMING ORGANIZATION NAME AND ADDRESS Department of Civil Engineering Montana State University Bozeman, MT 59717		10. PROGRAM ELEMENT, PROJECT, TASK AREA & WORK UNIT NUMBERS
11. CONTROLLING OFFICE NAME AND ADDRESS Office of Naval Research 800 N. Quincy Street Arlington, VA 22217		12. REPORT DATE September 1981 13. NUMBER OF PAGES
14. MONITORING AGENCY NAME & ADDRESS(if different from Controlling Office)		15. SECURITY CLASS. (of this report) Unclassified 15a. DECLASSIFICATION/DOWNGRADING SCHEDULE

16. DISTRIBUTION STATEMENT (of this Report)

Approved for public release; distribution unlimited

17. DISTRIBUTION STATEMENT (of the abstract entered in Block 20, if different from Report)

Approved for public release; distribution unlimited.

18. SUPPLEMENTARY NOTES

19. KEY WORDS (Continue on reverse side if necessary and identify by block number)

Biofouling, Biofilms, heat exchangers, heat transfer coefficients, frictional resistance, scaling, corrosion

20. ABSTRACT (Continue on reverse side if necessary and identify by block number)

This report describes experimental systems and preliminary experiments on (1) Biofilm growth and structure, (2) Biofilm effect on heat transfer resistance (3) Biofilm effect on frictional resistance, (4) Growth kinetics of bacterial suspensions, and (5) Biofilm and inorganic particulate interrelationships. This information will be used to develop a unified theory for biofilm

(see attached sheet)

DD FORM 1 JAN 73 1473 EDITION OF 1 NOV 65 IS OBSOLETE
S/N 0102-LF-014-6601

Unclassified
SECURITY CLASSIFICATION OF THIS PAGE (When Data Entered)

development and associated energy losses in tubular heat exchangers.

Specific sections deal with (1) apparatus and techniques used in the study, (2) comparison of growth rates and structure of biofilms containing Pseudomonas aeruginosa and Sphaerotilus natans (3) growth kinetics for suspensions of Pseudomonas aeruginosa with glucose as a substrate (4) calcium scaling rates in heat exchanger tubing at heat fluxes compatible with biofilm growth.

TABLE OF CONTENTS

INTRODUCTION

Microfouling of surfaces in marine environments is a problem which affects a wide variety of systems from ship hulls to heat exchangers. System performance as well as operating costs suffer from energy losses due to increased frictional and heat transfer resistance. Most studies to date have avoided addressing fundamental questions concerning behavior of microorganisms in fluid flow systems and their effect on frictional and heat transfer resistance.

The fouling process begins with transport of microbial cells and their firm adhesion to the surface. The factors which affect these processes such as surface material, surface active films, and shear stress determine the length of the induction period prior to the rapid growth phase.

The rapid growth phase is characterized by logarithmic accumulation rate within a biological matrix consisting of both organic and inorganic constituents. The extent and rate of growth are moderated by factors such as nutrient availability and shearing forces at the fluid-biofilm interface. Ultimately, a steady state biofilm thickness develops where loss of biofilm mass to the bulk fluid balances growth rate.

Resulting frictional and heat transfer resistance are closely related to specific properties of the biofilm. Viscoelasticity and roughness of the biofilm have significant effects on frictional and convective heat transfer resistance, while biofilm thickness and thermal conductivity influence conductive heat transfer resistance.

This report for the first funding period, May 15, 1980 through May 15, 1981, describes preliminary results of our research. There are two complementary parts to the research. One part consists of experiments for investigating formation and structure of biofilm. Both microscopic and macroscopic properties of the biofilm are being studied. Mathematical models

of biofilm growth have been developed and are being refined using laboratory data. The other part of the research concerns the influence of biofilms on energy losses and also includes effects of particulate inclusions and inorganic constituents within the biofilm on energy losses.

The report is divided into four sections as follows:

(1) Apparatus and techniques

(2) Biofilm formation and structure

(3) Effects of biofilm and inorganic scale on energy losses

(4) Publications

APPARATUS AND METHODS

Annular Fouling Reactor System

The annular fouling reactor system consists of eight annular fouling reactors (AFR) and a support system which includes water treatment facilities, continuous bacterial inoculation, and measurement instrumentation. Figure 1 is a schematic diagram of this system. Only two of these reactors were used for the results discussed in this report.

Annular Fouling Reactors: The annular reactors are constructed of acrylic plastic and consist of two concentric cylinders, a stationary outer cylinder and a rotating inner cylinder. Figure 2 illustrates details of the reactors. Rotational velocity is electronically controlled and continuously displayed. A torque transducer mounted on the shaft of each reactor between the rotating cylinder and the motor drive continuously monitors changes in fluid frictional resistance caused by biofilm development. The torque is continuously displayed and recorded by an Apple Computer system. Each reactor contains four (4) thin removable slides which are used for biofilm sampling. The slides form an integral fit with the inside wall of the outer cylinders. The reactors are completely mixed by virtue of the pumping action of four draft tubes and an impeller mounted at the bottom of the inner cylinder. Advantages of the annular configuration include the following:

1. No concentration gradients exist in the bulk fluid due to complete mixing. This simplifies mathematical descriptions and sampling.
2. Fluid shear stress at the wall can be varied independent of mean residence time.
3. High surface area to volume ratio.

Dilution water to the AFR's is (1) treated with activated carbon

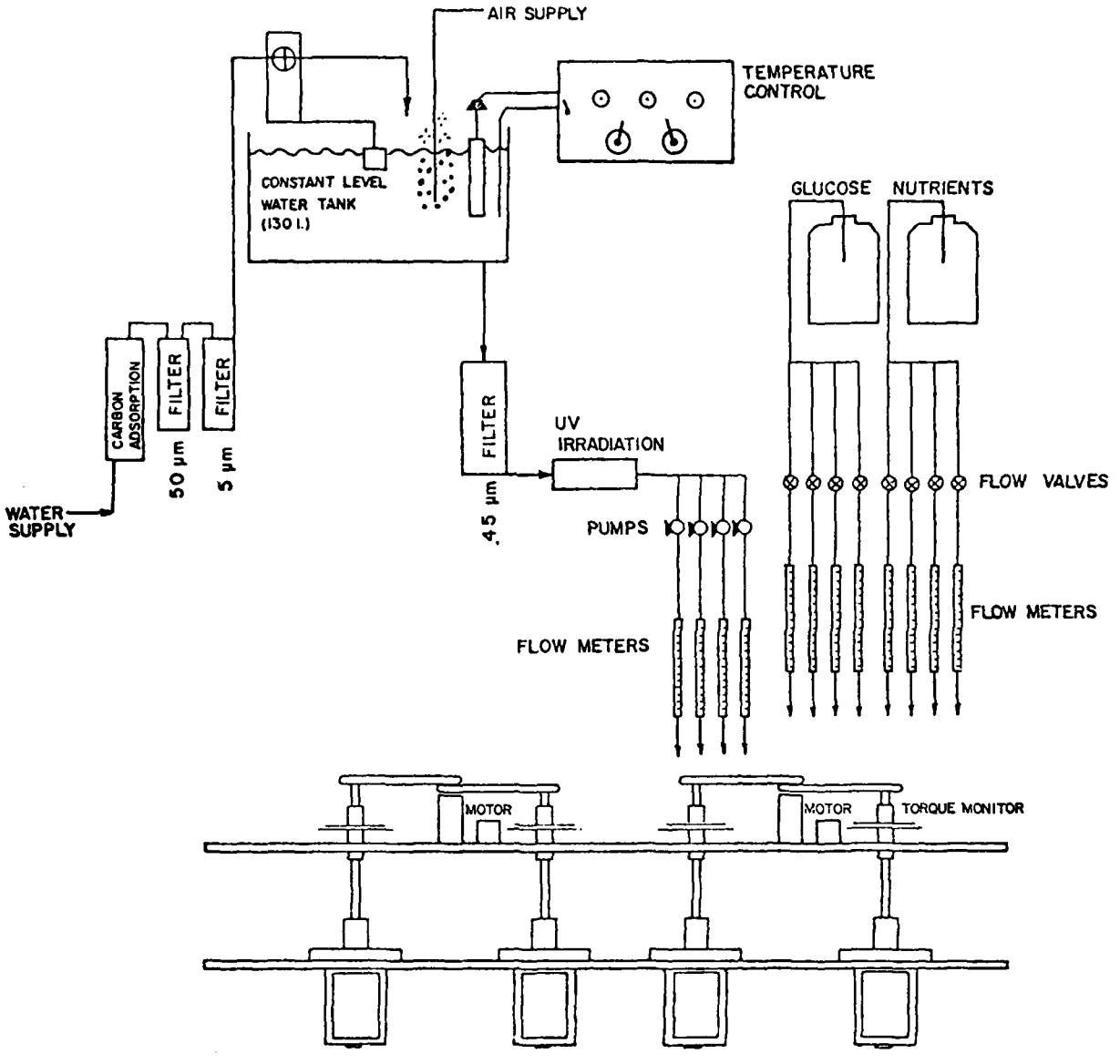

Figure 1. Annular Fouling Reactor System.

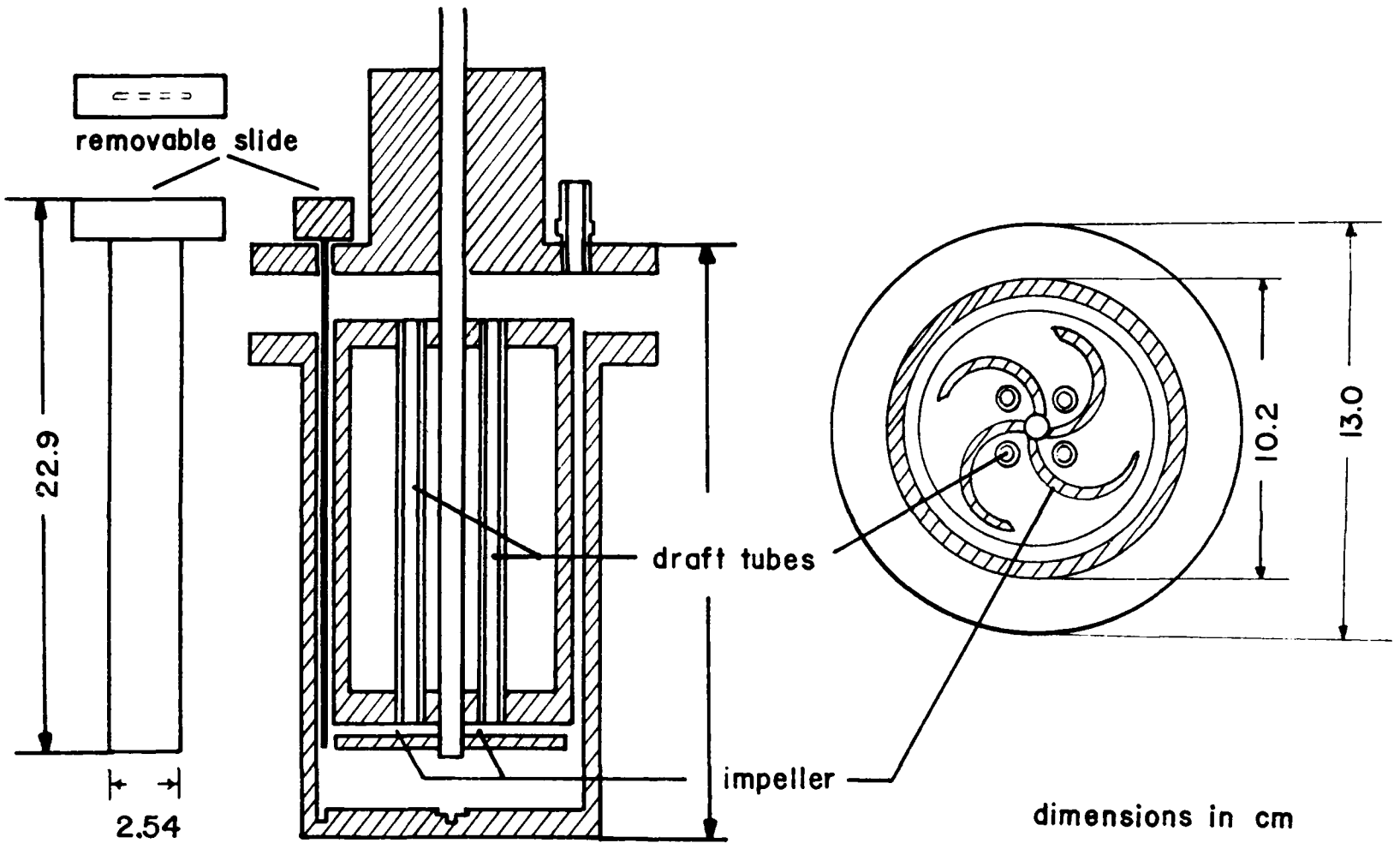

Figure 2. Annular Fouling Reactor Details

to remove residual chlorine and soluble organics, (2) filtered in a filtration cascade (down to 0.45 μm) to remove suspended material, and (3) treated in a UV irradiation trough for sterilization. Dilution water is continuously fed into the reactors by peristaltic pumps. Volumetric flowrates are monitored with in-line flowmeters.

Sterile nutrient solution is fed to the AFR's by gravity flow. Flowrates are controlled with Dial-A-Flo® valves and monitored with in-line flowmeters.

Prior to entering the AFR's dilution water passes through a temperature adjustment/aeration chamber which maintains reactor temperature at 30 ± 0.05°C and provides a dissolved oxygen concentration near saturation in the reactor influent.

Chemostat system: The chemostats consist of Berzelius Pyrex beakers with side arms and rubber stoppers. Figure 3 illustrates details of the reactors. Stainless steel baffles and magnetic stirring disks provide complete mixing of the liquid solution. A polypropylene scraping disk in each reactor provides a method of removing attached microorganisms from the inner surfaces of the glass to prevent wall growth. Anti-backflow devices on the influent and effluent lines prevent contamination of the substrate feed solution and reactor solution due to the backflow of microorganisms.

Sterile substrate solutions are fed to the chemostats by gravity flow. Flow rates are controlled with Dial-A-Flow® valves and monitored with in-line flow meters.

Chemostat solution temperature is controlled at 25 ' 1°C by a thermistor temperature controller and immersion heater located in the chemostat temperature control reservoir (Fig. 4).

The chemostat is continuously aerated with filtered laboratory air fed through the influent anti-backflow device.

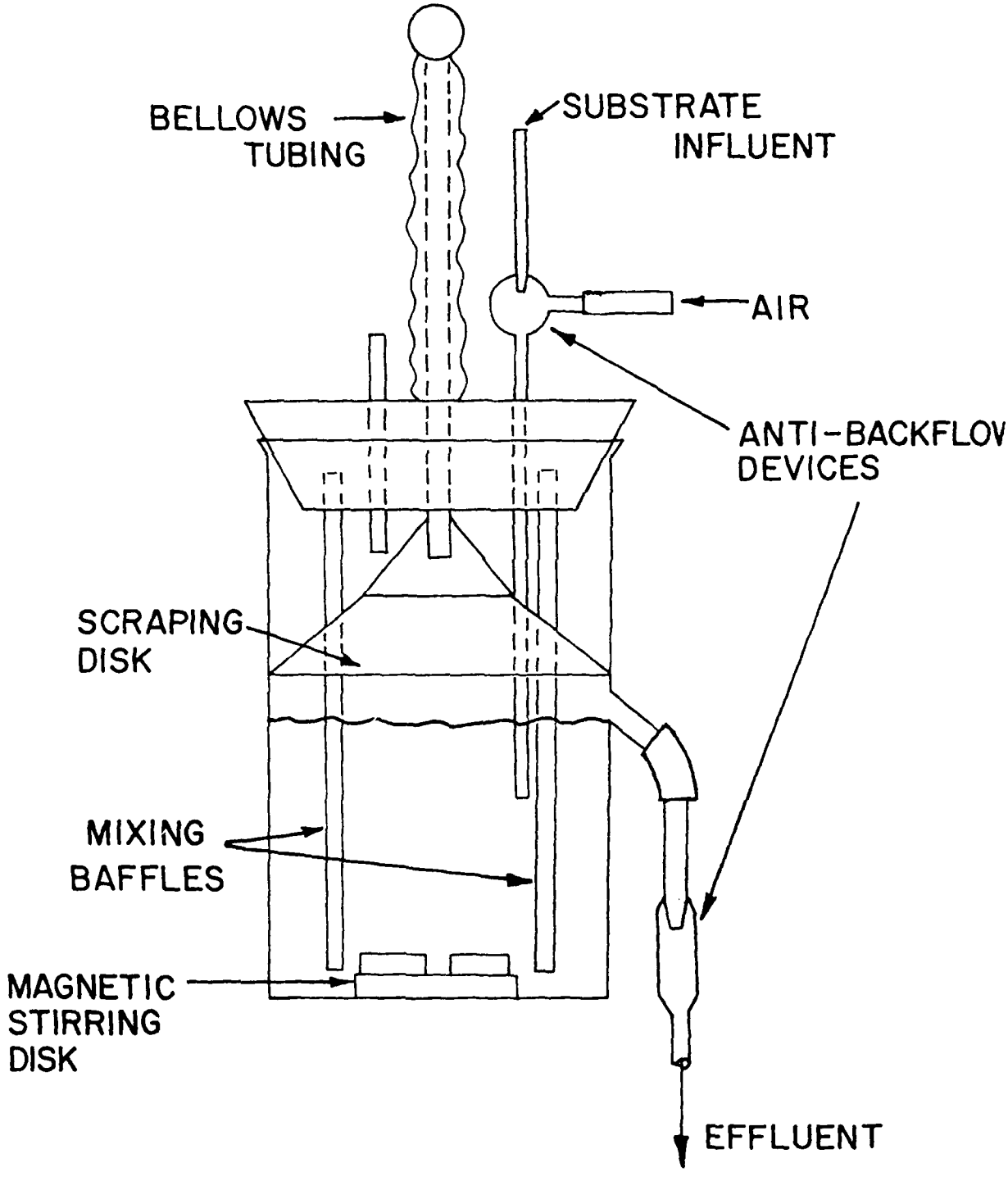

Figure 3. Chemostat Details

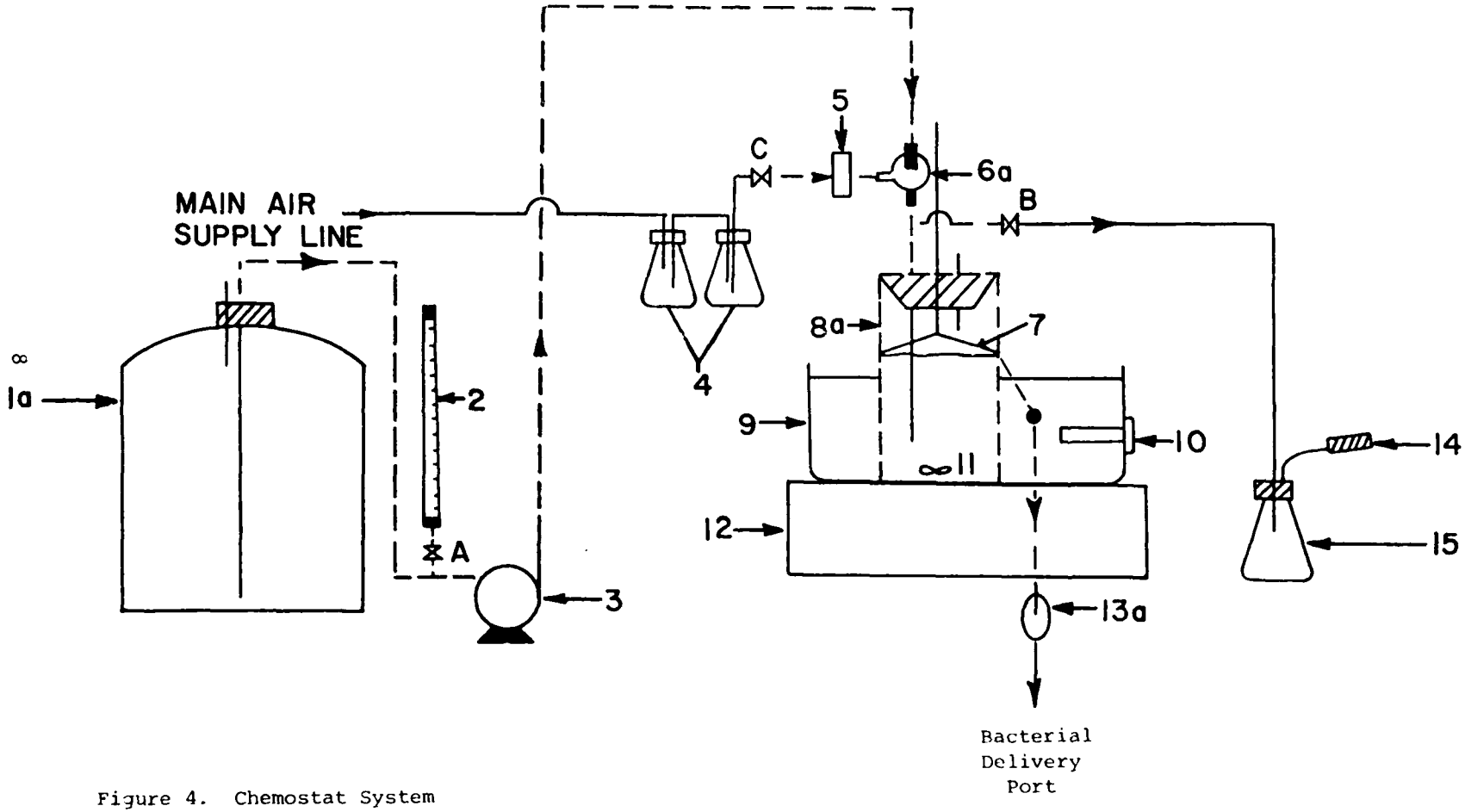

Figure 4. Chemostat System

Legend (Figure 4)

1a. Medium Reservoir(< autoclaved)

2. Sterile Pipette for measuring flow rate

3. Peristaltic pump

4. Air filters (glass wool packed)

5. Inline air filter (0.45 µm)

6a. Device to avoid back contamination

7. Scraper

8a. Chemostat

9. Water Bath

10. Temperature Controller

11. Magnetic Stirring Bar

12. Magnetic Stirrer

13a. Device to avoid back Contamination

14. Air Filter

15. Sampling Flask

A,B,C Pinch Clamps

Dashed lines indicate items autoclaved prior to operation.

Instrumentation: Electronic instrumentation is used to continuously measure torque and rotational speed. Data is stored on magnetic tape for retrieval.

An Apple II Plus microcomputer accepts data from eight separate torque/rpm transducers and displays the information on a video monitor. Results are updated every 30 sec. A modular diagram of the instrumentation is shown in Fig. 5.

The torque transducers are of the torsion bar type and measure torque in the range of 0 to 10 inch-ounces ($0-7.06 \times 10^{-3}$ N-m). They were specifically designed and constructed in this laboratory for interfacing to a microcomputer. Calibration curves for the transducers are shown in the appendix.

Substrate solution: The glucose mineral salts medium shown in Table 1 has been used as a nutrient solution for chemostat and AFR experiments reported. Solutions are sterilized by autoclaving.

Analytical methods: Epifluorescence microscopy is used to enumerate the total number of bacterial cells present in biofilm or bulk solution samples (Hobbie et al. 1977). Known volumes of the samples are homogenized in a Sorvall Omnimixer (Dupont Instruments, Newtown, CT) and serial dilutions prepared using filtered DI water. The resulting solutions are then stained with Acridine Orange and filtered through membrane filters.

The filters are viewed using a Leitz Ortholux II microscope equipped with a mercury-xenon ultraviolet lamp. Cells fluoresce green or orange against a black background and are easily counted in the range of 30-100 bacteria per field. Ten fields are counted from each dilution, with arithmetic means and standard deviations computed and recorded as either cells/ml solution or cells/cm^3 biofilm.

Total and soluble organic carbon (TOC and SOC) are determined using an ampule analysis technique (Oceanography International Corp., College Station, TX). Soluble samples are prepared by filtration through Nuclepore membrane filters (Nuclepore Corp., Pleasanton, CA., No. 111107, average pore size 0.45 μm).

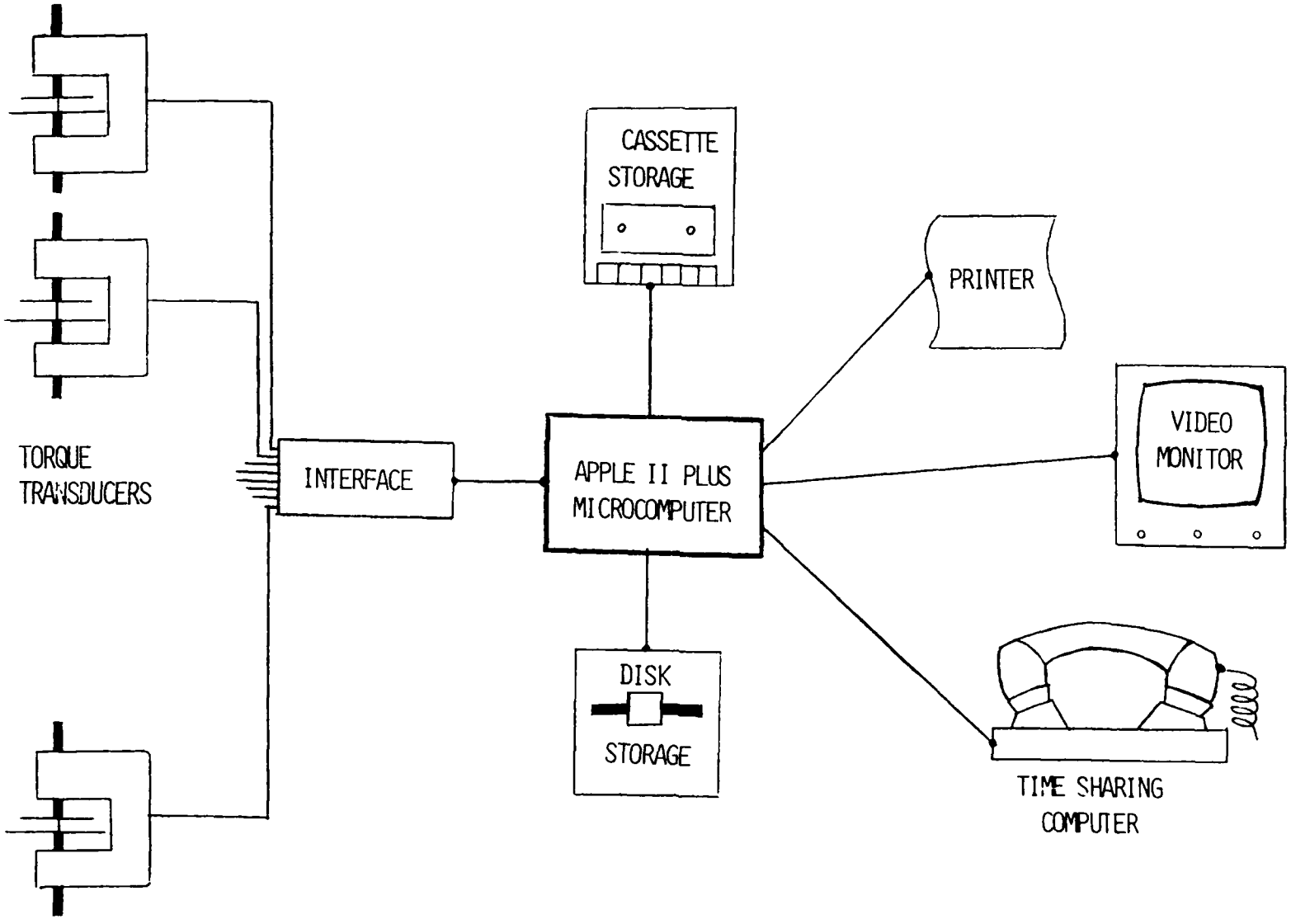

Figure 5. Torque Instrumentation

TABLE 1

GLUCOSE MINERAL SALTS MEDIUM[11]

Glucose	10.0 mg
NH_4Cl	3.6
$MgSO_4 \cdot 7H_2O$	1.0
$CaCl_2$	0.1
$FeCl_3 \cdot 6H_2O$	0.02
K_2HPO_4 (buffer)	18.0
KH_2PO_4 (buffer)	3.0
Vitamin B_{12}	0.05 µg
Distilled Water	1.0 liter

For glucose concentrations other than 10 mg/l, the concentrations of mineral salts are proportionally adjusted.

Cellular carbon is determined by enumerating the total number of bacterial cells by epifluorescence microscopy, estimating the average volume per cell and multiplying the above quantities by literature values for the specific gravity per cell ($1.07 g/cm^3$), the dry wt/wet wt ratio (0.22) per dell, and the average mass of carbon per cell (0.5 mg C per mg cell).

Polymer carbon is determined by measuring the TOC, SOC, and cellular carbon concentrations of biofilm or bulk solution samples and performing the following calculation:

$$\text{polymer carbon} = \text{TOC} - \text{SOC} - \text{cellular carbon}$$

Glucose concentration is determined by the Glucostat semi-micro procedure (Worthington Biochemical Co., Freehold, N.J.). The calibration curves consistently exhibit linear behavior in the desired concentration range.

Suspended solids are determined by filtering at least 100 ml of sample through a Nuclepore membrane. After filtration, the filters are dried at 60°C for a minimum of 3 hours and then weighed.

The thickness of microbial film in the AFR is determined with the stage micrometer of a microscope (Bausch and Lomb, Inc., Rochester, N.Y.) in a method adapted from that of Sanders (1964). The removable slide is withdrawn from the reactor, placed in a vertical position for one minute to allow excess water to drain, and then placed on the microscope stage. The 10x objective (100x magnification) is lowered until the biofilm surface is in focus and the fine adjustment dial setting of the stage micrometer is recorded. The objective is then lowered further until the inert plastic growth surface is in focus (Figure 6). The difference in fine adjustment settings is compared with a calibration curve (Figure 7) and the thickness determined. The reported biofilm thickness is the mean of 4 or 5 measurements along the slide from top to bottom.

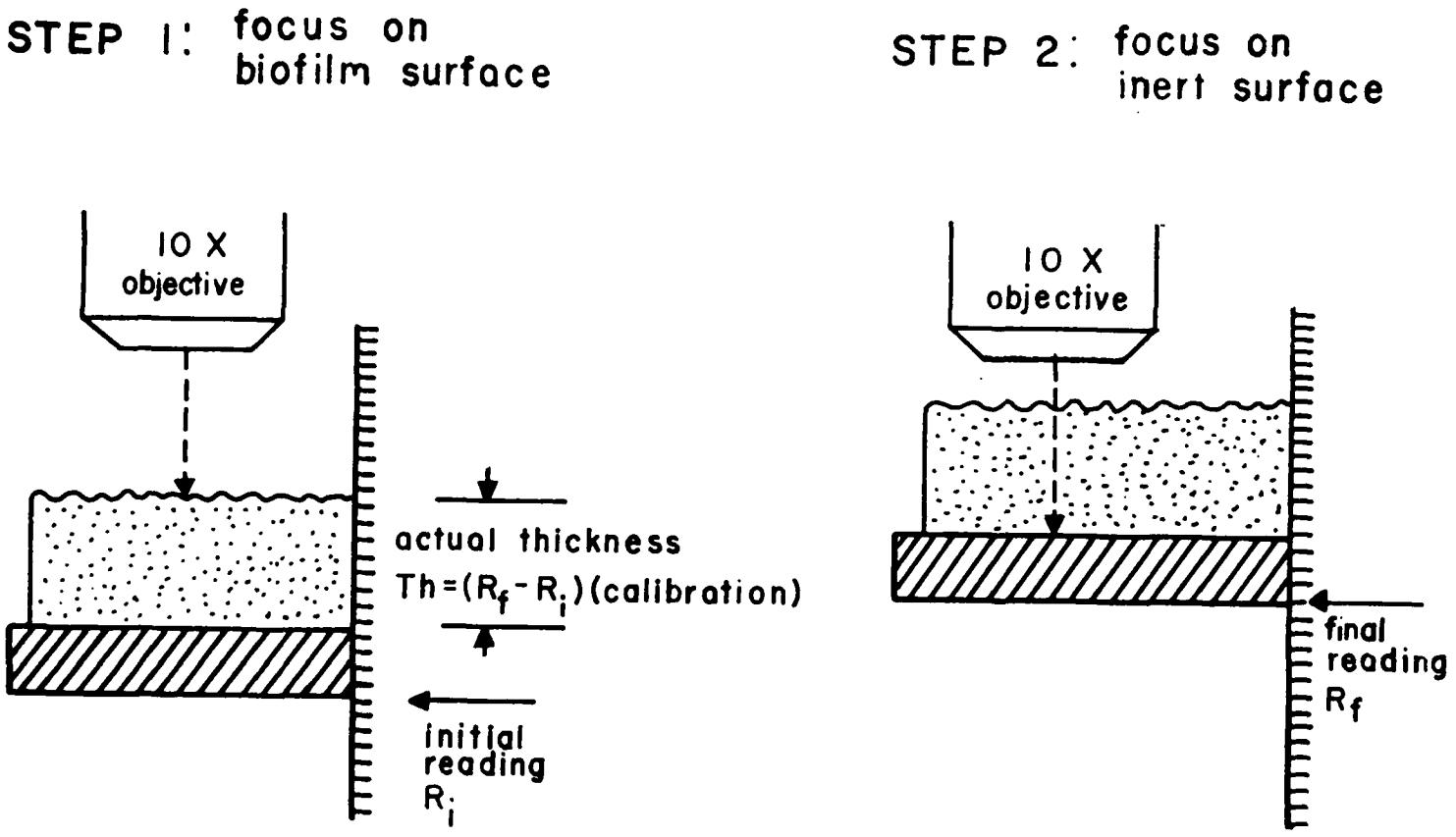

Figure 6. Microscopic Method for Measurement of Biofilm Thickness

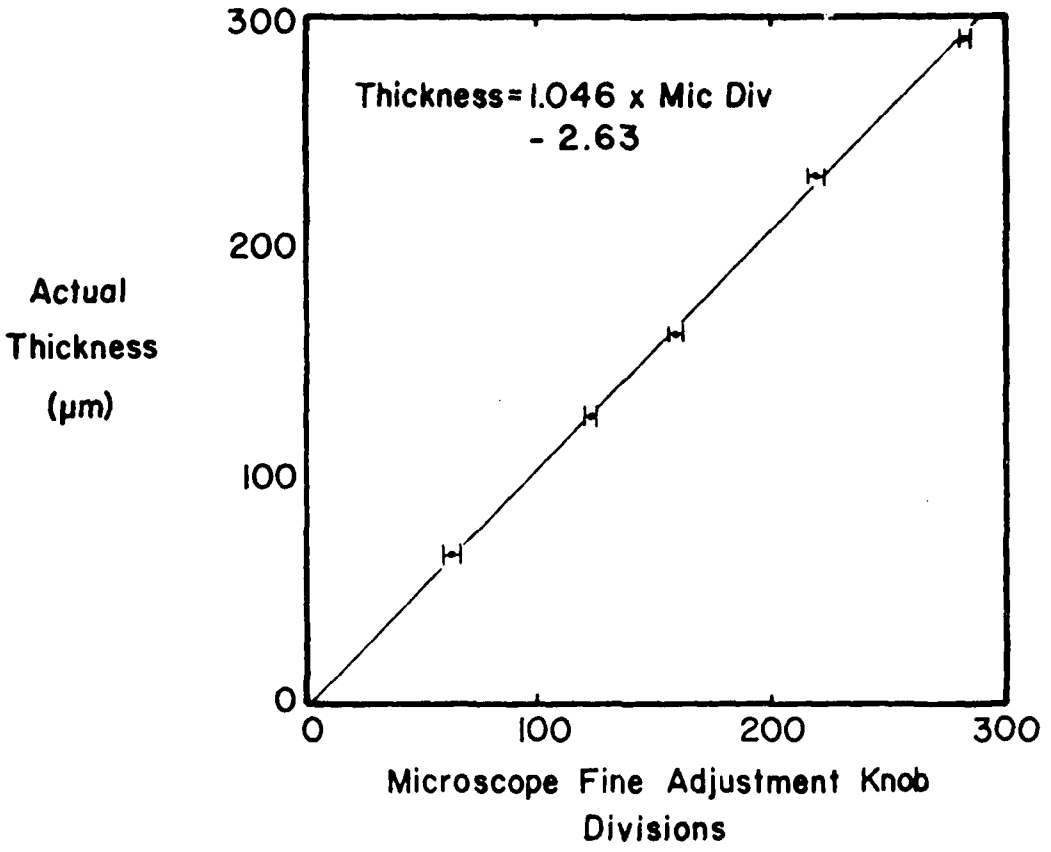

Figure 7. Calibration Curve for Film Thickness Measurement. Each Point is an Average of Repeated Measurements on a Metal Shim With the Actual Thickness Determined With a Vernier Micrometer.

Periodically, samples are removed from one of the AFR's for SEM. Small sections of a removable slide are clipped off and fixed in 0.067 M cacodylate buffer with 10% EM grade glutaraldehyde. Samples are subsequently put through a series of acetone dehydrations followed by critical point drying and sputter coating.

Tubular Fouling Reactor System

The tubular fouling reactor system (TFR) consists of a test block heat exchanger and a support system which includes water supply treatment facilities and measurement instrumentation. Figure 8 is a schematic diagram of the system.

Test block heat exchanger: The test block heat exchanger consists of two adjacent aluminum cylindrical blocks (12.5 cm dia.) clamped to the section of tubing being tested (Fig. 9). The block is heated by electrical resistance heating elements. The inner wall of the aluminum block and outer wall of the tubing are machined to close tolerances to provide intimate contact. A heat transfer compound is applied to maximize heat transfer at this interface.

A thermal gradient is set up between the heated outer surface of the block and water flowing through the tubing being tested. In the first block (downstream section), two thermistors measure temperatures at two radial distances from the tube axis.

Support system: The water supply support system recycles water through the test heat exchanger and a second refrigerated heat exchanger. Heat is removed by this refrigerated heat exchanger, controlled by a temperature controller (Yellow Springs Instrument, Inc., Yellow Springs, Ohio), in order to maintain a constant bulk water temperature.

Dilution water, nutrients, and inorganic salts are fed to the recycled water at constant rates while excess fluid is removed as waste. A pH controller feeds hydrochloric acid (6N) or sodium hydroxide (6N) to the recycled

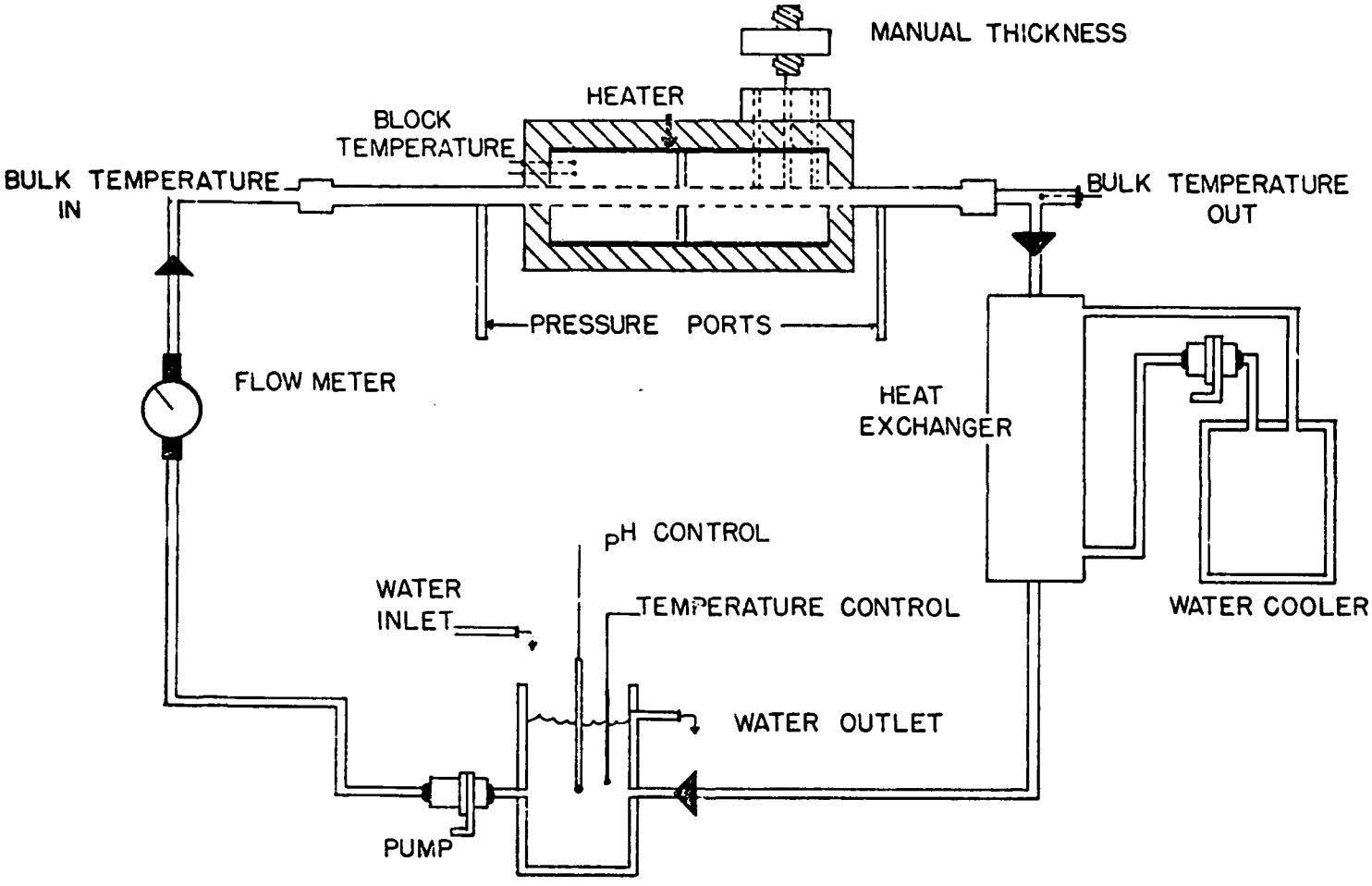

Figure 8. Tubular Fouling Reactor System

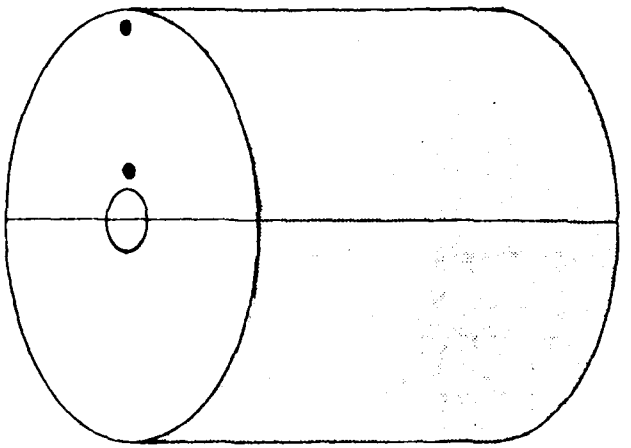

$R_1 = 0.95$ cm

$R_2 = 8.09$ cm

$R_i = 1.50$ cm

$R_{ii} = 7.37$ cm

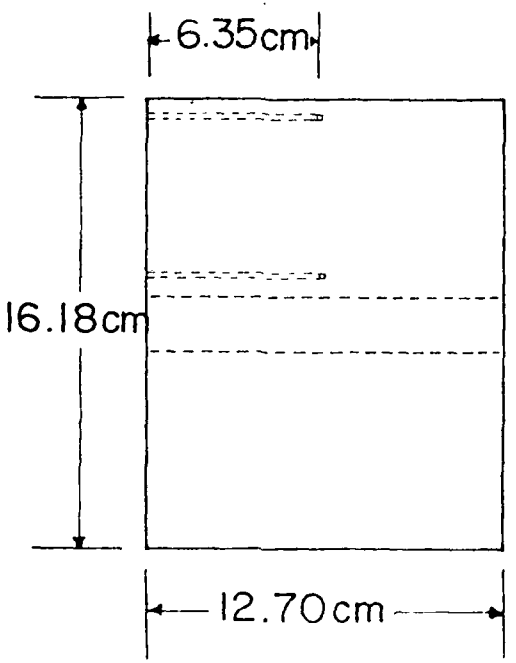

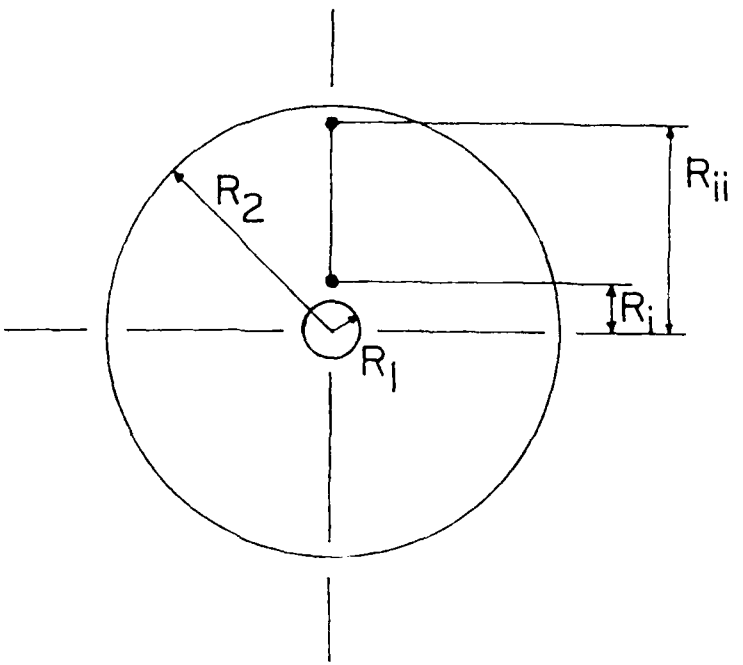

Figure 9. TFR Aluminum Block Detail

water as needed to maintain a constant pH in the bulk water. (New Brunswick Scientific, New Brunswick, N.J.).

For all practical purposes, the TFR system is a uniformly mixed CSTR since fluid residence time is much greater than fluid recycle time.

Continuous measurements: The following variables are continuously measured and monitored by microcomputer:

(1) inner and outer aluminum block temperatures

(2) input and output bulk water temperatures

(3) pressure drop across aluminum block test section

(4) volumetric flow rate

Data is displayed on a CRT monitor and is updated every 30 seconds. Every hour data is recorded on cassette tape for storage and subsequent retrieval.

Periodic measurements: A manual thickness measuring device is attached to the second block (upstream section). Thickness of a fouling deposit is measured by lowering an electrically insulated probe via a micrometer into a port which passes through the tube wall. The tip of the probe is not insulated and, upon contact with the fouled surface, an electric current can be detected passing through the probe into the tube wall. Probe distance to the inside tube wall is determined prior to beginning an experiment when the tube is clean. Thickness is determined by subtracting probe distance to the fouling deposit from the distance to the clean tube wall. Calcium is measured by EDTA titration as described in Standard Methods, 1971.

Chemostat System

Chemostats, as described in the section on the AFR, produce a continuous inoculum of well-defined bacterial populations to any of the fouling reactors.

Chemostat studies are vital to our investigations for a number of reasons including the following:

1. To ensure a microbial feed to the biofilm reactors which partially defines a physiological state for the cells.

2. To perform material balances for biofilm reactors.

Detailed studies using these chemostats have helped define operating parameters necessary for stable production of biomass. A complete schematic of a chemostat and its support system is shown in Fig. 4.

The system is designed to maintain aseptic conditions as follows:

(1) The reservoir containing culture medium is autoclaved at 121°C (15 psig) for 20 minutes.

(2) The entire chemostat system including support apparatus indicated in Figure 4 is autoclaved.

(3) All tubing is made of silicone rubber to withstand repeated autoclaving.

(4) The air break device (Figure 4) aids in avoiding back-contamination from the outlet of the chemostat.

(5) The chemostat air supply is maintained sterile by passing it through two Erlenmeyer flasks packed with glass wool followed by a 0.45 μm in-line filter.

Pure cultures (from TSB agar plates) are used to prepare the inoculum for the chemostats. One hundred ml of medium in a 250 ml Erlenmeyer flask are autoclaved (20 min, 15 psig, temp. 121°C) and then inoculated with organisms from a plate and allowed to grow in a constant temperature water bath (reciprocatory shaker) for 8-24 hours. This method for preparing the inoculum minimizes growth lag in the chemostat.

After inoculation, the chemostat is operated without continuous nutrient feed until a significant microbial population is obtained. Then, the nutrient pump is started and flowrate (dilution rate) is adjusted. The chemostat is operated at that dilution rate until steady state is attained. Six residence times (i.e., turnovers) are allowed to attain steady state.

Temperature of the chemostat is maintained at 25°C and pH is controlled

by the buffering capacity of phosphate in the medium (pH7).

Chemostat samples are periodically streaked and organisms identified to confirm culture integrity.

Mathematical model: A chemostat model based on aggregate properties such as biomass concentration, yield, and organic carbon concentration, has been used to analyze chemostat experimental data.

- Steady State Glucose Carbon Material Balance

$$F\,(s_i - s) = \frac{\mu \times V}{Y_x} + r_p(p_x + p_s)\,V$$

net rate of glucose input by flow | rate of glucose removal for cellular reproduction | rate of glucose removal for polymer production

- Steady State Cellular Carbon Material Balance

$$F\,x = \mu \times V \quad \text{or} \quad \frac{F}{V} = \mu = D$$

rate of cellular output by flow | rate of cellular reproduction

- Steady State Polymer Carbon Material Balance

$$F\,(p_x + p_s) = r_p\,(p_x + p_s)\,V$$

rate of polymer output by flow | rate of polymer production

- Yield Condition

$$\Delta s = \Delta s_x + \Delta s_p$$

total substrate removed | substrate removed for cellular reproduction | substrate removed for polymer reproduction

dividing by the quantity of cells produced (Δx),

$$\frac{\Delta s}{\Delta x} = \frac{\Delta s_x}{\Delta x} + \frac{\Delta s_p}{\Delta x}$$

total substrate removed per cells produced	substrate removed for cellular reproduction per cells produced	substrate removed for polymer production per cells produced

however

$$\frac{\Delta s_p}{\Delta x} = \frac{\Delta s_p}{\Delta (p_x + p_s)} \quad \frac{\Delta (p_x + p_s)}{\Delta x}$$

where

$\Delta (p_x + p_s)$ = total polymer produced

substituting and noting that $\frac{\Delta s}{\Delta x}$ is the reciprocal of yield,

$$\frac{1}{Y} = \frac{1}{Y_x} + \frac{1}{y_p} \quad \frac{\Delta (p_x + p_s)}{\Delta x}$$

Hence the system is described by four independent equations. However, these equations contain 5 unknown quantities (μ, Y_x, r_p, Y_p, Y). An additional independent equation can be generated as follows:

$$Y = \frac{\mu \times V}{F (s_i - s)}$$

Endogenous respiration is not considered in the above development. Deviations in the proposed model will occur, particularly at low dilution rates, if endogenous respiration is an important process. Under these circumstances, an endogenous respiration coefficient, k_e, will be included in the model by substituting $\mu = (D + k_e)$ into the first two equations and solving for the additional unknown (k_e) as follows:

substituting $\mu = (D + k_e)$ into the first equation

$$F (s_i - s) = \frac{(D + k_e)\ xV}{Y_x} + \frac{r_p (p_x + p_s)\ V}{Y_p}$$

rearranging and linearizing,

$$\frac{F\ (s_i - s)}{x\ V} - \frac{r_p\ (p_x + p_s)}{x\ Y_p} = \frac{D}{Y_x} + \frac{k_e}{Y_x}$$

Consequently, plotting the l.h.s. of the equation versus D will result in a straight line where

$$\text{slope} = \frac{1}{Y_x} \qquad \text{intercept} = \frac{k_e}{Y_x}$$

Results: Studies have been completed on a pure culture of Pseudomonas aeruginosa. Kinetic parameters obtained were: $\mu_{max} = 0.37\ h^{-1}$; $K_s = 6.9$ mg/l; Y = 0.42 g biomass/g substrate. Figure 10 is a plot of the data obtained from this study.

Microbiological Techniques.

Specific organisms: A number of specific organisms are maintained including those associated with marine fouling:

Pseudomonas aeruginosa

Pseudomonas atlanticus, T_6C

Pseudomonas alcaligenes

Flavobacterium species

Vibrio alginolyticus

Desulfovibrio desulfuricans

Sphaerotilus natans

Enterobacter aerogenes

Bacillus cereus

Leuconostoc mesenteroides

1 - P. aeruginosa is a soil or water organism which has a remarkable capacity for survival in terrestrial and aquatic environments. They are polysaccharide producers and often found as pollutants in natural water systems. Growth kinetics and biofilm production by this organism is

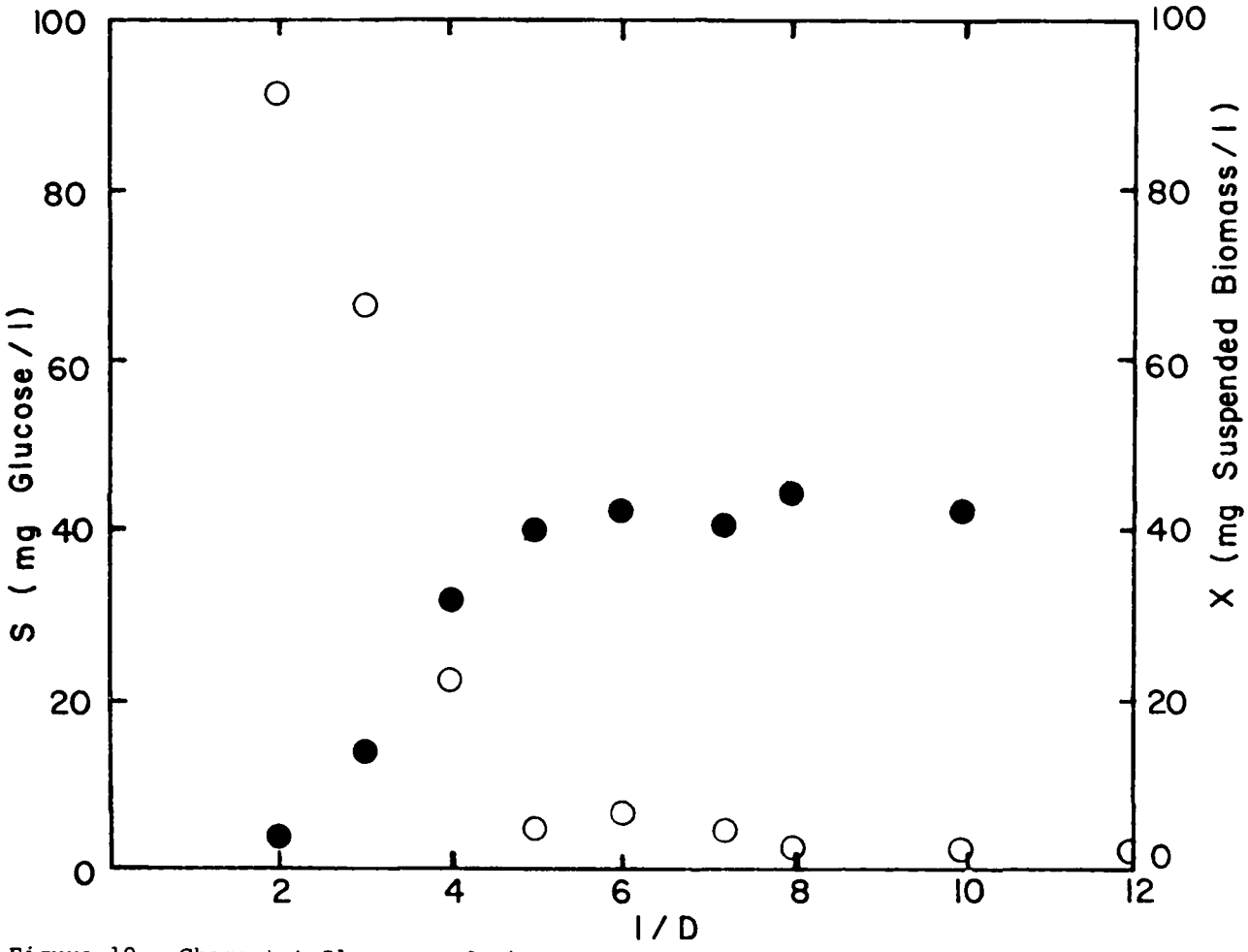

Figure 10. Chemostat Glucose and Biomass Concentrations for a single Pseudomonas aeruginosa ground study.

being studied in the AFR systems.

2 - Sphaerotilus natans is being studied in the AFR systems in pure and mixed cultures. Sphaerotilus forms sheaths (up to 1-5 mm in length) in natural water. We have observed excessive fluid frictional losses when Sphaerotilus biofilms form in the TFR or AFR.

3 - Desulfovibrio desulfuricans is an obligate anaerobe which reduces sulfate and often accelerates corrosion of metals. The growth kinetics of this organism are being determined in order to relate their growth to corrosion rates.

4 - Leuconostoc mesenteroides, Bacillus cereus, Enterobacter aerogenes, and Sphaerotilus natans were used to study the influence of temperature on biofilm formation.

5 - Pseudomonas atlanticus (T_6C), P. alcaligenes, Flavobacterium and Vibrio alginolyticus. These are all marine organisms which grow rapidly and produce a slimy film on surfaces. We will be studying the biofilm formation produced by these organisms on different metals (titanium and copper-nickel) treated in different ways (chlorine and Cathelco®).

Identification: Microbial identification procedure is divided into two complementary steps. Specimens are first isolated and processed through preliminary visual and gram stain identification. They are then further identified using the API 20E System for identification of Enterobacteriaceae and other gram-negative bacteria.

In the identification of the test organisms, the specimens are processed as soon as possible. Proper plating medium and incubation conditions are very important for organism survival and subsequent identification. Most of our specimens are plated on tryptic soy agar supplemented with 0.3% yeast extract or EMB and incubated at 28 - 35°C. Plates are streaked for

purification and maintained on slants of TSA-Ye at 5°C. Marine specimens are plated on marine agar. Synthetic salt water (Instant Ocean®) is used for culturing marine organisms. Gram stains as well as colony and cell morphology are observed before further identification.

The API 20E system for the identification of Enterobacteriaceas and other gram negative bacteria is a convenient microtube system designed for 23 standard biochemical tests for colony(ies) of bacteria isolated from plating medium. Information concerning the API system is included in the appendix.

Table 2 shows the scheme followed for the identification of gram negative organisms.

Preservation: To maintain an organism alive, uncontaminated, and without variation or mutation, in other words, as close as possible to the original isolate, methods must be employed to preserve the bacteria. Not all species respond in a similar manner to a given method and the availability of equipment, storage space, and skilled labor often dictates the method employed. (La page et at, 1970).

The traditional method of preserving bacterial cultures is through periodic transfer to fresh media. The interval between subcultures varies with the organism, the medium employed, and the external conditions. Some bacteria must be transferred every other day, others only after several weeks or months. Three conditions must be determined using this method for the preservation of cultures: (i) suitable maintenance medium, (ii) ideal storage temperatures, and (iii) the frequency between transfers.

The quick freezing method is the technique most often used in our laboratory. Results are good and the method is simple. Cell suspensions are mixed with glycerol, quick frozen in liquid nitrogen for 25 seconds, and stored at approximately -20°C.

TABLE 2

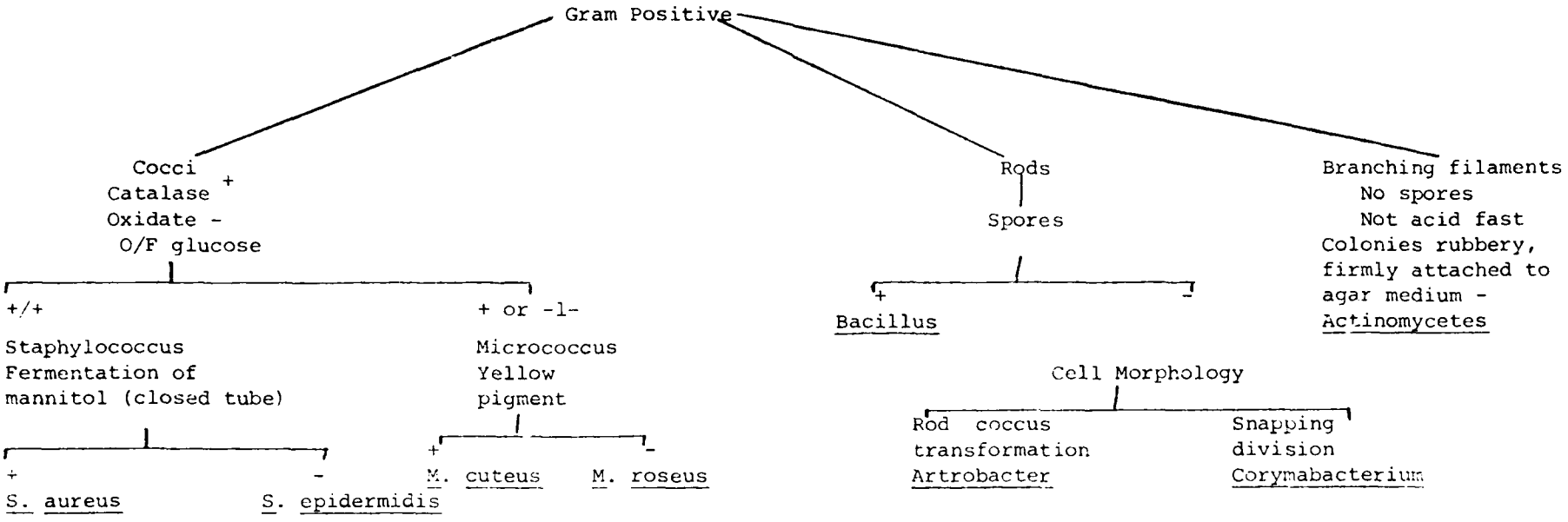

LeChevallier, M. W., Seidler, R. J., and Towns, T. M. (1980). Enumeration and characterization of standard plate count Bacteria in chlorinated and raw water supplies. Applied and environmental Microbiology, 40, p. 924.

The physiological condition of the culture is very important in the survival of the bacterium to liquid nitrogen freezing. In general, actively growing cells at the mid to late logarithmic phase of growth are created. The cells are concentrated and distributed into sterile "quick freezing" vials containing glycerol at 25 volume per cent. In scant growth, suspend the cells from one slant in 1.4 ml of the suspending medium. Then pour this over a second slant, suspend and use 0.5 ml of this for each vial.

Rapid warming results in the greatest recovery of microorganisms from the frozen state. This has also been the experience at the American Type Culture Collection. To recover frozen cultures, thaw them rapidly with moderate agitation in a 37°C water bath until the ice melts. Immediately after thawing, remove from the water bath and if an ampule was used rather than a glass vial, wipe with 70% ethanol to disinfect. Open the ampoule or vial and aseptically transfer the culture to fresh medium.

Check the viability of the culture to determine the effectiveness of the procedure for a given species. The expected shelf life of different bacteria is shown in Table 3.

TABLE 3. Expected shelf life of representative bacteria preserved by various methods

Genus	Serial transfer[a]	Mineral oil	Sterile soil	Deep freeze	Freeze-dried	Liquid nitrogen
Acetobacter	1-2 mo	1 yr		1-3 yr	>30 yr	>30 yr
Achromobacter	1 mo	1-2 yr		1-3 yr	>30 yr	>30 yr
Acinetobacter	weekly				>30 yr	>30 yr
Actinobacillus	weekly	2-3 yr			>30 yr	>30 yr
Actinomyces	1 mo		1-2 yr	2-3 yr	>30 yr	>30 yr
Agrobacterium	1-2 mo	1-2 yr	1-2 yr		>30 yr	>30 yr
Arthrobacter	1-2 mo			1-2 yr	>30 yr	>30 yr
Bacillus	2-12 mo	1 yr	1-2 yr	2-3 yr	>30 yr	>30 yr
Bacteroides	weekly			1 yr	>30 yr	>30 yr
Bifidobacterium	weekly				>30 yr	>30 yr
Chromatium	1 mo				> 6 yr	>10 yr
Clostridium	6-12 mo	1-2 yr		2-3 yr	>30 yr	>30 yr
Corynebacterium	1-2 mo	1 yr		1-2 yr	>30 yr	>30 yr
Enterobacter	1-4 mo	1-2 yr			>30 yr	>30 yr
Escherichia	1-4 mo	1-2 yr			>30 yr	>30 yr
Erwinia	1-4 mo	1-2 yr			>30 yr	>30 yr
Flavobacterium	1 mo	2 yr			>30 yr	>30 yr
Gluconobacter	1 mo				>30 yr	>30 yr
Haemophilus	weekly	1 mo (37°C)			>30 yr	>30 yr
Klebsiella	1-4 mo	1 yr		1-2 yr	>30 yr	>30 yr
Lactobacillus	weekly				>30 yr	>30 yr
Methanobacterium	1 mo				>10 yr	>10 yr
Methanomonas	1 mo				>10 yr	>10 yr
Micromonospora	1 mo		1-2 yr	1 yr	>30 yr	>30 yr
Neisseria	1 mo				>30 yr	>30 yr
(N. gonorrhoeae)	weekly	1 mo (37°C)			>30 yr	>30 yr
(N. meningitidis)	weekly	1 mo (37°C)			>30 yr	>30 yr
Nocardia	1-4 mo	1 yr		1-2 yr	>30 yr	>30 yr
Proteus	1-2 mo	1 yr		1-2 yr	>30 yr	>30 yr
Pseudomonas						
Spirillum	weekly	6 mo		1 yr	>30 yr	>30 yr
Staphylococcus	1-2 mo			1 yr	>30 yr	>30 yr
Streptococcus	1-2 mo	1 yr			>30 yr	>30 yr
Streptomyces	1-8 mo	1-2 yr	2-3 yr	1-3 yr	>30 yr	>30 yr
Xanthomonas				1-2 yr	>30 yr	>30 yr

[a]Transfer schedule depends on media used. The times listed are approximations, and species variation occurs within genus.

FORMATION AND STRUCTURE OF A FOULING BIOFILM.

Introduction

Biofilm development at a surface is the net result of several physical, chemical and microbial processes including the following:

1. Transport of dissolved and particulate matter from the bulk fluid to the surface
2. Firm microbial cell attachment to the surface
3. Microbial transformations (growth, reproduction, etc.) within the biofilm resulting in production of organic matter.
4. Partial detachment of the biofilm due primarily to fluid shear stress.

In most cases, the net result of these processes is a sigmoidal progression of biofilm accumulation as indicated in Figure 11. The progression has been arbitrarily divided into three (3) phases: induction, growth and plateau. Biofilm accumulation during the induction period results in no change in frictional resistance. Induction is followed by a period of rapid accumulation - the growth phase. Finally, a plateau in accumulation is reached. Factors which affect these processes are:

- Transport of material from the bulk fluid to the surface and attachment to the surface. Materials can be soluble (microbial nutrients and organics) or particulate (viable microorganisms, detriturs, or inorganic particles). Also, suspended particles of sufficient mass may control films by "scouring" action.
- Microbial metabolism within the film. Microbial growth in the biofilm and extracellular polymers produced by the microorganisms contribute to the biofilm deposit and promote adherence of inorganic suspended solids.
- Fluid shear stress at the surface of the film. Such forces can limit the overall extent of the fouling deposit by reentraining attached material.
- Temperature. Temperature affects the rates of all biologically important reactions.
- Surface material and roughness. Surface properties can influence micro-mixing near the surface and corrosion processes. Some metal surfaces may release toxic components into the biofilm inhibiting growth and/or attachment. Some metals produce loosely held oxide films under the biofilms. When the oxide film sloughs, the biofilm is also removed.
- Fouling control procedures. Chlorine, the most commonly used

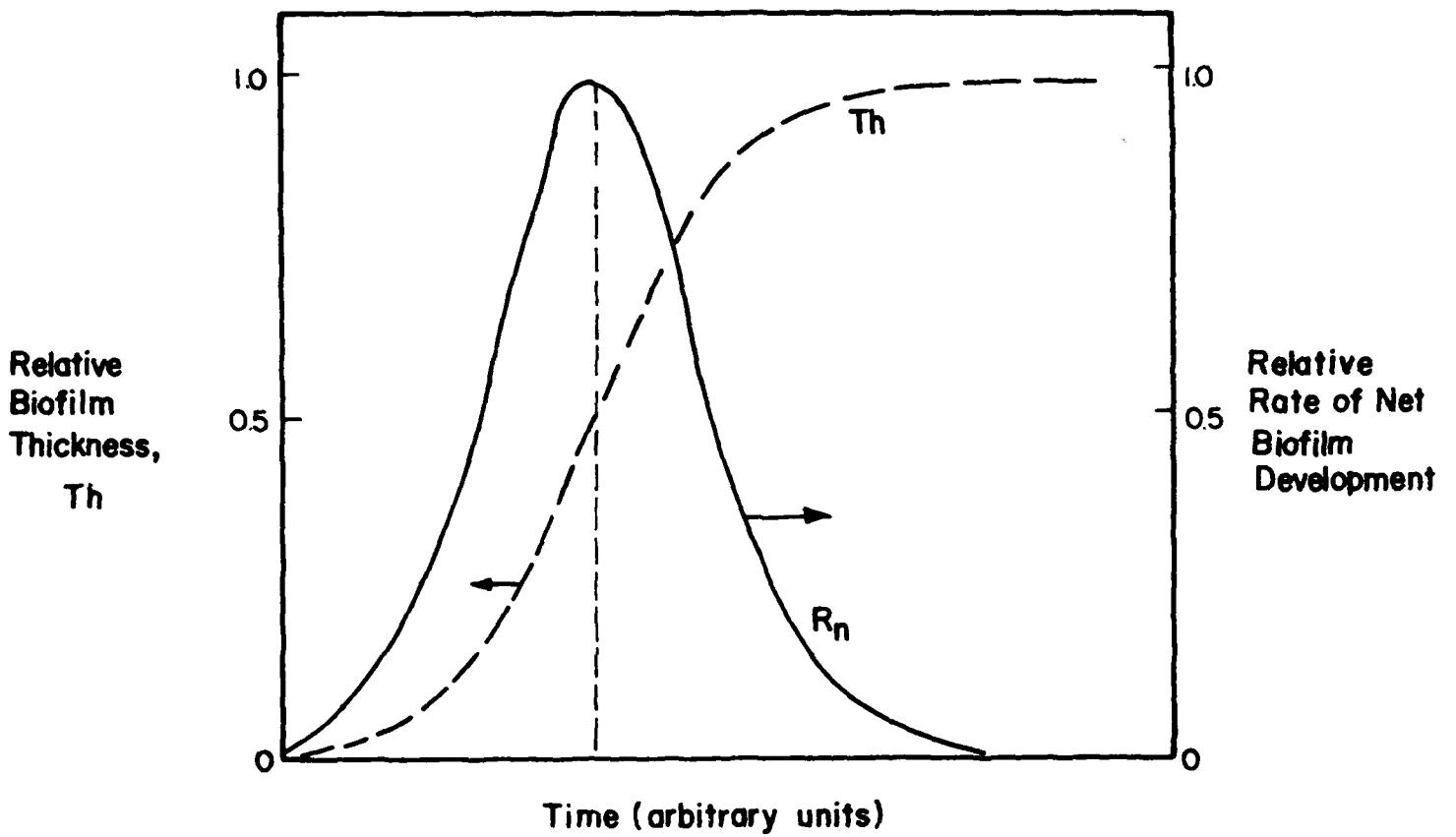

Figure 11. Sigmoidal Progression of Biofilm Accumulation

chemical, oxidizes biofilm polymers causing disruption and partial removal. Inactivation of a portion of the microbial population also occurs. Altered biofilm "roughness" and decreased viable cell numbers will influence "regrowth" rates of the biofilm. Mechanical cleaning can physically remove portions of the attached film.

Transport: When a "clean" surface first contacts water with biological activity, organic substances and microbial cells must be transported to the surface before biofilm development can begin. Consequently, the rate of transport determines the length of the "induction" period, i.e., the initial period during which no macroscopic effects of the biofilm are evident. In very dilute solutions (e.g., open ocean), the rate of transport may control the overall rate of biofilm development for long periods. Rate of transport is proportional to the concentration difference between the bulk fluid and the surface. In dilute solutions, this is small. The flow regime (zero, laminar or turbulent) also significantly influences transport rates and should be defined carefully in any experimental system used for biofilm studies. Surface characteristics are also critical to the repeatability and applicability of the results because a rough surface will increase transport and attachment rates.

Adhesion of Microbial Cells to the wetted Surface: Previous research (Marshall et al., 1971; Zobell, 1943) suggests the existence of a two-stage adhesion process: (1) reversible adhesion followed by, (2) an irreversible adhesion. Reversible adhesion refers to an initially weak adhesion of a cell which can still exhibit Brownian motion but is readily removed by mild rinsing. The adhesive forces which hold the cell at the wall during reversible adhesion probably include the following:

- electrostateic
- London-van der Waals
- interfacial tension

° covalent bonding

Conversely, irreversible adhesion is a permanent bonding to the surface, ususally aided by the production of extracellular polymers. Cells attached in this way can only be removed by rather severe mechanical treatment. Marshall (1976) and Corpe (1970) have implicated polysaccharides and glycoproteins in irreversible adhesion. (Figure 12).

Most of the research on cell adhesion has been conducted at very low fluid shear stress or in quiescent conditions. (Fletcher, 1977). These conditions suggest sedimentation or diffusion may control the rate of adhesion. Also, there is yet to be a demonstration of reversible adhesion in turbulent flow.

In turbulent flow, the net rate of adhesion is the quantity most easily measured. The net rate of adhesion is the difference between the rate of adhesion and rate of detachment. Detachment results from several forces including the following:

fluid dynamic forces
    shear forces
    lift (upsweeps)
taxis

Upsweeps result in turbulent bursts of fluid which may move away from the surface into the bulk flow. Upsweeps generate a lift force normal to the surface which can influence detachment. Drag or viscous shear forces act in the direction of flow on attached cells and are approximately 1000 times greater than the lift forces acting on attached cells. Note that although viscous shear may dislodge a particle, unless a lift force is present, the particle will presumably roll along the surface until another surface adhesion site is found.

The nature of the surface is an important factor affecting adhesion. Wettability or critical surface tension, is the property used most frequently

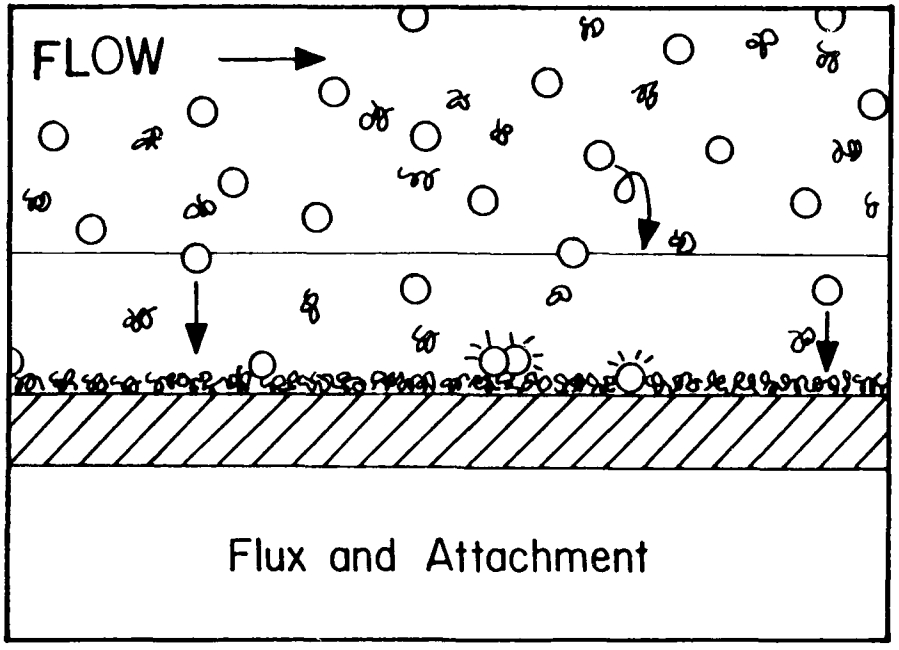

Figure 12. Bacterial Attachment.

to describe surface characteristics in microbial attachment studies (Dexter, 1976; Fletcher and Loeb, 1979).

One intriguing hypothesis is that iron (Fe^{+3}) plays an important role in initial attachment of bacteria and initiates some forms of scaling by altering surface characteristics. A layer of hydrated ferric oxide is believed to form on the surface prior to any initial fouling (Fig. 13). The highly nucleophilic hydroxyl groups can attract cations such as Ca^{++} and Mg^{++} or electrophilic centers such as silicon found in soluble forms of silica ($Si(OH)_4$). Through simple substitution reactions, covalent or coordinate covalent bonding can occur resulting in a tight, initial scaling layer on the fouled surface. Alternated layers of divalent cations and hydrated silica can form a multilayered fouling deposit, or serve as nucleation sites for scale crystal growth.

This same type of mechanism may conceivable promote biofouling. Molecules on the surface of bacteria contain electrophilic functional groups such as ketones (RR'C=O) and acids (RCOOH). These groups can react with nucelophilic hydroxyl groups of hydrated ferric oxide or silica and form covalent bonds with the surface. Divalent calcuim and magnesium ions can also strengthen the biological matrix through additional polymer bridging (Fig. 14).

One mechanism for initial attachment of bacteria has been previously discussed and requires a layer of deposited organic molecules before bacteria can attach. Both of these mechanisms are similar in that they create highly wettable surfaces.

Metabolism: Restricting our discussion to chemosynthetic organisms, the attached microbial cells assimilate reduced organic or inorganic compounds, nutrients, and oxygen or some other electron acceptor. The process yields energy with which the cells reproduce, maintain their internal structure, and

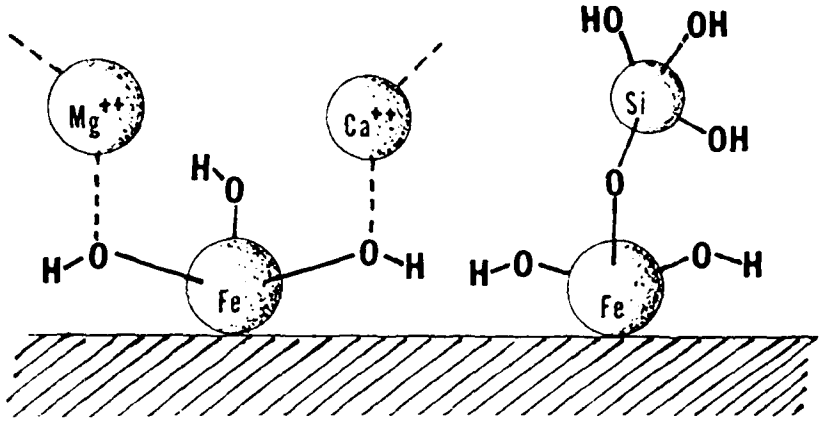

Figure 13. Hypothetical Role of Iron in Promoting Fouling.

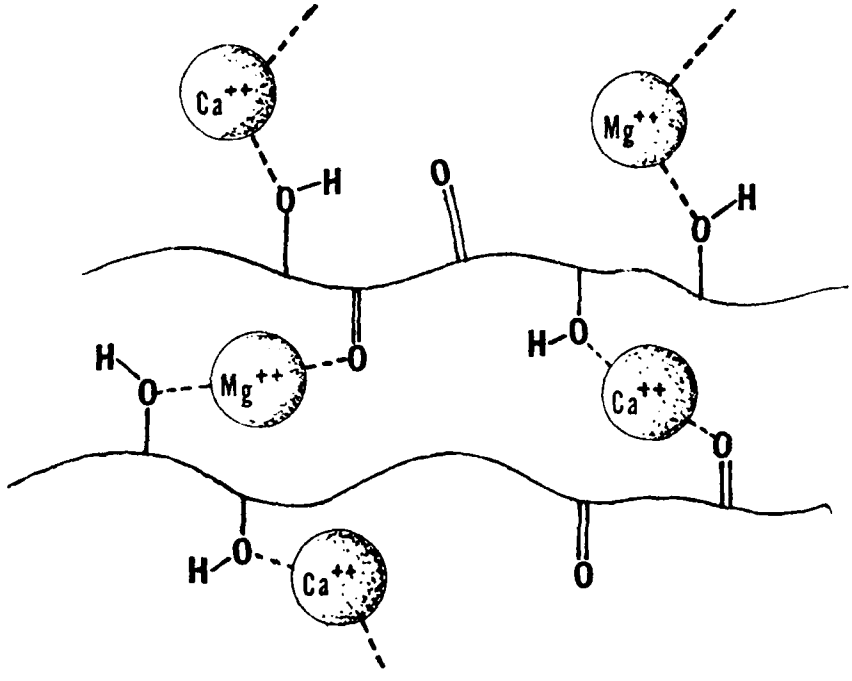

Figure 14. Hypothetical Role of Divalent Cations in Strengthening Biopolymer Matrix.

form extracellular products. Therefore, growth, maintenance and product formation are fundamental processes carried out by microbial cells in the presence of sufficient nutrients (Table 4). If nutrients are depleted, or toxic substances are present, death and lysis may occur.

Observed substrate removal rate, q_s, cannot be used to distinguish between growth, maintenance, product formation, and death but q_s is easy to measure. Trulear and Characklis (1980) have observed substrate removal rate in an AFR. The substrate removal rate, increases in proportion to biofilm thickness up to a critical thickness beyond which removal rate remains constant (Fig. 15). The critical, or "active", thickness is observed to increase with substrate concentration. This behavior is confirmed by other investigators (LaMotta, 1974; Kornegay and Andrews, 1967; Zelver, 1979) and is attributed to nutrient diffusional limitations within the biofilm. Once the biofilm thickness exceeds the depth of substrate (or oxygen) penetration into the biofilm (Fig. 16), the removal rate is unaffected by further biofilm accumulation. This diffusional limitation may weaken the biofilm matrix and lead to detachment.

If anaerobic conditions develop in the lower biofilm layer, the ubiquitous sulfate reducing bacteria may proliferate. Using the thermodynamically favorable energy potential between sulfate and lower oxidation states of suflur, these bacteria can oxidize organics in the absence of oxygen. In fact, in the presence of oxygen they exist in a dormant state. One of the unfavorable side effects of anaerobic bacterial growth is the production of acidic hydrogen sulfide and the corrosion of ferrous surfaces which it produces.

It seems clear from other data (Bryers, 1979) that product formation (primarily polysaccharide) is significant in the early stages of biofilm

Table 4. A matrix representation for the fundamental microbial rate processes.

FUNDAMENTAL PROCESS		REACTANTS → stoichiometry → PRODUCTS							
Process	Rate	Substrate s	Nutrient z	Electron Acceptor e	Biomass x_T	Biomass x_d	Product p_e	Product p_i	Metabolite a
Growth	μ	-	-	-	+		+	(+)	+
Maintenance									
exogenous	m	-	-	-			+		+
endogenous	k_e		+	-	-	(+)	+	-	+
Product Formation	k_p	-	-	-			+	+	+
Death									
loss of viability	k_d				-	+			
lysis	k_L	(+)	(+)		-	(+)	+		
OBSERVED RATE		q_s	q_z	q_e	μ_n		q_p		q_a

q = specific production or removal rate (t^{-1})

μ = specific growth rate or specific biomass production rate (t^{-1})

x_T = total biomass concentration (ML^{-3})

x_d = inert solids concentration (ML^{-3})

p_e = extracellular microbial product concentration (ML^{-3})

p_i = intracellular microbial product concentration (ML^{-3})

s = substrate concentration (ML^{-3})

z = nutrient concentration (ML^{-3})

e = electron acceptor concentration (ML^{-3})

μ_n = net solids production rate (t^{-1})

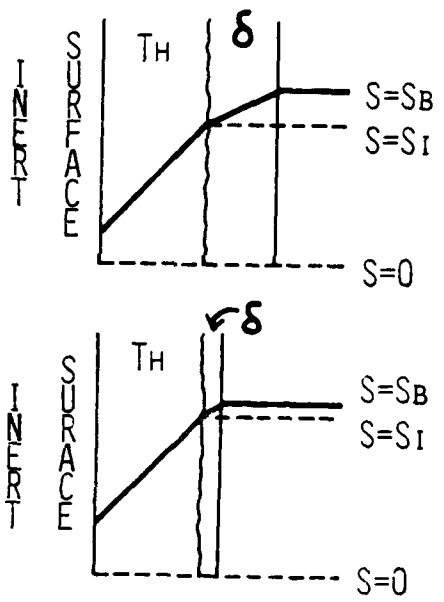

LIQUID PHASE RESISTANCES

Figure 15.

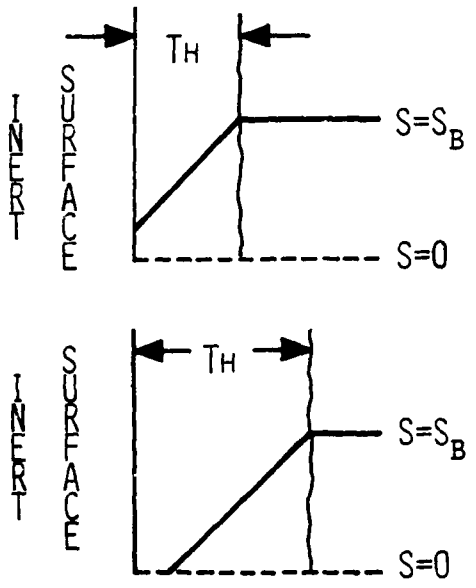

Figure 16. Diffusional Resistance in Biofilms.

formation. Maintenance requirements or biomass decay become important as the biofilm gets thicker and substrate does not entirely penetrate the biofilm. Evaluation of these other process rates is critical for determining stoichiometric coefficients and predicting biofilm development rates. Inorganic constituents in the biofilm may further complicate understanding of the processes occurring. It is difficult to specifically identify fouling deposit compostion in real systems. Biofouling may be intimately associated with precipitation/crystallization processes and the interaction may produce a deposit with characteristics significantly different from either biofilm or inorganic deposits. Consequently, one of our goals is to understand the associations of inorganic precipitates, bacteria, and sediment in a deposit at at a heated wall.

Factors which affect microbial growth also influence scaling processes:

1. Increasing transport from bulk fluid to the fouling surface will increase scaling rate.
2. Surface properties such as microroughness or surface charge will affect scaling rate by providing a driving force for nucleation.
3. The degreee of localized supersaturation of scaling ions affect scaling rate just as nutrient concentration in the bulk fluid affects bacterial growth rate.

Supersaturation can occur, not only from temperature or pressure changes, but also from thermodynamic instabilities generated in regions bordering the microscopic crevices and cracks in a surface.

In general, scale formation requires supersaturation, nucleation, and sufficient contact time for depostiion.

Detachment of Biofilm: As the biofilm grows thicker, the fluid shear stress at the biofilm interface generally increases. Also, as biofilms grow thicker, the potential for substrate, oxygen or nutrient limitation in

the deeper portions is great. These limitations may weaken the biofilm matrix and cause detachment (Figure 17). Trulear and Characklis (1979) report that the biofilm detachment rate increases with increasing biofilm mass (Figure 18). Trulear (1979) also reports that detachment rate increases with fluid shear stress (Figre 19).

Influence of Fluid Velocity

The substrate removal rate is dependent on fluid velocity (Fig. 20). At low fluid velocities, a relatively thick mass transfer boundary layer (δ_m) can cause a liquid phase diffusional resistance which decreases substrate concentration at the liquid-biofilm interface and thereby decreases substrate removal rate (Fig. 15).

The effect of fluid velocity on the plateau (or steady state) biofilm thickness is illustrated in Figure 21 for various substrate loadings. At high substrate loadings, increasing fluid velocity increases biofilm detachment rate which minimizes the plateau biofilm thickness. However, at low substrate loadings, fluid velocity seems to have no measureable effect on the plateau thickness. Trulear and Characklis (1979) have demonstrated that plateau biofilm mass exhibits a maximum when fluid velocity is increased. At low fluid velocity, mass transfer limits the rate of biofilm production. Therefore, increasing fluid velocity increases substrate flux into the biofilm and net biofilm development rate increases. As fluid velocity continues to increase, biofilm detachment rate becomes the dominant process and net biofilm development begins to decrease.

Influence of Temperature on Biofilm Processes

Temperature, like fluid velocity, is an important environmental factor influencing biofilm processes. Microbial growth is the net result of a complex sequence of enzymatic reactions whose individual rates are related to temperature. However, growth and metabolism are not the only temperature-dependent processes contributing to biofilm development. Temperature also affects mass

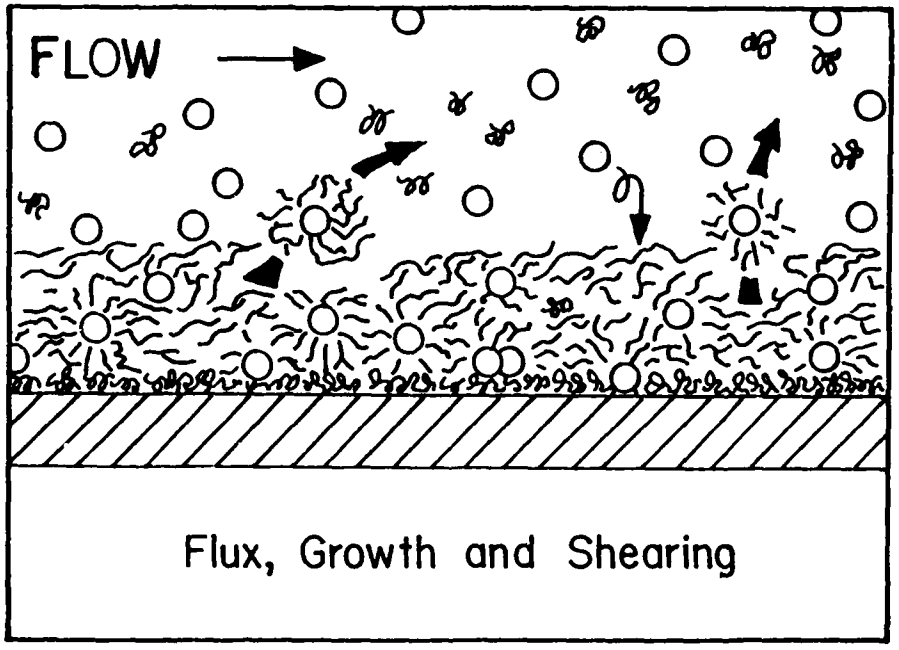

Figure 17. Factors Affecting Biofilm Detachment.

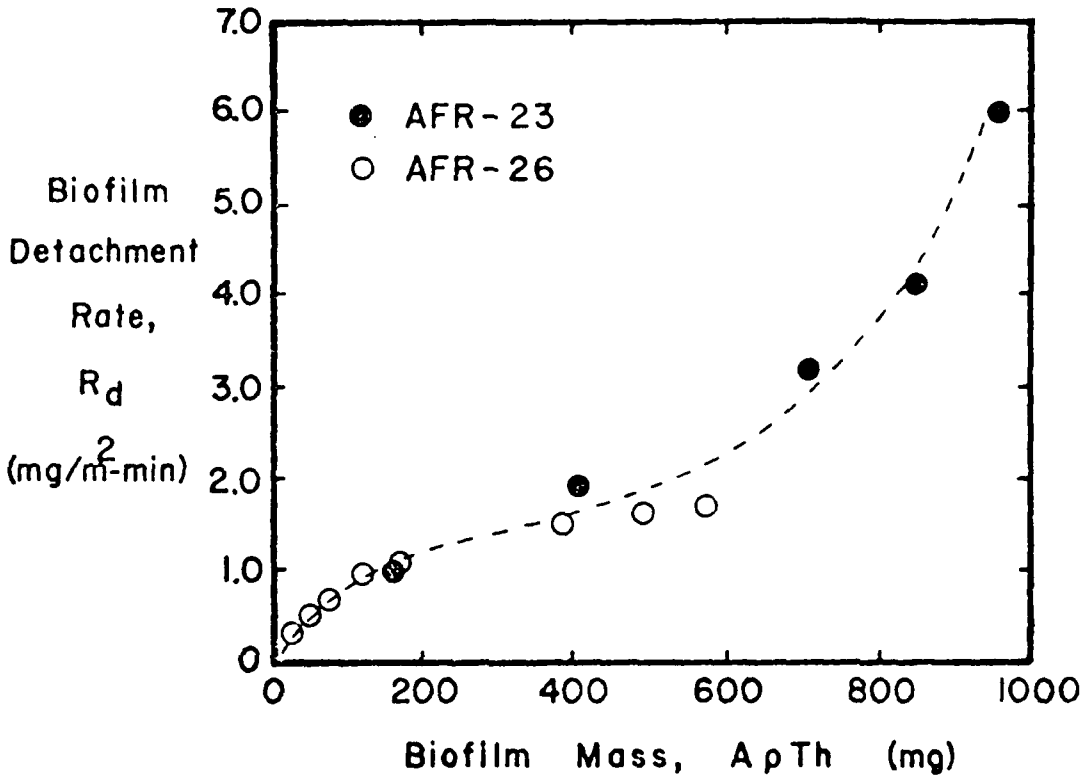

Figure 18. Relationship Between Biofilm Detachment Rate and Biofilm Mass.

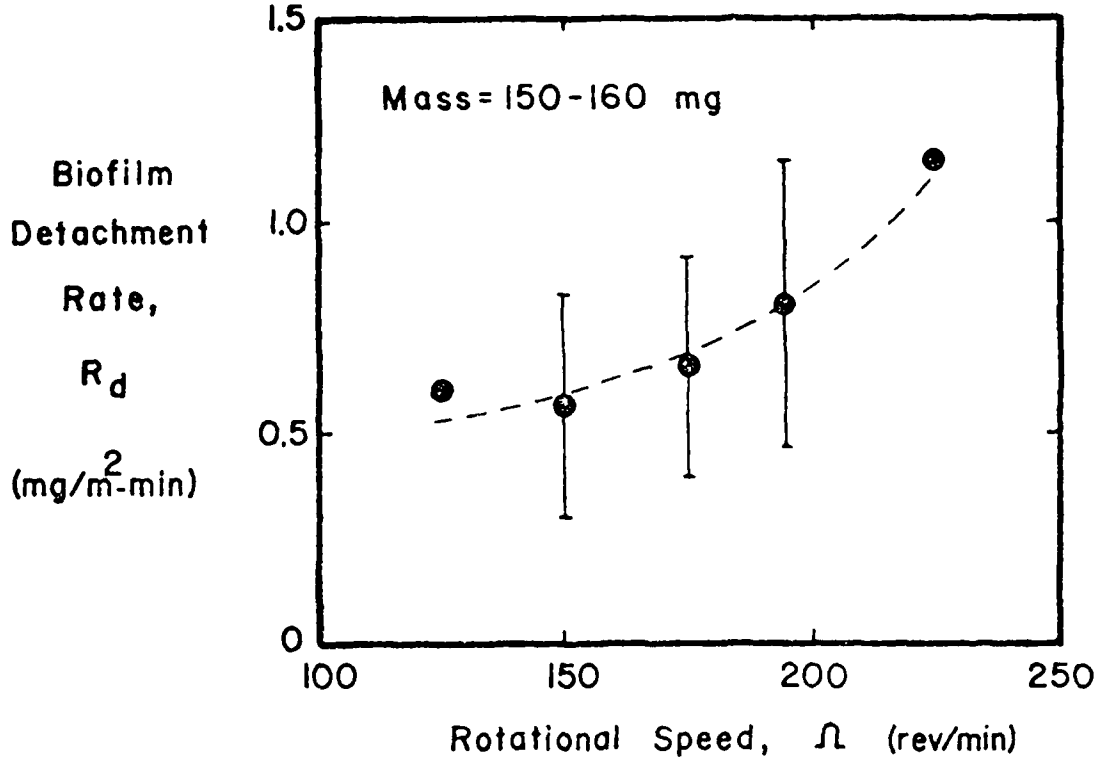

Figure 19. Dependancy of Biofilm Detachment Rate with Rotational Speed.

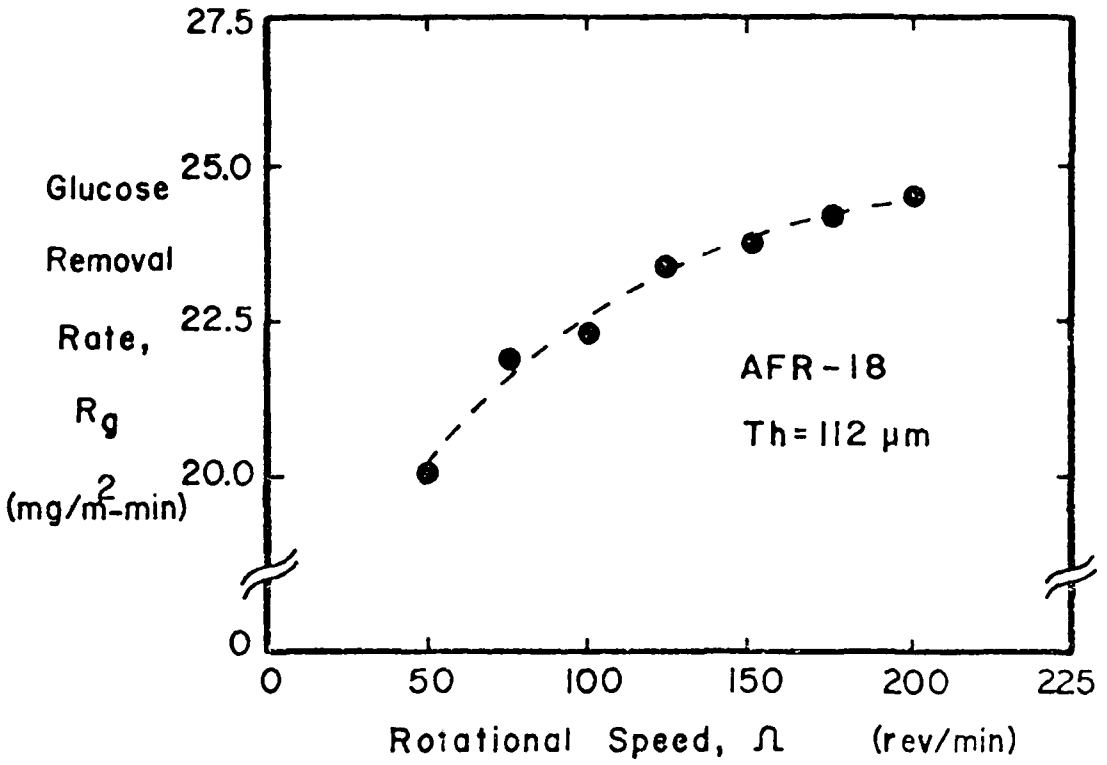

Figure 20. Dependancy of Substrate Removal and Fluid Velocity.

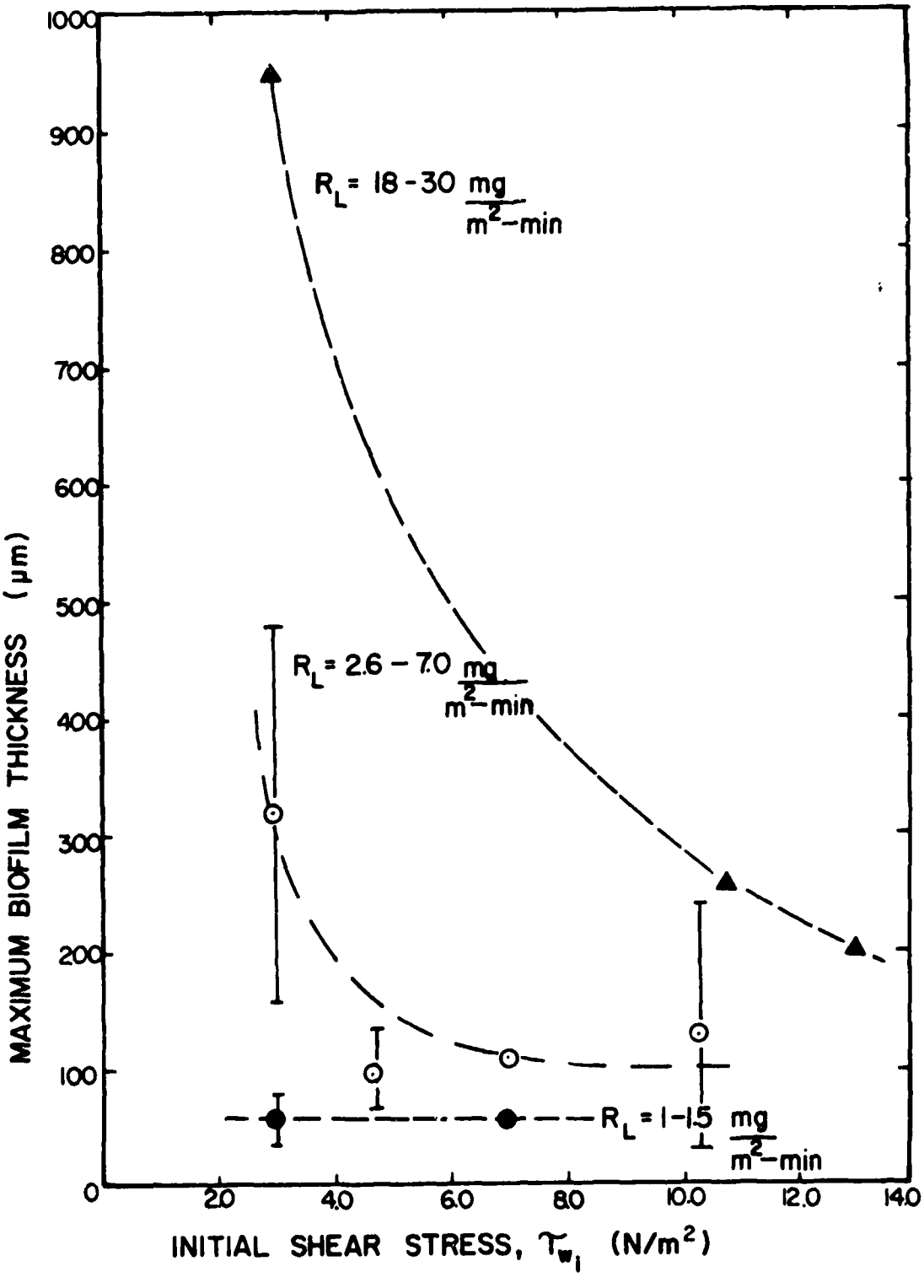

Figure 21. Maximum Biofilm Thickness as a Function of Initial Shear Stress.

transfer rate of nutrients from the bulk water to biofilms and diffusion rate of nutrients within biofilms. Diffusion rate of toxic compounds within biofilms may determine their effectiveness in fouling control. Temperature also significantly affects biofilm properties resulting in modified transport coefficients for mass, heat and momentum within the biofilm.

The induction phase of biofilm development is significantly altered by temperature (Figure 22). The shortest induction phase was observed in temperature range of optimum growth for the microbial population used in these experiments. Figure 23 demonstrates the influence of temperature on biofilm development rate as measured by biofilm thickness. The effect on friction factor is not so evident (Figure 24). Temperature also influences biofilm properties such as density (Figure 25). A more comprehensive discussion of temperature effects can be found elsewhere (Characklis, 1980; Stathopoulos, 1981).

In summary, biofilm accumulation rate and many related processes increase with temperature up to a critical temperature at which a maximum rate is reached (Figre 26). In experiments thus far, the critical temperature has always coincided with the optimum temperature for growth of microorganisms.

Influence of Nutrient Concentration

When the concentration of organic nutrients in the bulk water increases, the effect on the biofilm is to:

(1) increase the rate and extent of accumulation

(2) increase the density

(3) change the morphology or dominant species

Fluid velocity and nutrient concentration in the bulk water influence transport rate of nutrients to the biofilm surface. Transport of nutrients and oxygen is ultimately the cause of the affects listed above.

Trulear and Characklis (1980) used glucose as the nutrient for biofilm growth. Their maximum net biofilm accumulation rate, $\rho \left(\frac{dTh}{dt}\right)_{max}$, increased

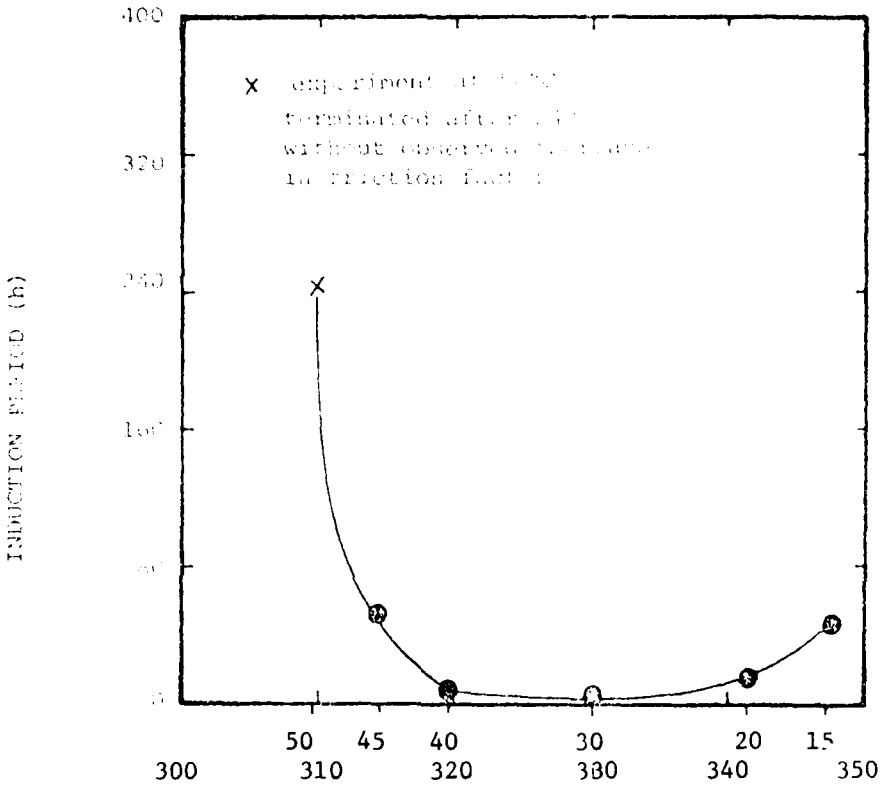

Figure 22. Influence of temperature on the induction period as determined by increasing in friction factor.

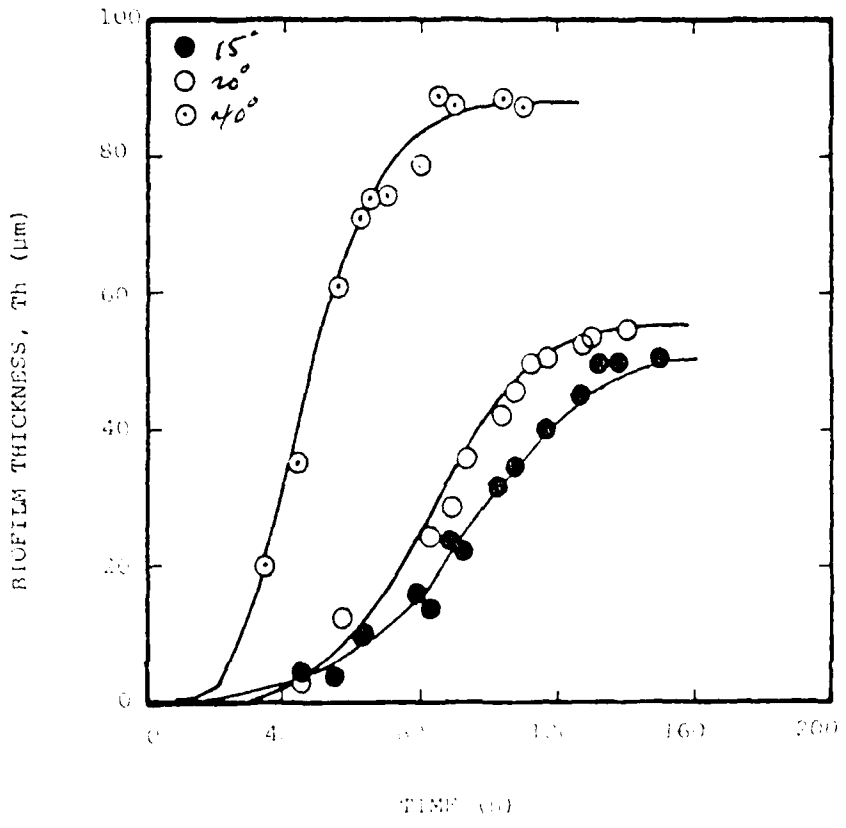

Figure 23. The change in biofilm thickness during experiments at 15, 20 and 40°C. The lines represent time smoothed data.

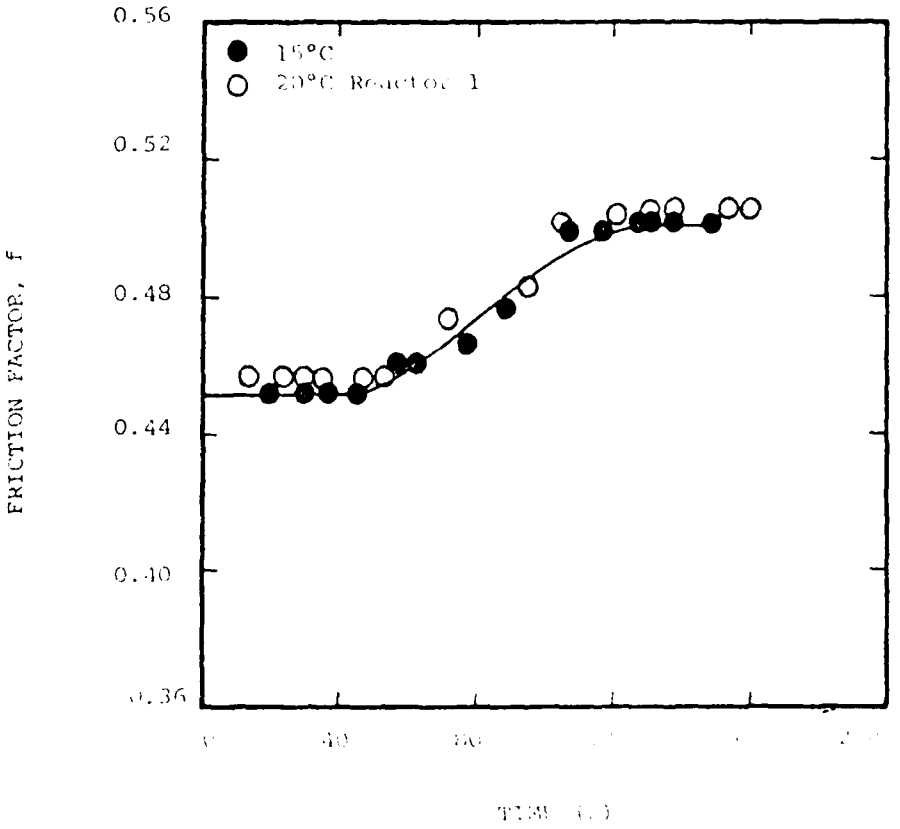

Figure 24. The change in friction factor during experiments at 15 and 20°C. The line reflects time-smoothing of the data.

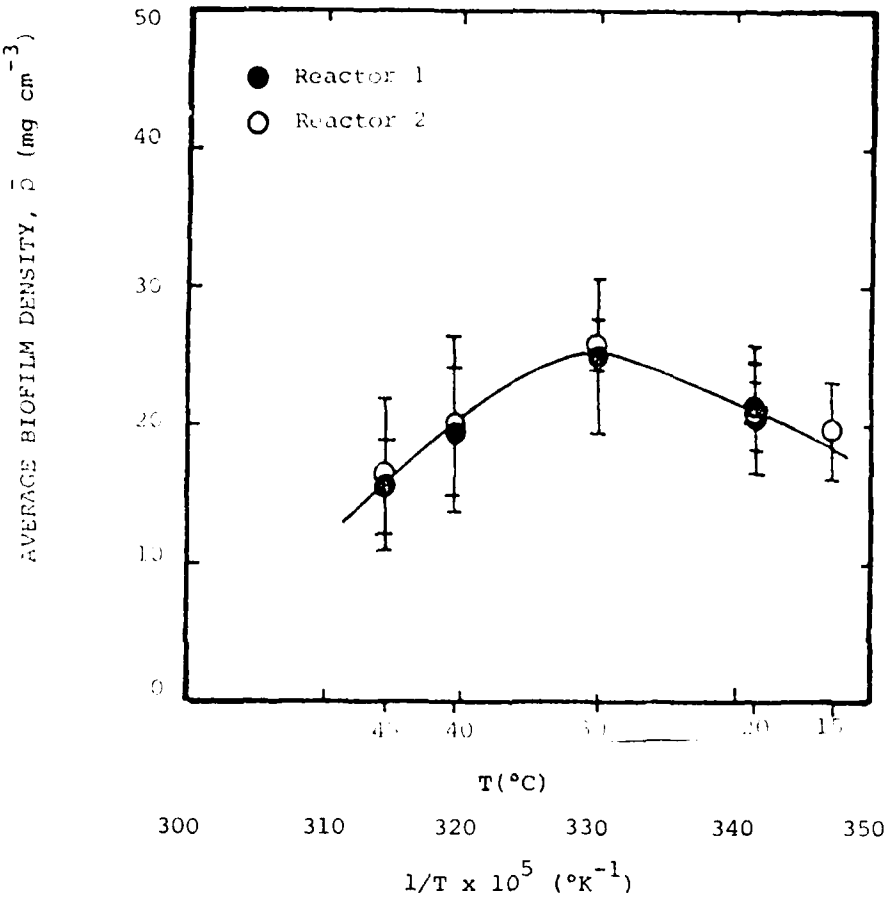

Figure 25. Effect of temperature on average biofilm density.

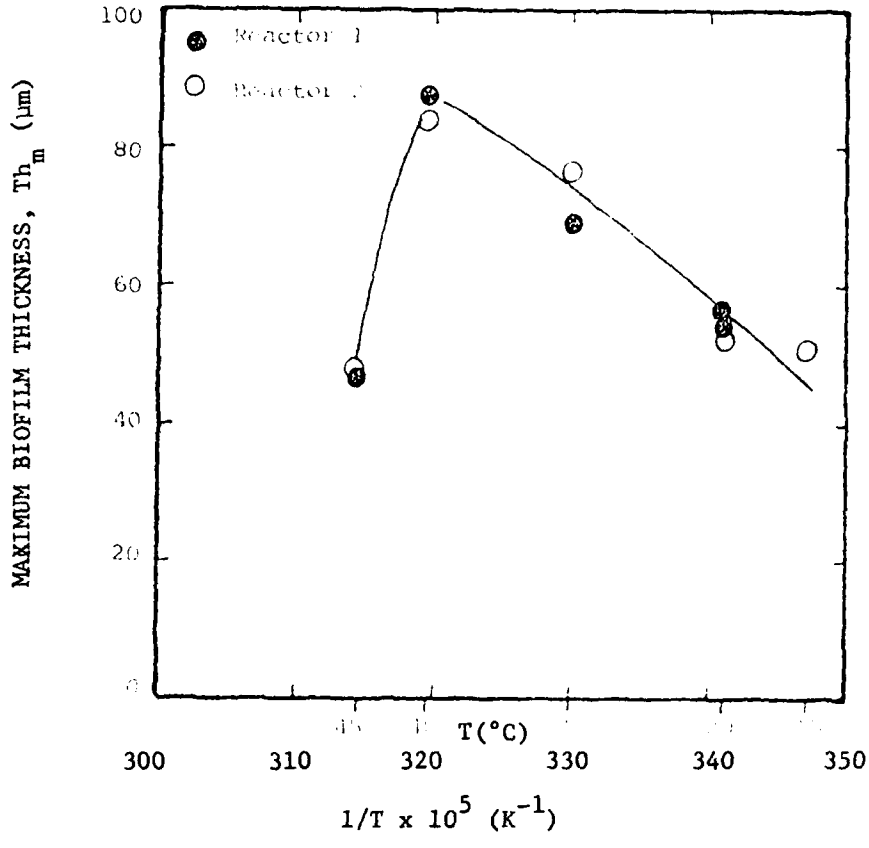

Figure 26. Effect of temperature on the maximum biofilm thickness.

with glucose loading (Figure 27) due to an increased glucose concentration in the reactor. The relation was not linear and the data suggest $\rho\ (\frac{dTh}{dt})_{max}$ will reach a maximum asymptotic value at higher glucose loading rates.

The plateau value for attached biofilm mass, $\rho\ Th_p$, increased with glucose loading (Figure 28), however, the rate of increase diminished significantly once the glucose loading rate approached 10 mg/m^2-min. This behavior may have been due to a limitation in oxygen at the higher glucose loading rates.

The plateau biofilm thickness, Th_p, decreased with glucose laoding (Figure 29) although $\rho\ Th_p$ increased. This was due to an increase in biofilm density with glucose loading rate (Figure 30). Zelver (1979), using a tubular reactor system, also observed an increase in biofilm density with glucose loading. However, in Zelver's experiments, both plateau biofilm thickness and mass increased with glucose loading.

Biofilm morphology was observed microscopically during biofilm thickness measurements. Largely filamentous biofilms were observed in experiments with low glucose loading rates. With increasing glucose loading the biofilm structure shifted to a non-filamentous matrix dominated by dense patches of microbial colonies.

The observed trends in biofilm density and morphology suggest that the density of the biofilm decreases with increasing filamentous structure.

Photomicrographs of the filamentous biofilms observed by Trulear and Characklis closely resemble photographs of attached Sphaerotilus growth (Dias et al, 1968). Furthermore, Dias et al. report that low influent glucose favored greater numbers of filamentous Sphaerotilus in the mixed population slimes developed.

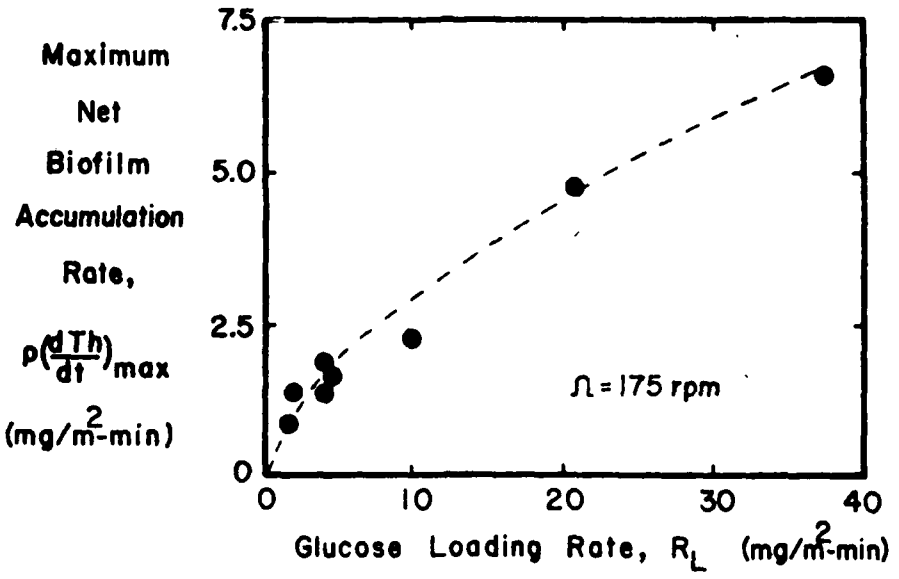

Figure 27. Change in the Maximum Net Biofilm Accumulation Rate with Glucose Loading Rate.

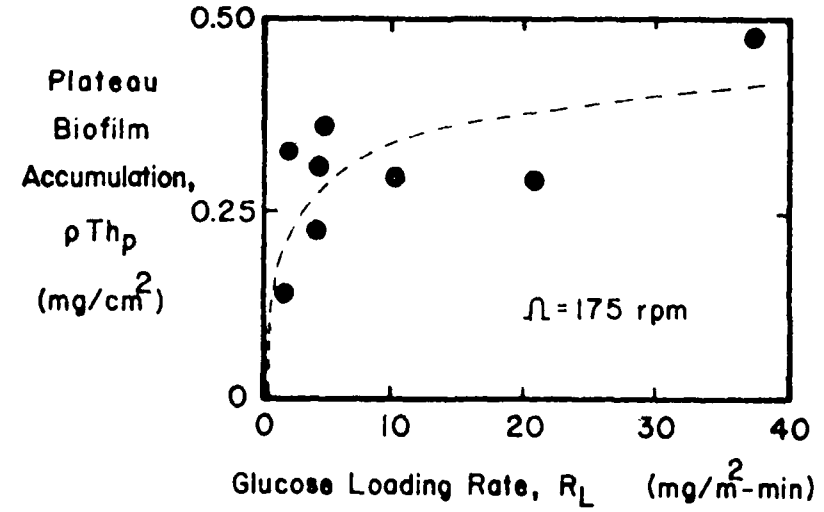

Figure 28. Change in Plateau Biofilm Accumulation with Glucose Loading Rate.

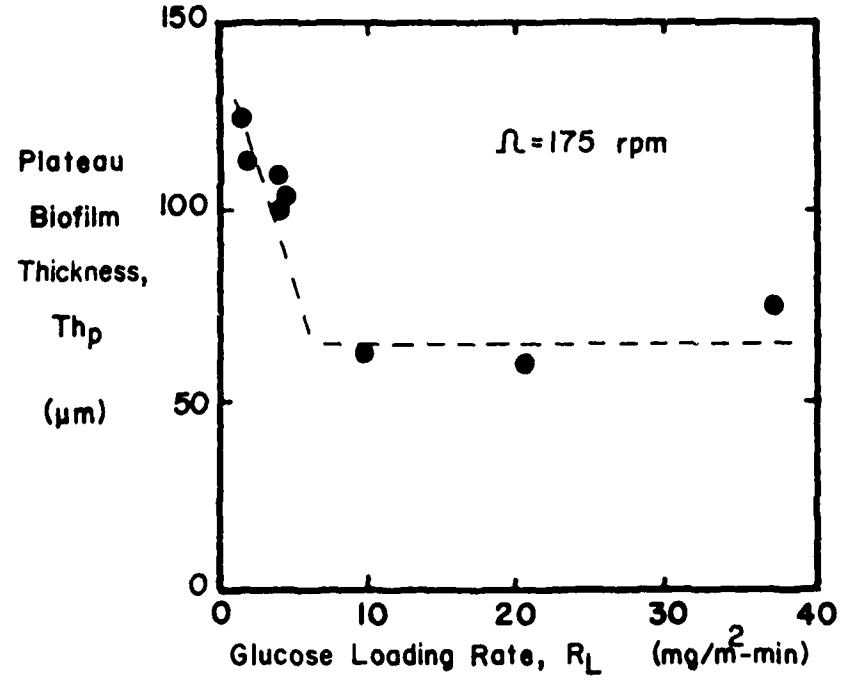

Figure 29. Change in Plateau Biofilm Thickness with Glucose Loading Rate.

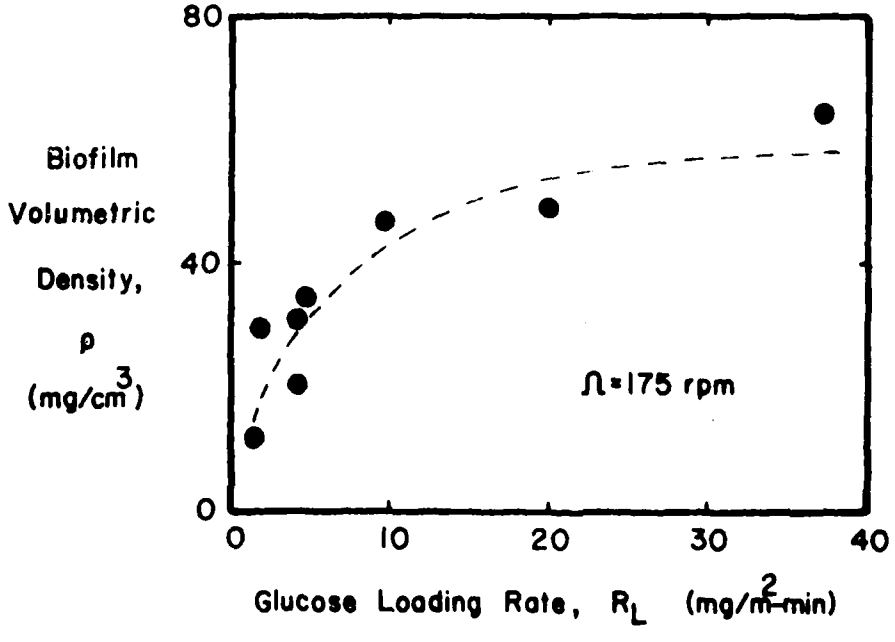

Figure 30. Relation Between Biofilm Volumetric Density and Glucose Loading Rate.

The results obtained concerning biofilm density and morphology suggest that different microbial species are selected for preferentially in the biofilm depending on the level of influent glucose. At the low glucose loading rates, filamentous organisms would have a physiological advantage over other morphological forms since they could protrude into the bulk fluid and "see" more glucose.

The concentration of inorganic species in the bulk water may also affect the physical and biological structure of biofilms. For example, nitrogen limitation can result in production of copious quantities of microbial extracellular polysaccharides. Calcium, magnesium and iron affect intermolecular bonding of biofilm polymers whcih are primarily responsible for the structural integrity of the deposit. In fact, EDTA is effective, in detaching biofilm (Characklis, 1980). In heat exchangers, corrosion products and inert suspended solids can adsorb to the biofilm matrix and influence its chemical composition. Table 5 reports the range of inorganic composition observed in selected biofilms.

Mature Biofilm Experiments

Experiments have been conducted in the AFR system using monoculture inocula of either Spherotilus natans or Pseudomonas aeruginosa. The experiments were initiated by first developing steady state chemostat cultures of the desired organism and then pumping portions of the chemostat cultures into each of the two AFR's for a period of 12 hours. This procedure provides a defined microbial inoculum for initial AFR surface colonization. At the end of the initial 12 hour period, AFR dilution water and nutrient feed were turned on for the duration of each experiment. Dilution water flow rate and nutrient feed concentation provided an influent glucose concentration of 5 mg/l and an AFR hydraulic residence time of 10 minutes. The remainder of this section will summarize and compare the results from two

Table 5. Chemical properties of biofilms obtained from fouled surfaces experiencing excessive frictional losses (after Characklis [6]).

	REFERENCE				
	[1]	[2]	[2]	[3]	[4]
Water	87	85.6	90	95	96
Volatile Fraction	2.5	2.7	1.9	2.4	3.2
Fixed Fraction	10.5	11.7	8.1	2.6	0.8
Si (as percent fixed fraction)		7.0	11.8	12.5	
Fe		18.5	7.9	1.4	
Al		7.5		3.9	
Ca		1.0	5.6		
Mg		2.5		3.2	
Mn		59.5	56.3	4.9	

1. Pollard & House, 1959.
2. Minkus, 1954.
3. Arnold, 1936.
4. Characklis, 1980.

AFR experiments, Experiment 3 which was inoculated with S. natans and Experiment 4 which was incoulated with P. aeruginosa. Biofilm Thickness: the S. natans biofilm reached a steady state biofilm thickness which was approximately 3 times thicker than the P.aeruginosa steady state biofilm thickness (Fig. 31). Also the S. natan biofilm reached steady state thickness considerably sooner than the P. aeruginosa biofilm.

Torque (Frictional resistance) : The S. natans biofilm caused a significant increase in the torque required to rotate the AFR inner cylinder (Fig. 32). Conversely the P. aeruginosa biofilm caused no increase in torque (not shown). Previous results reported by Trulear and Characklis (1980) suggest that the behavior is related to the filamentous structure of Sphaerotilus-dominated biofilms.

Partitioning of organic carbon in the biofilm: Results indicate that biofilms were composed primarily of extracellularrganic carbon (polymeric material). The S. natans biofilm was approximately 80% extracellular carbon and 20% cellular carbon whereas the P. aeruginosa biofilm contained approximately 90% extracellular carbon and 10% cellular carbon (Fig. 33). Comparing the extracellular polymer fractions of each biofilm, the P. aeruginosa extracellular carbon was approximately five times denser than the S. natans extracellular carbon. Conversely, the cellular carbon fractions of each biofilm were approximately the same density (Fig. 34).

Mathematical Model for Mature Biofilm Accumulation

A general mathematical model for microbial processes in a continuous stirred tank reactor (CSTR), based on material balances, is presented. This model considers microbial activity in the bulk fluid as well as the reactor surfaces. Results from the AFR and TFR systems can be interpreted using this model since both are operated as CSTR's. This model takes into account most of the variables discussed such as fluid

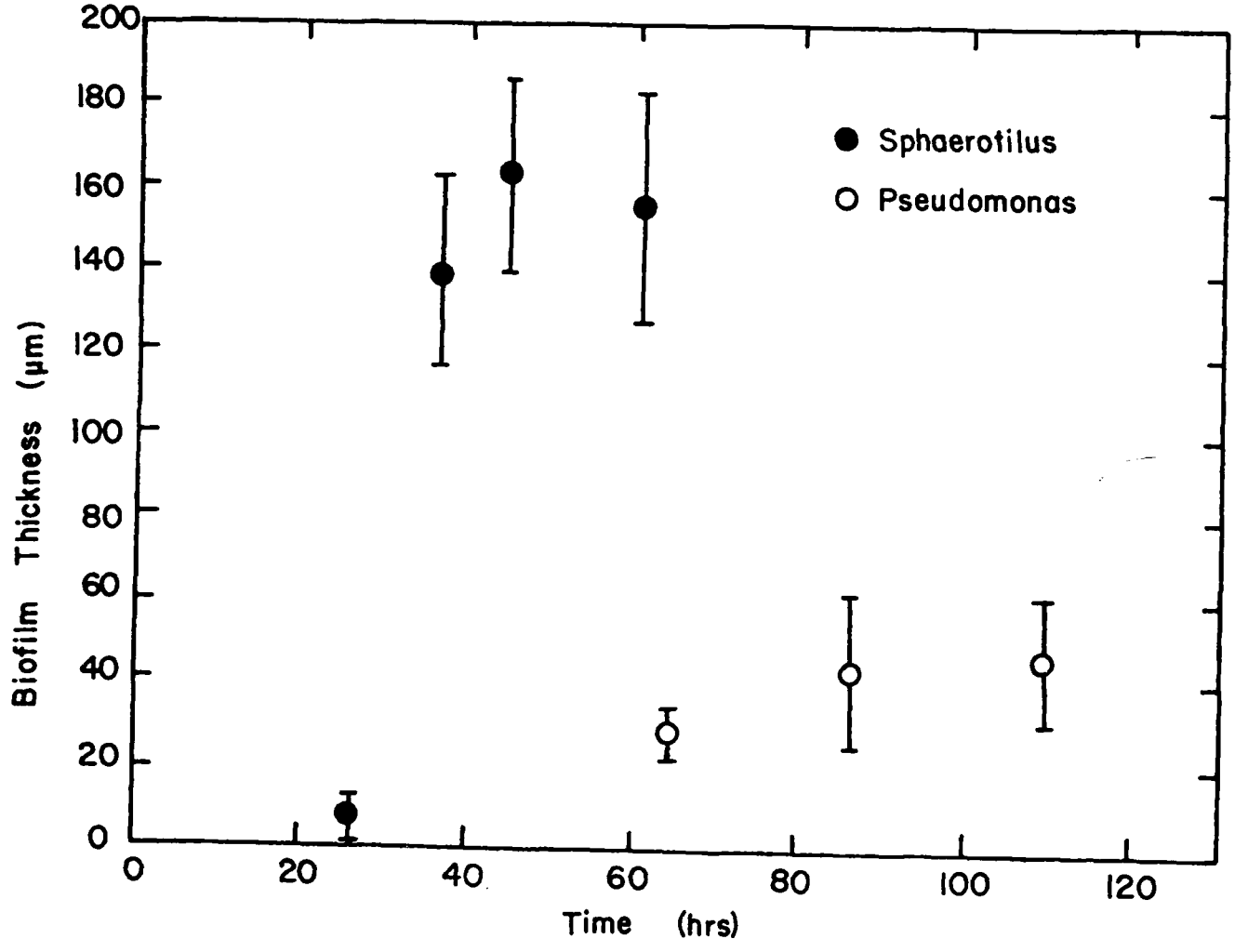

Figure 31. Biofilm thickness of S. natans vs Ps. aeruginosa.

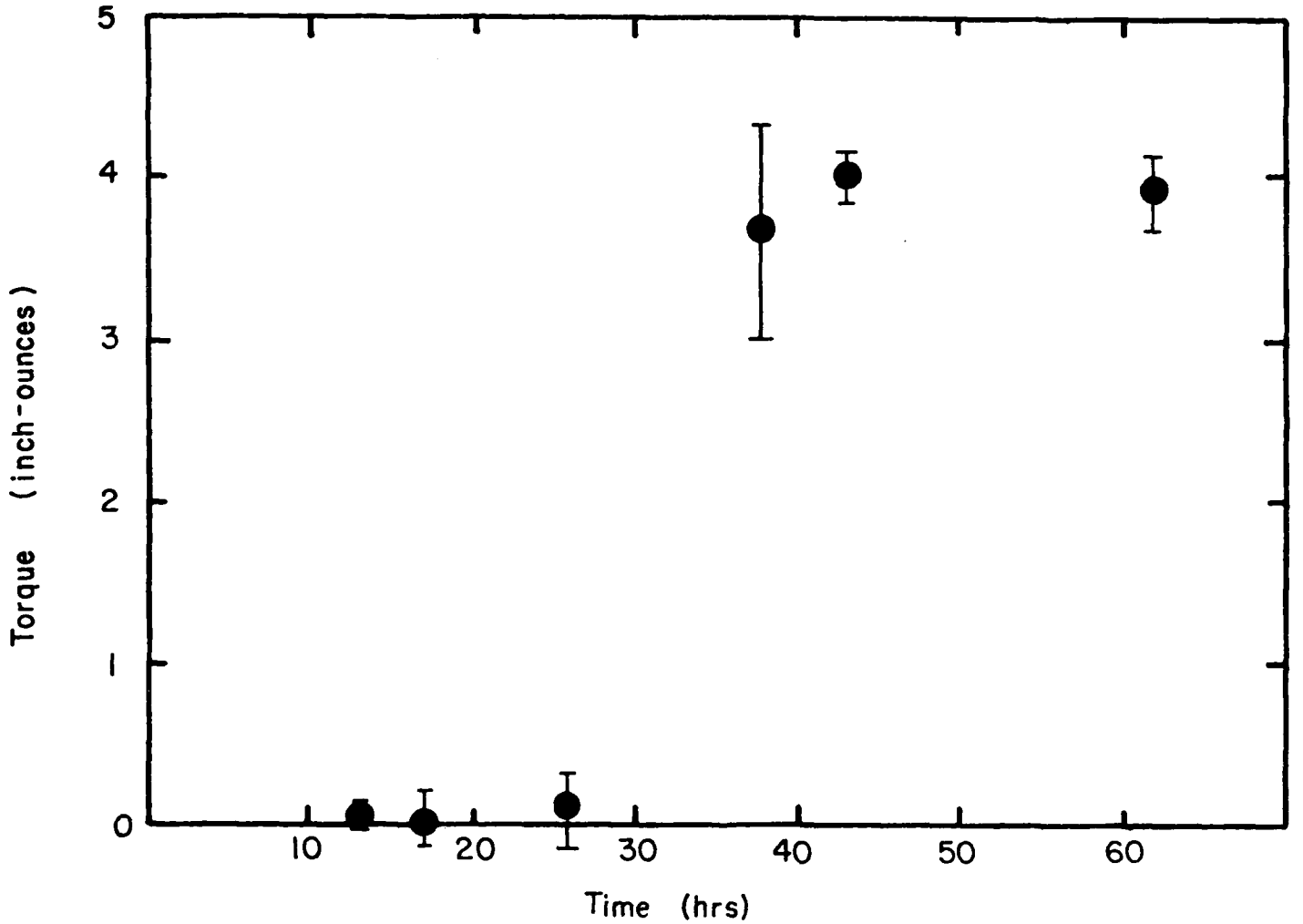

Figure 32. Average Torque increase during growth of S. natans.

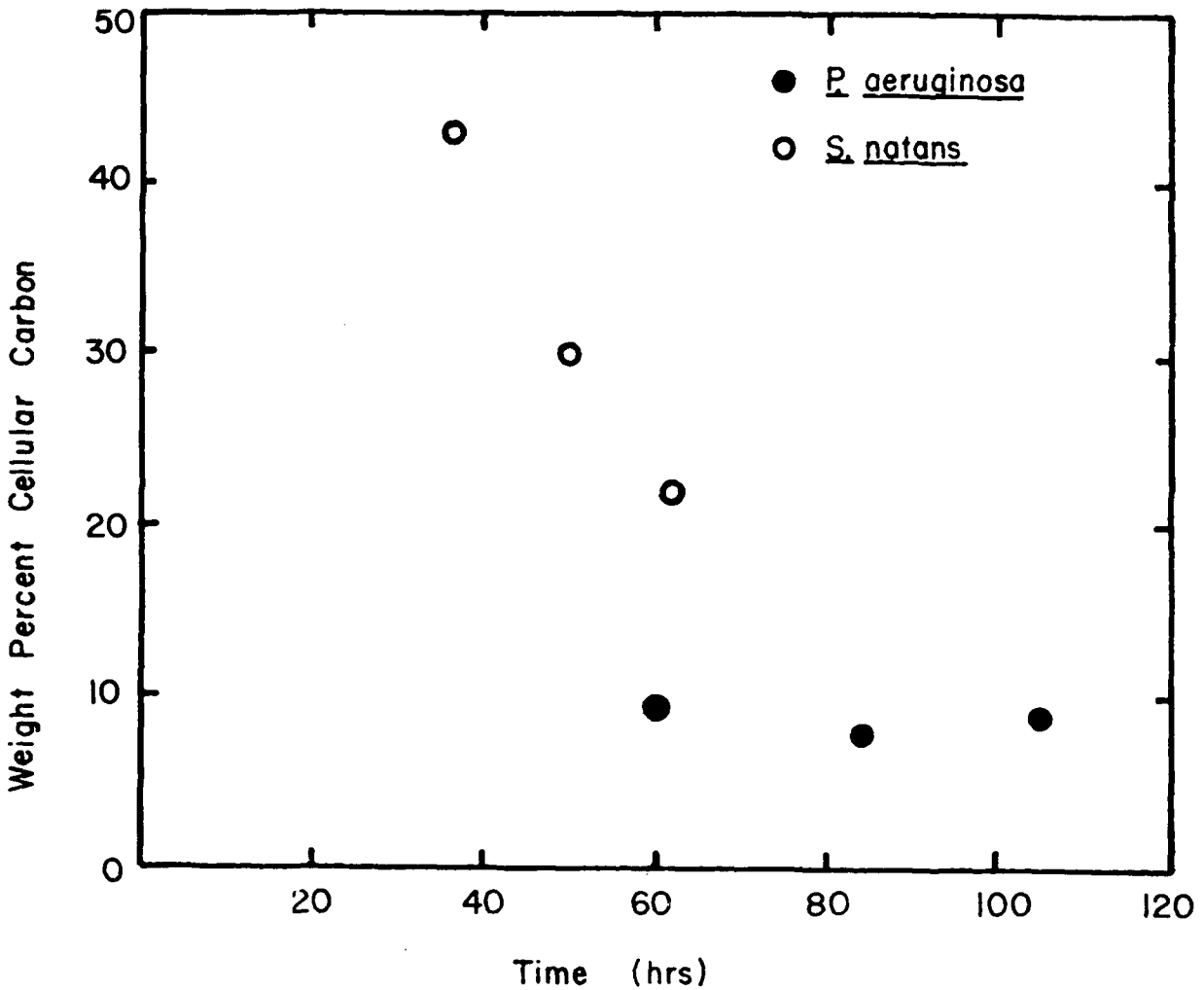

Figure 33. Fraction of cellular carbon in Biofilms during accumulation.

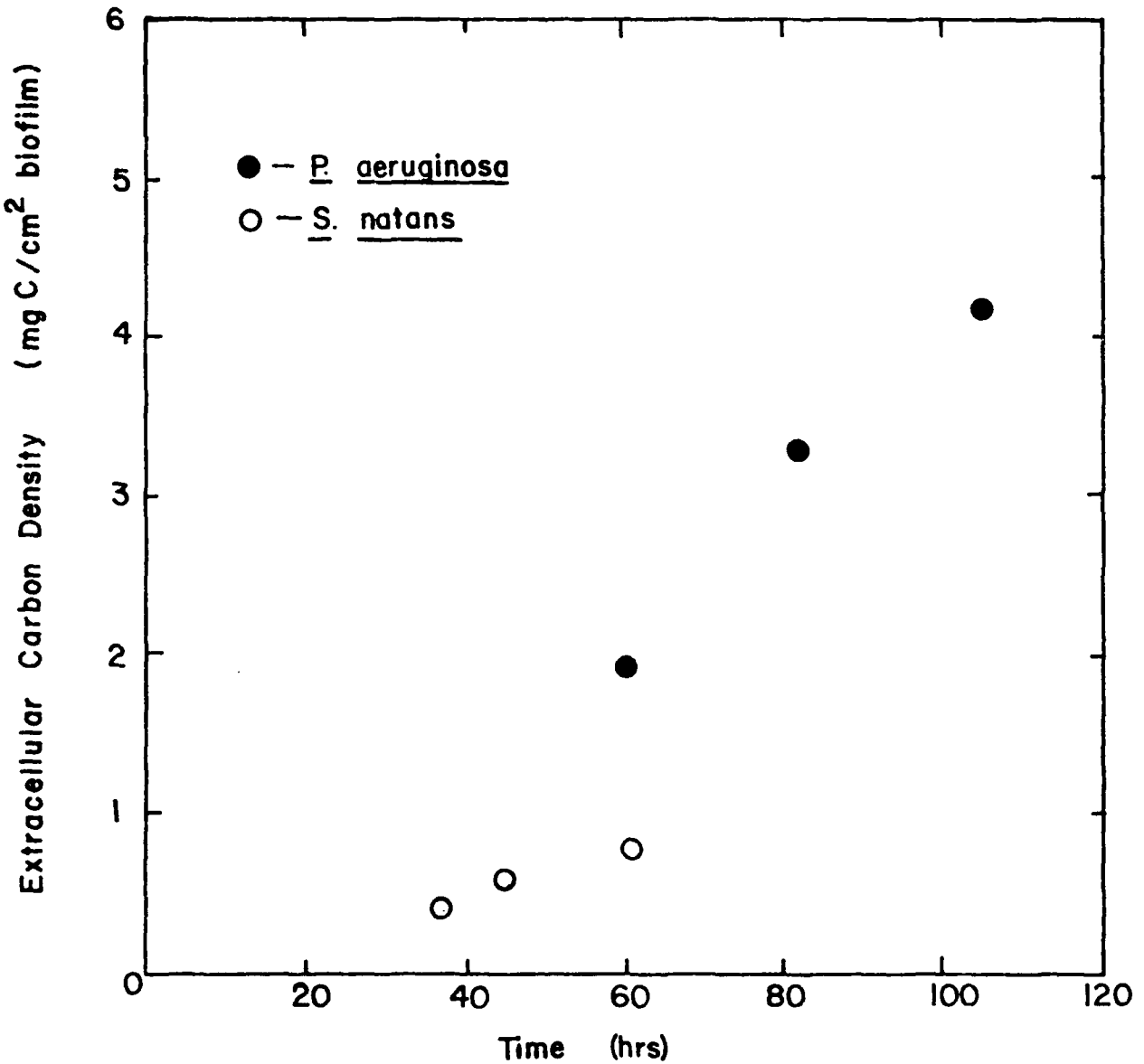

Figure 34. Extracellular carbon density during Biofilm accumulation.

velocity, substrate concentration, biomass concentration and a host of parameters characteristic of the system. Temperature effects appear in every kinetic coefficient of the model. Stathopoulos (1981) has measured the influence of temperature on μ_m, K_s, Y_B, R_D, R_E and m.

This model assumes no structure for the biofilm. This simplifies mathematical representation of the system since only single parameters are needed for each biofilm property. As long as oxygen and nutrients fully penetrate the biofilm this is a reasonable assumption.

- Glucose Carbon Material Balance

$$V\frac{ds}{dt} = F(s_i - s) - \alpha R_g A - (1-\alpha)R_g A - \frac{\mu x V}{Y_x} - \frac{r_p(p_x + p_p)V}{Y_p}$$

net rate of glucose accumulation	net rate of glucose input by flow	rate of glucose removal for biofilm cellular reproduction	rate of glucose removal for biofilm polymer production	rate of glucose removal for suspended cellular repeoduction	rate of glucose removal for suspended polymer production

- Total Biomass Carbon Material Balance

$$M_T = (x + p_x + p_s) V + (x_b + p_b) A Th$$

Total system biomass	liquid phase biomass	biofilm biomass

The change with time in total system biomass is as follows:

$$\frac{dM_T}{dt} = V\frac{dx}{dt} + V\frac{d(p_x + p_s)}{dt} + A Th \frac{dx_b}{dt} + A Th \frac{dp_b}{dt} + A(x_b + p_b)\frac{dTh}{dt}$$

however $(x_b + p_b) = \rho$ = biofilm carbon density

substituting,

$$\frac{dM_T}{dt} = V\frac{dx}{dt} + V\frac{d(p_x + p_s)}{dt} + A Th \frac{dx_b}{dt} + A Th \frac{dp_b}{dt} + A \rho \frac{dTh}{dt}$$

- Suspended Cellular Carbon Material Balance

$$V \frac{dx}{dt} = - F x + \mu x V + R_{d_x} A$$

net rate of suspended cellular accumulation	rate of suspended cellular output by flow	rate of suspended cellular reproduction	rate of biofilm cellular detachment

- Suspended Polymer Carbon Material Balance

$$V \frac{d(p_x - p_s)}{dt} = - F (p_x + p_s) + r_p (p_x + p_s) + R_{d_p} A$$

net rate of suspended polymer accumulation	rate of suspended polymer output by flow	rate of suspended polymer production	rate of biofilm polymer detachment

- Biofilm Cellular Carbon Material Balance

$$A \, Th \frac{dx_b}{dt} = \alpha R_g A Y_{x_b} - R_{d_x} A$$

net rate of biofilm cellular accumulation	rate of biofilm cellular reproduction	rate of biofilm cellular detachment

- Biofilm Polymer Carbon Material Balance

$$A \, Th \frac{dp_b}{dt} = (1 - \alpha) R_g A Y_{p_b} - R_{d_p} A$$

net rate of biofilm polymer accumulation	rate of biofilm polymer production	rate of biofilm polymer detachment

- Total Biofilm Carbon Material Balance

$$A \rho \frac{dTh}{dt} = R_g A Y_{bio} - R_{d_{bio}} A$$

net rate of total biofilm accumulation	rate of total biofilm production	rate of total biofilm detachment

- Biofilm Glucose Removal Condition

$$(\alpha\ R_g A) + (1 - \alpha)\ R_g A = R_g A$$

- Biofilm Detachment Condition

$$R_{d_{bio}} = R_{d_x} + R_{s_p}$$

Hence the system is described by 8 independent equations containing 8 unknown quantities (α, R_g, R_{d_x}, R_{d_p}, Y_{x_b}, Y_{b_p}, Y_{bio}, $R_{d_{bio}}$).

FOULING DEPOSITS AND ENERGY LOSSES

Fouling deposits can cause energy losses in water transmission lines and heat exchangers in two ways:

1. Fluid frictional resistance
2. Heat transfer resistance

Frictional Resistance

Increase in fluid frictional resistance due to biofilm accumulation when flow rate is maintained constant causes an increase in pressure drop and power requirements for pumping. Conversely, if pressure drop is held constant, flow capacity is reduced. In systems where scale thickness is comparable to that of typical biofilms, frictional resistance is usually dramatically less than that due to biofilms. This implies that the effective roughness for scale is significantly less than that for biofilms.

Frictional resistance can be represented by a dimensionless friction factor given by the following equation:

$$f = 2.0 \frac{d}{L} \frac{\Delta p}{\rho_f v_m^2}$$

The change in friction factor and biofilm thickness with time is shown in Fig. 35 for a laboratory tubular reactor. Dehart (1979) has observed similar behavior in a tubular reactor in the field.

The friction factor is related to the Reynolds number and the equivalent sand roughness k_s through the empirical Colebrook-White relation. This equation correlates friction factor to Reynolds number of various "Commercially rough" pipes throughout the hydraulically smooth, transition, and fully rough regimes. The Colebrook-White equation, solved for the equivalent sand roughness k_s yields

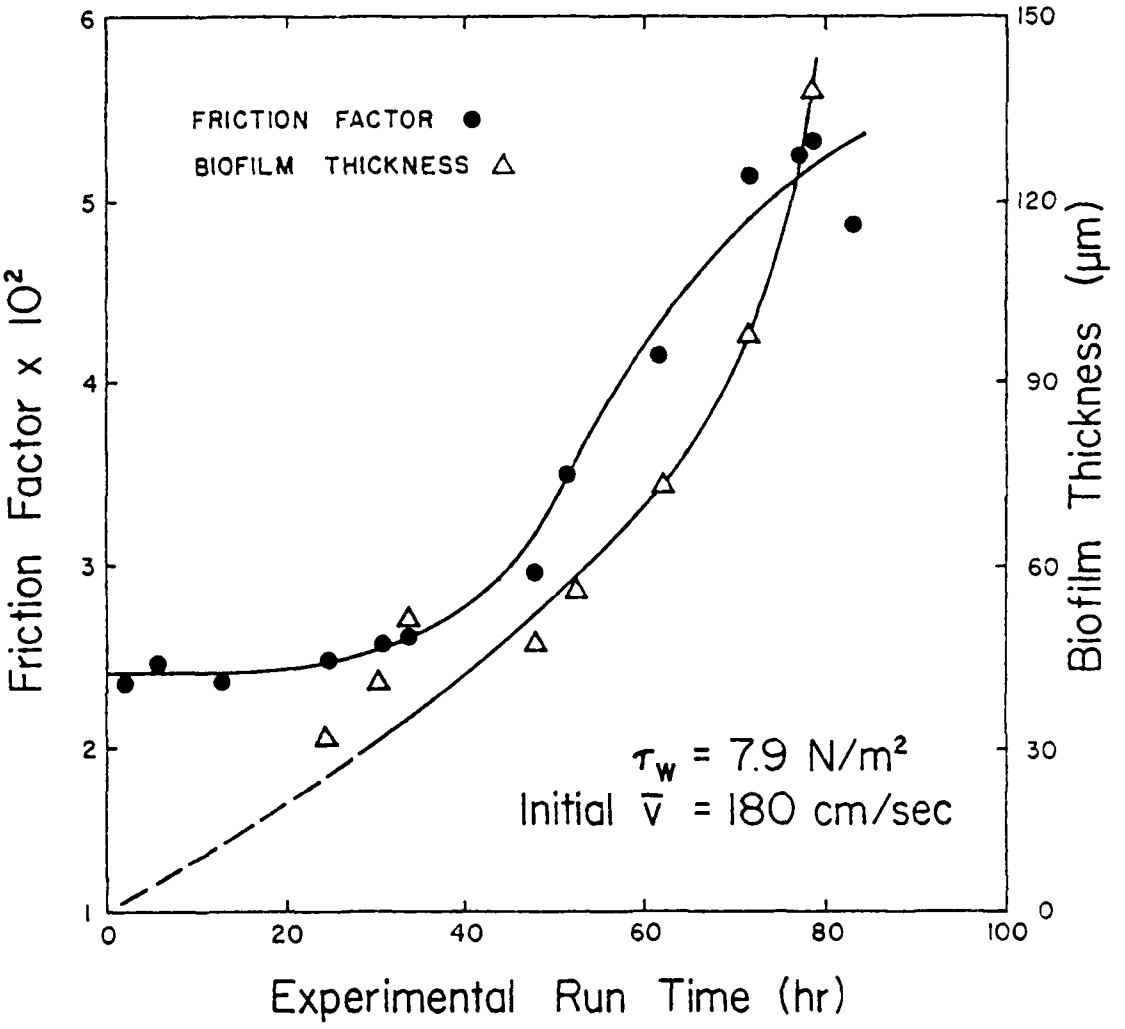

FIGURE 35. CHANGE IN FRICTION FACTOR AND BIOFILM THICKNESS DURING A TYPICAL EXPERIMENT.

$$k_s = \frac{d}{2}\ 10^{(0.87 - 0.50f^{-1/2})} - \frac{18.70}{Re\ f^{1/2}}$$

This expression can be used to compute an equivalent sand roughness for the biofilm from a measurement of the flow rate and pressure drop. Figure 36 indicates the progression of k_s with time and Figure 37 presents the change in k_s with biofilm thickness for the range of shear stress investigated by Zelver (1979).

Determination of the flow regime (smooth, transitional or fully rough depends on the magnitude of k_s relative to the size of the viscous sublayer (δ_1):

$$\delta_1 = \frac{10d}{Re}\ \left(\frac{f}{2}\right)^{-0.5}$$

More specifically, when $k_s < \delta_1$, the pipe is considered hydraulically smooth; when $14\ \delta_1 > k_s > \delta_1$ the flow is in the transitional regime; when $k_s > 14\delta_1$, the flow is in the fully rough regime (Schlichting, 1968).

Frictional resistance of biofilms grown under constant pressure drop (i.e., constant shear stress) have been compared to the frictional resistance of pipes with a rigid roughness as given by the Colebrook-White equation. The follcwing was observed:

1. Frictional resistance due to biofilms shows a similar dependency on Reynolds number as frictional resistance due to commerically rough pipe surface.
2. Frictional resistance is dependent on biofilm thickness.
3. Frictional resistance does not increase above the hydraulically smooth pipe value until a critical biofilm thickness is attained.

The Blasius-Stanton or Moody diagram (Moody, 1944) can be used to compare frictional resistance due to biofilm with frictional resistance of rigid rough surfaces. The Blasius-Stanton diagram is a plot of friction factor vs. Reynolds number for a series of pipes with different equivalent sand roughness; the friction factor in a pipe with a rigid rough surface depends on both the relative roughness and the Reynolds number.

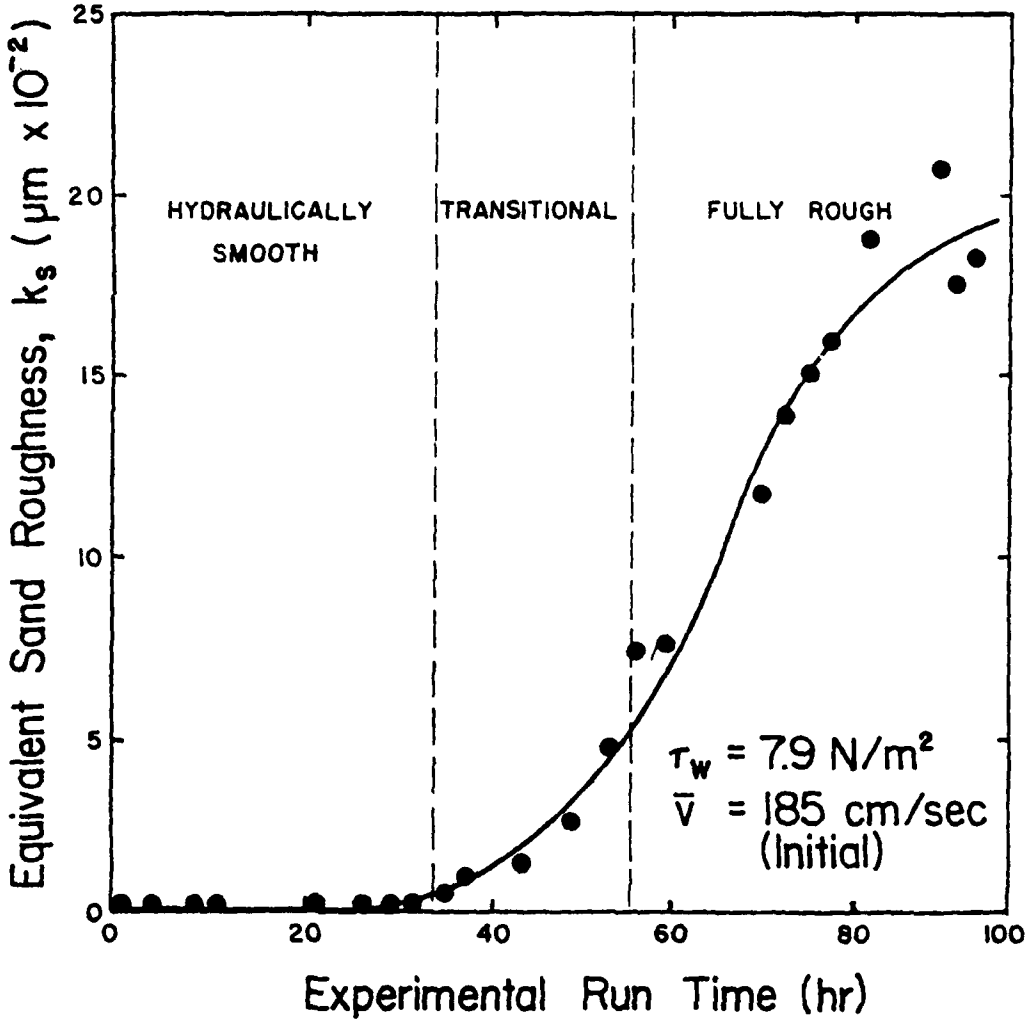

Figure 36. Equivalent Sand Roughness for Biofilm as a Function of Time for a Typical Experiment.

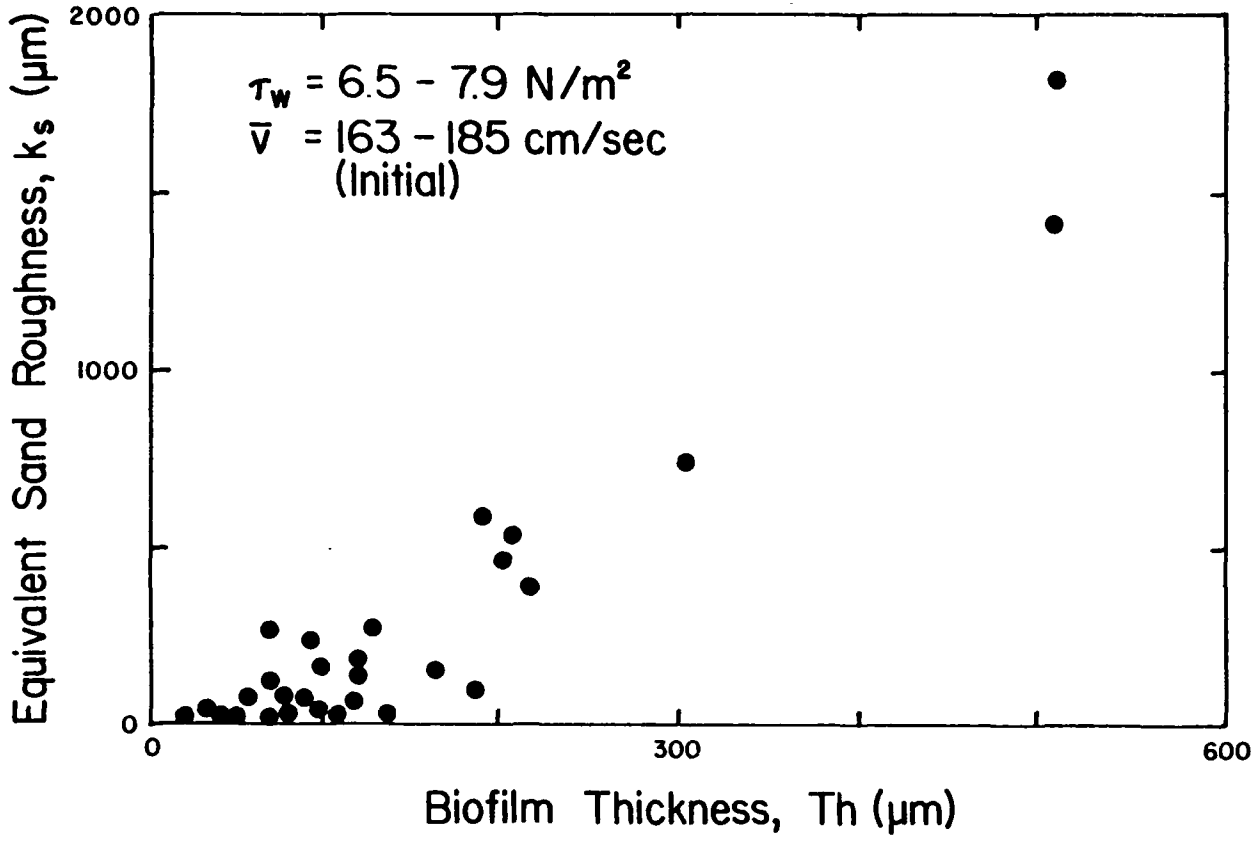

Figure 37. Equivalent Sand Roughness for Biofilms of Various Thicknesses

The relationship between friction factor and Reynolds number for a fouled circular tube is presented in Figure 38. The friction factors and Reynolds numbers presented have not been corrected for the pipe constriction resulting from the biofilm. This figure shows the dependency of friction factor on Reynolds number is the same as for a tube with a rigid rough surface within the range of Reynolds number investigated (5,000 to 48,000). This data was obtained by reducing, in steps, the shear stress from its initial value in a given experiment and calculating friction factor and Reynolds number at each step. The shear stress was reduced from the initial condition to minimize detachment of biofilm during the experiment.

Figure 39 indicates the relationship between friction factor and Reynolds number within a single experiment at different stages of biofilm development; friction factor increases with biofilm thickness. The relationship between biofilm thickness and friction factor for all of Zelver's experiments at a wall shear stress from 6.5-7.9 N m^{-2} is shown in Figure 40. Friction factor is dependent on biofilm thickness after a critical thickness (Th_c) approximately equal to the thickness of the viscous sublayer (δ_1) is attained.

Conceptually, Th_c corresponds to the stage of biofilm development at which surface irregularities protrude through the viscous sublayer. Until this stage, the biofilm lies completely within the viscous sublayer ($k_s < \delta_1$) and friction factor does not increase (the tube is hydraulically smooth). For a wall shear stress of 6.5-7.9 N m^{-2}, the viscous sublayer is approximately equal to 40 micrometers; this compares well with the observed Th_c = 30-35 micrometers for the same wall shear stress range.

Although the frictional resistance effects of biofilm can be adequately described by formula and concepts suitable for rigid rough

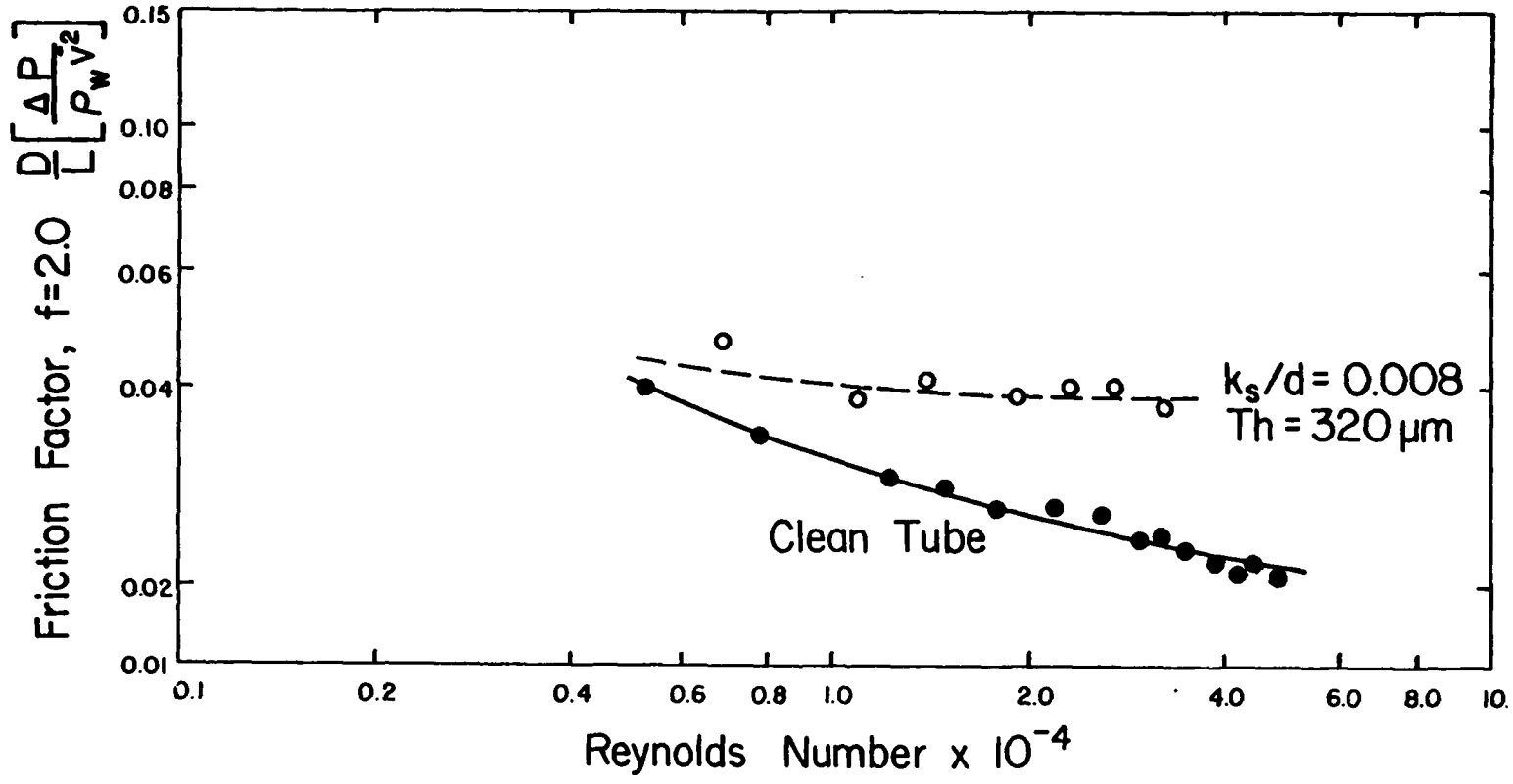

Figure 38. Relationship Between Friction Factor and Reynolds Number for a Biofouled Tube.

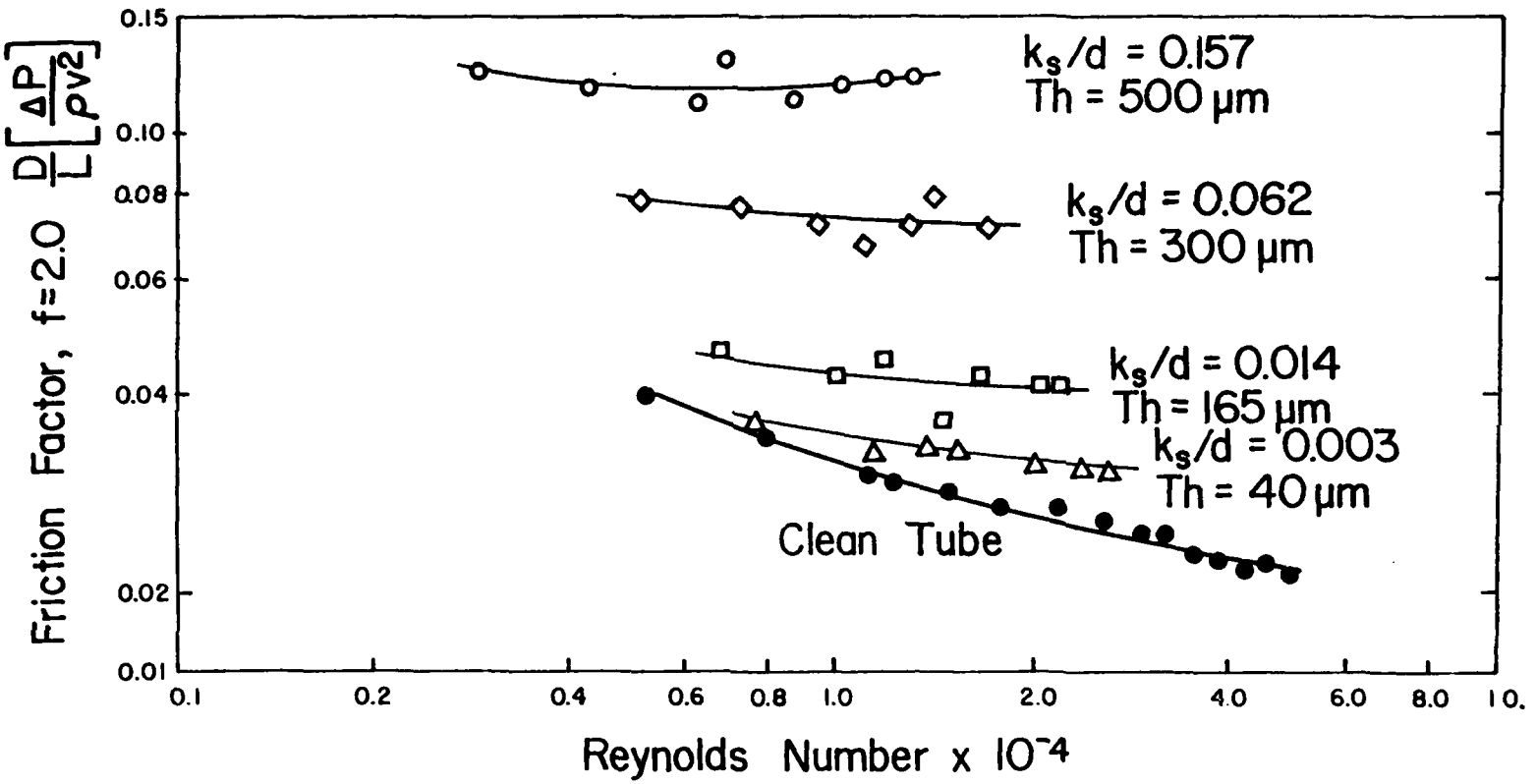

Figure 39. Relationship Between Friction Factor and Reynolds Number During Biofilm Development.

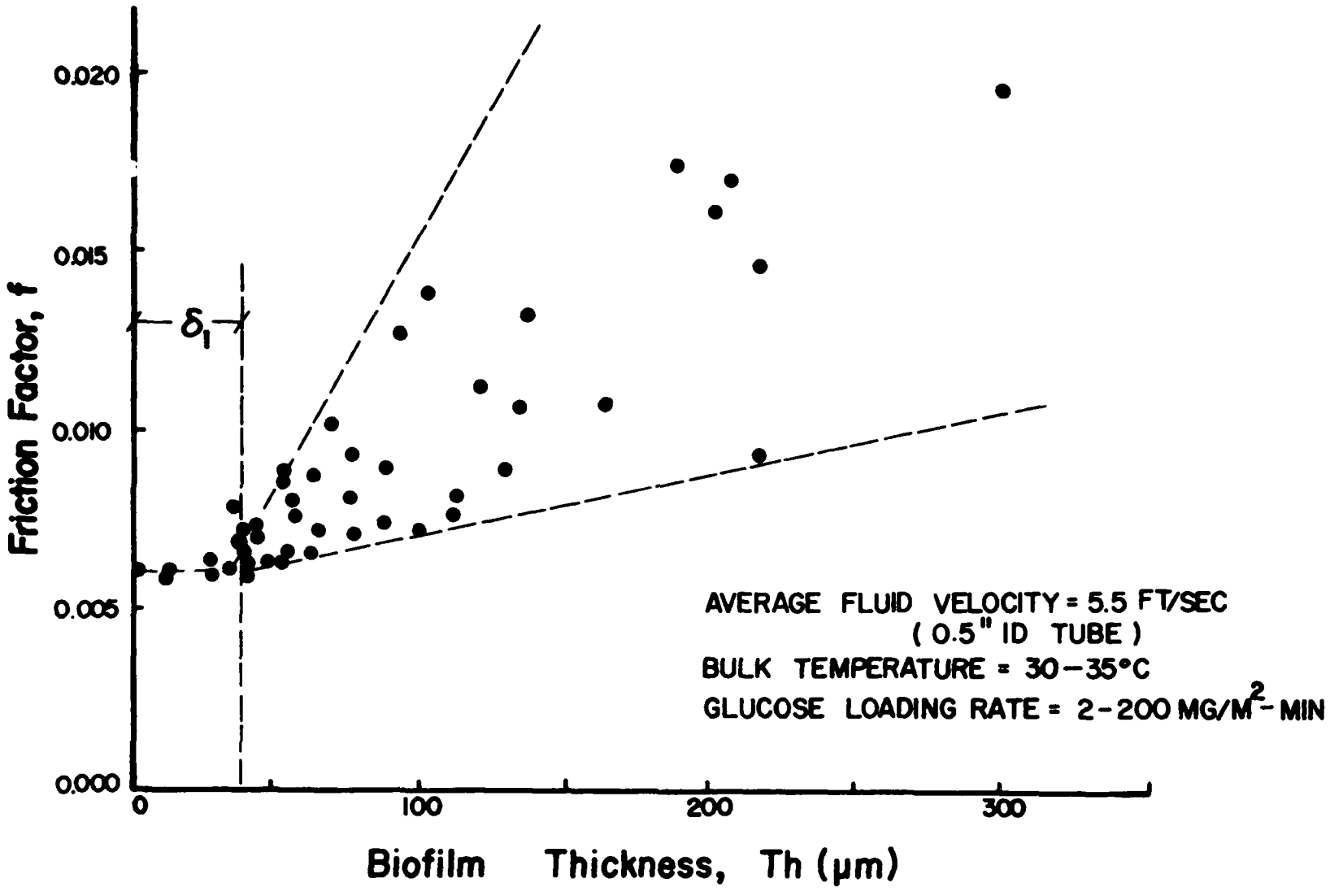

Figure 40. Evidence for Critical Thickness for Biofilm Frictional Resistance

surfaces, the conclusion should not be drawn that indeed the biofilm presents a rigid rough surface to the flow. Such a notion is an over-simplification and cannot account for all experimental observations (Picologlou et al., 1980).

Finally, frictional resistance measurements provide a relatively simple method for determining liquid mass transfer resistance in some biofilm systems since frictional resistance and liquid mass transfer resistance are related (LaMotta, 1974).

Heat Transfer Resistance

Biofilm development and resulting fluid frictional resistance have been discussed and both influence heat transfer. Changes in heat transfer resistance arise from the combined effects of increased biofilm thickness (conductive heat transfer) and increased frictional resistance (convective heat transfer).

$$\begin{matrix}\text{overall heat} \\ \text{transfer resistance}\end{matrix} = \begin{matrix}\text{conductive heat} \\ \text{transfer resistance}\end{matrix} + \begin{matrix}\text{convective heat} \\ \text{transfer resistance}\end{matrix}$$

Conductive heat transfer can be related to biofilm thickness and its effective thermal conductivity. Experimental biofilm thermal conductivity determinations indicate no significant difference from that of water at the same temperature (Nimmons, 1979). This is not surprising since biofilm is approximately 98-99% water.

Convective heat transfer results from fluid mixing or motion, and can be related to momentum transfer or frictional resistance. Colburn (1933) correlated convective heat transfer in tubes to friction factor and properties of the fluid. The Colburn relationship is only useful when the biofilm is thicker than the viscous sublayer.

Overall heat transfer resistance due to biofouling film development can then be calculated if the following are known:

1. Biofilm thickness and biofilm thermal conductivity

2. Frictional resistance

3. Wall temperature and bulk temperature

Figure 41 describes a typical experiment conducted by Nimmons (1979) in a tubular reactor and illustrates the relative effects of conductive and convective heat transfer resistance on overall heat transfer resistance.

Heat transfer resistance was consistently observed to decrease upon initial exposure to the fouling fluid in Nimmon's experiments. He hypothesized the following sequence of events to explain his observations. As a clean heat exchanger (Fig. 42) is exposed to the fluid, a micro-layer of organics and microbial cells forms. The conductive thermal resistance is relatively insignificant for a thickness of a few micrometers and the fouling layer remains within the viscous and thermal boundary layers. However, the biofilm layer produces a microroughness increasing convective heat transfer. Assuming the biofilm thermal conductivity is equal to that of water, the effect of the biofilm on conductive heat transfer would be equal to a stagnant water film of the same thickness. As long as the biofilm thickness is less than the viscous sublayer thickness, changes in convective heat transfer are not accompanined by changes in friction factor (Fig. 43). When the roughness elements are of sufficient height to project beyond the viscous sublayer and into the turbulent zone, as increase in friction factor and a further decrease in convective heat transfer resistance are observed. At this point the Colburn relationships may be used to determine the convective heat transfer coefficient (Fig. 44). Based on this hypothesis and his experimental data, Nimmons estimated the thermal boundary layer to be approximately 10-15 μm. The expected value is 22 μm. The viscous sublayer thickness calculated from hydrodynamic considerations was

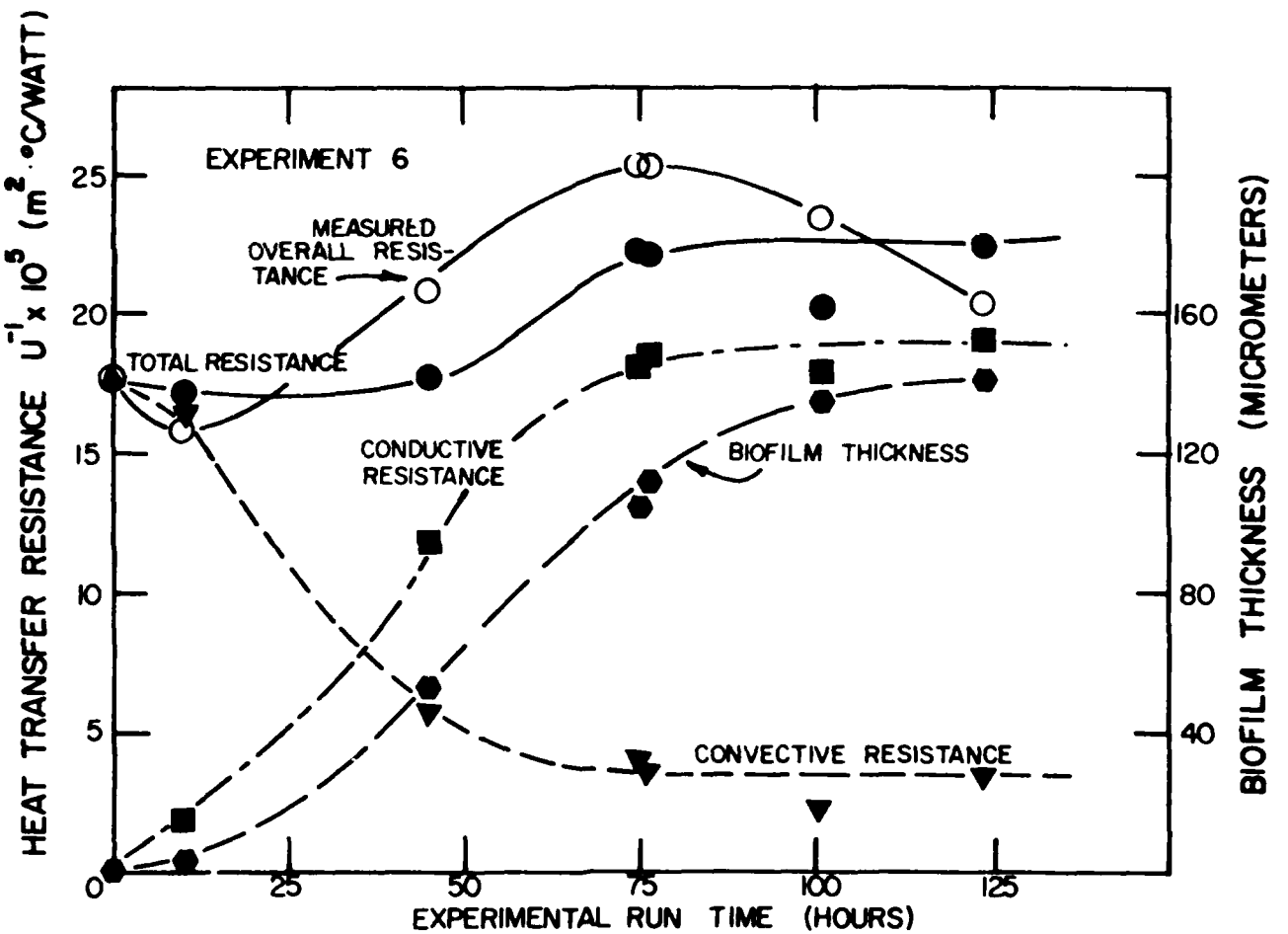

HEAT TRANSFER RESISTANCE CHANGES WITH TIME AS A RESULT OF BIOFILM DEVELOPMENT

Figure 41.

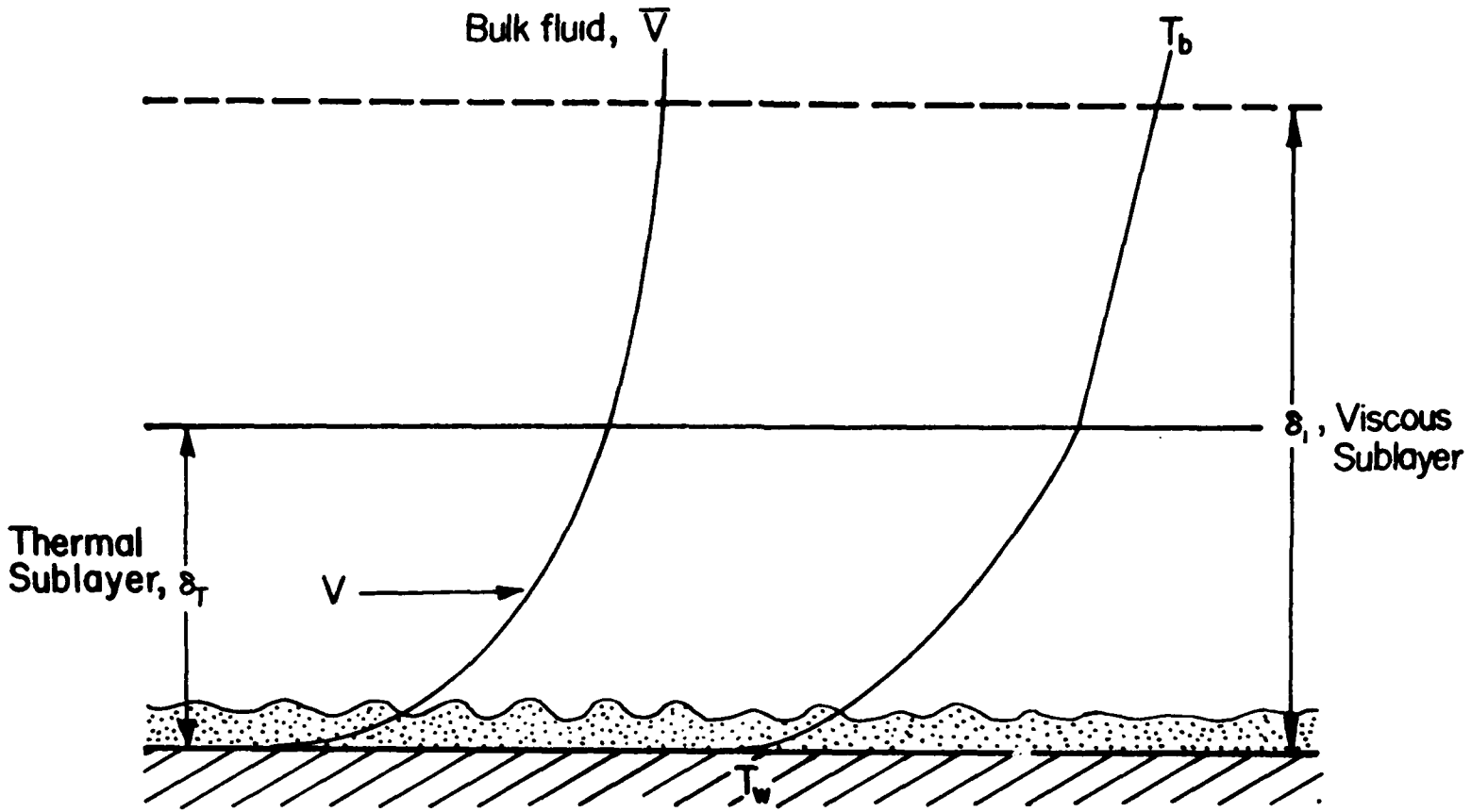

Figure 42. Initial Biofilm Development

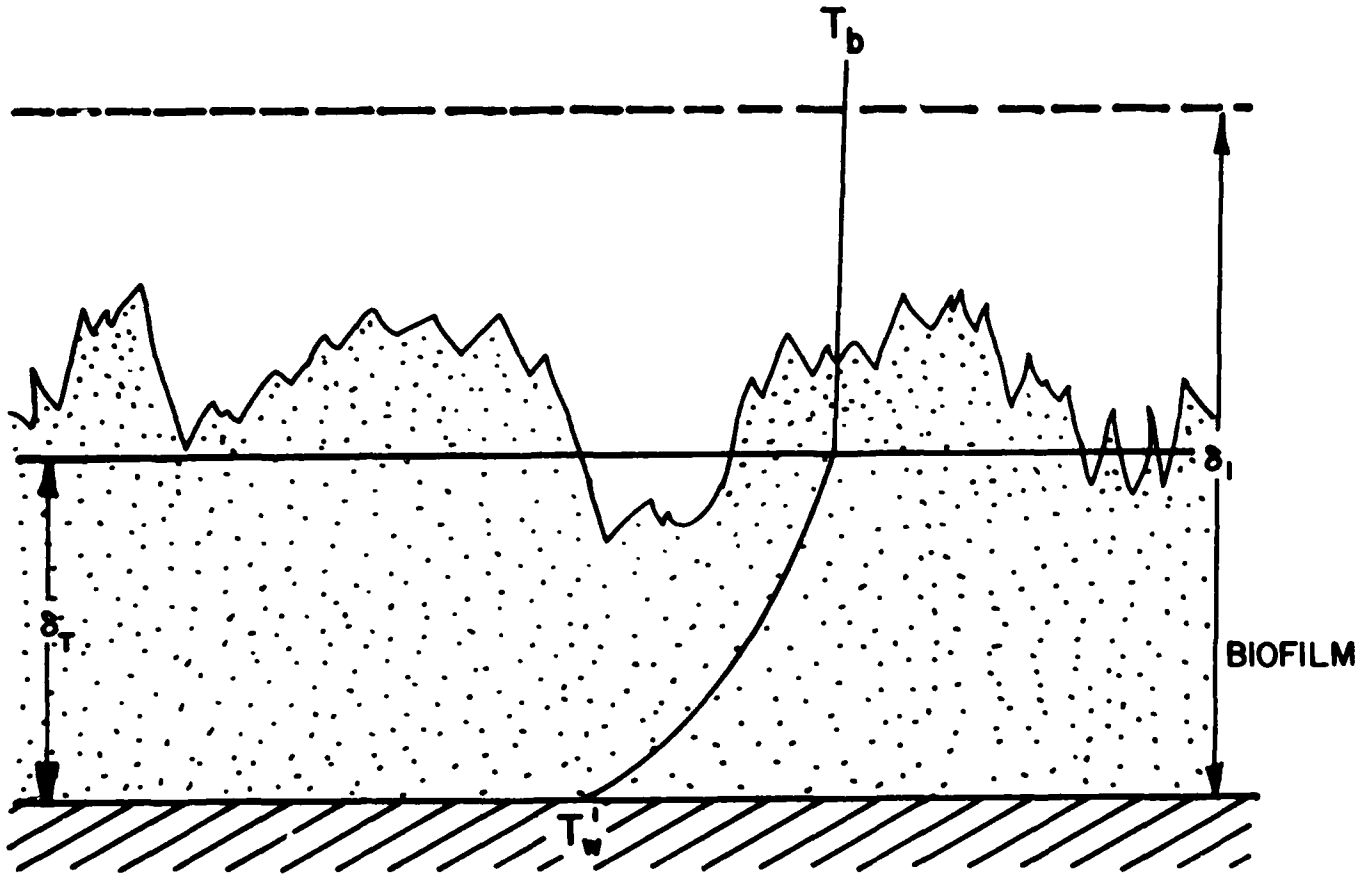

Figure 43. Biofilm Projection Beyond the Thermal Sublayer But Below the Viscous Sublayer.

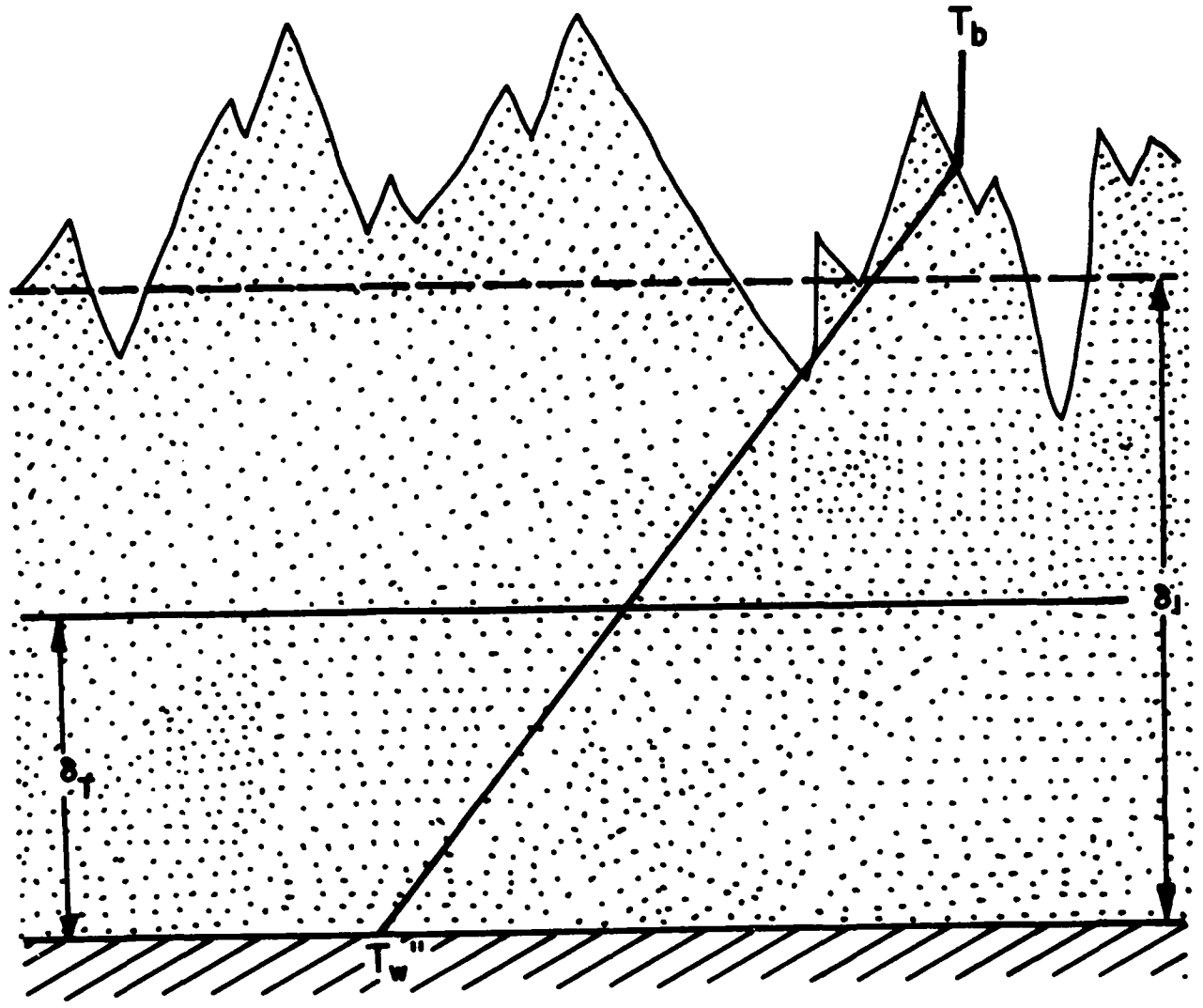

Figure 44. Biofilm Projection Beyond the Thermal and Viscous Sublayers and Into the Turbulent Zone.

44 μm as compared to 40 μm based on the observed onset of increased frictional resistance.

Nimmons computed the fouling factor, R_F, for his system and Figure 45 indicates its strong dependence on input substrate (glucose) concentration. Ranges of R_F measured in natural seawater systems are also included in Figure 45 for comparison purposes. Table 6 describes the experimental systems of Nimmons (data points), Ritter et al. (1977) and Fetkovich et. al. (1978). Neither carbon nor nutrient concentrations were determined in the latter two studies. However, carbon concentrations are estimated at between 0.5 - 10 mg l^{-1}.

Kirkpatrick et. al. (1980) have modelled the heat and mass transfer ocurring in a heat exchange tube as a biofilm develops. In a typical heat exchanger, results indicate a significant decrease in heat transfer. For systems of interest, the biofilm is relatively uniform over the length of the heat exchange tube. In tubes with combined heat and mass transfer, the biofilm thickness varies appreciable with fluid temperature. The assumed relationships between temperature and biofilm development rates in their model have been partially verified by Stathopoulos (1981).

Because thermal conductivity of scale deposits is much greater than that for biofilm, the conductive heat transfer resistance is significantly less. On the other hand, convective heat transfer resistance for "smooth" scale in turbulent flow is greater than that for the rough biofilm.

Scaling Experiments: The results of three scaling experiments are shown in Figure 46. T-2 and T-4 were run under identical conditions except that for T-2 the tube had no previous history of scaling. For T-3 and T-4 the tube was cleaned with EDTA (0.01M) and a soft bristled brush. T-3 received, in addition to 250 mg Ca^{++}, 200 mg/l of Na_2SiO_3.

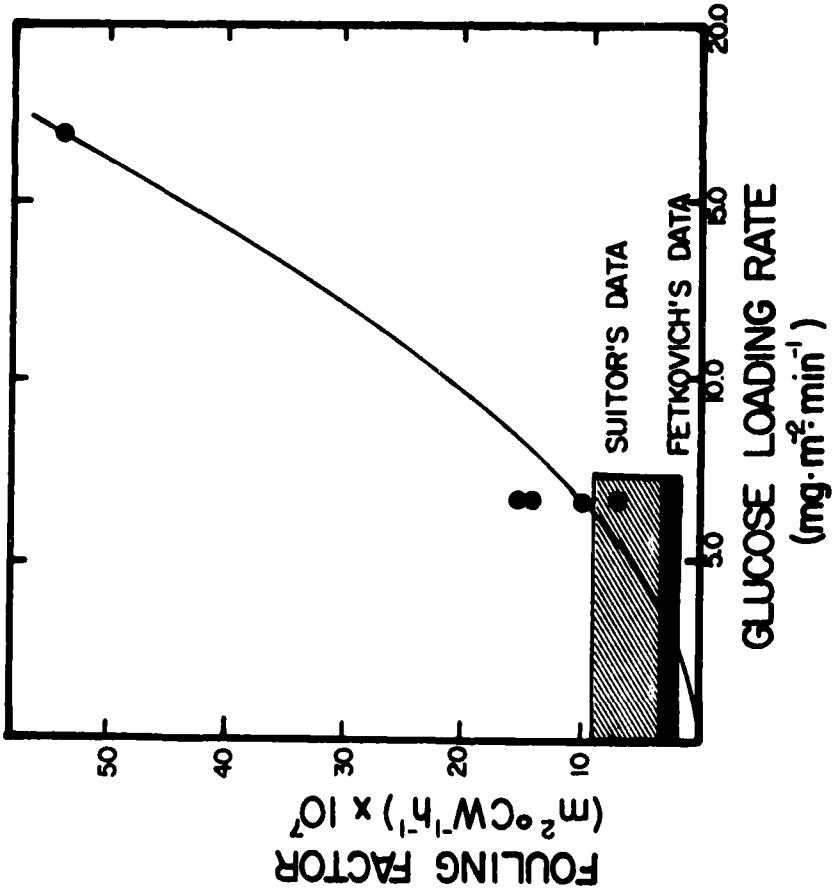

Figure 45. Fouling Factor vs Glucose Loading Rate.

Table 6. Description of experimental systems for R_F measurements reported in Fig. 45.

	Nimmons, 1979	Ritter and Suitor, 1977	Fetkovich et. al., 1978
Surface	Al 6061-T6	titanium	cupronickel
Surface Temperature (°C)	39-45	26-38	21
Fluid Velocity (cm s^{-1})	81	60-120	90-180

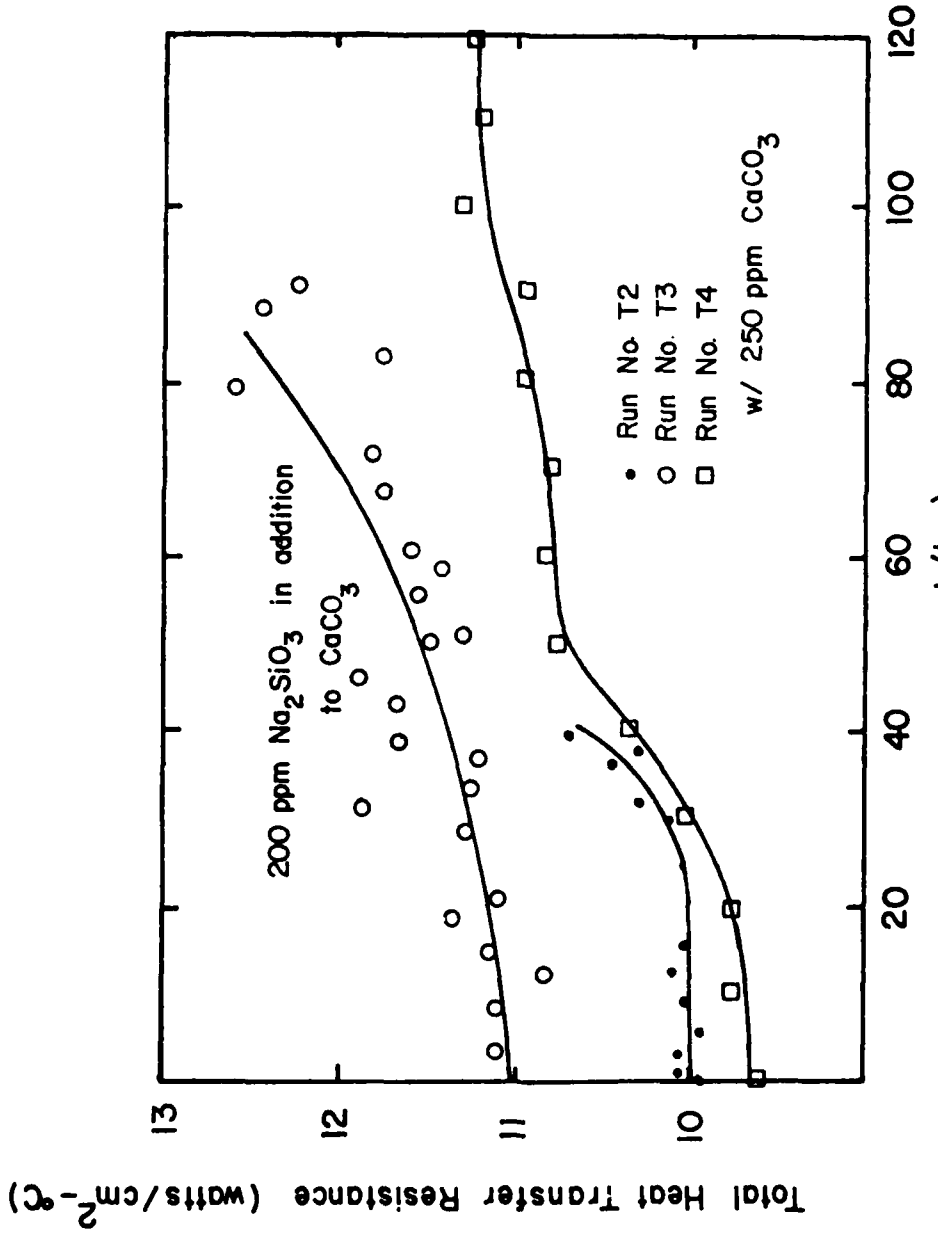

Figure 46. Heat transfer resistance increases due to scaling.

It appears that:

1. There was an induction period before scaling was observed for the "virgin" tube which was absent for subsequent runs.
2. The effect of adding soluble silica (Na_2SiO_3) was to decrease the maximum scaling rate.
3. Thin scales are relatively smooth compared to biofilm. Deposit relative roughness was calculated for experiment T-4 assuming a thermal conductivity for $CaCO_3$ of 0.026 watts/cm -°C (Zelver et al, 1981).

   The relative roughness was significantly less than that for biofilms of the same thickness (Table 7).

The copper-nickel alloy tubing used for experiments T-2 through T-4 contains a small amount of iron. When titanium tubing, which does not contain iron, was subjected to the same conditions, no scaling was observed.

Mathematical Model for Effect of Biofilm Accumulation on Heat Transfer and Frictional Resistance

A mathematical model simulating fouling biofilm development in a circular tube and its influence on heat transfer will be described. This model is being expanded to include biofilm-scale interaction.

Model Component 1 - Fouling Biofilm Development: Fouling biofilm development is the net result of several physical, chemical and biological processes including the following:

- transport and adsorption of inorganic and organic molecules at the wetted surface
- transport of microbial cells and other particulate material to the wetted surface
- adsorption and microbial adhesion to the surface

TABLE 7

INFLUENCE OF BIOFILMS AND CHEMICAL SCALE DEPOSITS ON FRICTIONAL RESISTANCE.

Type Deposit	Deposit Thickness (μm)	Relative Roughness (Dimensionless)
Biofilms†	40	0.003
	165	0.014
	300	0.062
	500	0.157
Scale		
$CaCO_3$	165*	0.0001
	224*	0.0002
	262*	0.0006

* Calculated from overall heat transfer resistance assuming a thermal conductivity for $CaCO_3$ of 0.026 Watts/cm °C.

† Characklis, 1980

- microbial reactions within the biofilm

- detachment of portions of the deposit by fluid shear

Net biofilm accumulation rate, R_B, reflects a combination of all the rate processes above:

$$R_B = R_A A + NAY - R_D A$$

Net rate of transport and adsorption has been described by Fletcher (1977) as follows:

$$R_A = k_A x \left(1 - \frac{\rho Th}{k_A'}\right)$$

The rate of biofilm production due to nutrient consumption N Y, has been experimentally determined by Trulear and Characklis (1981) as follows:

$$N\ Y = \frac{k_p\ \rho Th\ s}{k_p' + s}$$

The rate of biofilm detachment due to fluid shear, R_D, has been experimentally determined by Trulear and Characklis (1981). An approximate expression can be derived from their data as follows:

$$R_D = \rho Th\ k_D \exp\ (k_D'\ \tau_w)$$

Model Component 2 - Fluid Frictional Resistance: Picologlou et. al. (1980) have experimentally determined the influence of biofilm on fluid frictional resistance. Friction factor, f, was independent of Reynolds number, Re, for Re > 10,000 when Th exceeded the viscous sublayer thickness, δ_1. However, f was a function of biofilm roughness, ε. Therefore, the following expression describes the dimensionless friction factor (f) in a tube where $Th > \delta_1$ (Davies 1972):

$$f = \left[1.13 - 0.87 \ln\left(\frac{\varepsilon}{2r_I}\right)\right]^{-2}$$

Friction factor for any thickness and roughness is described by:

$$f = \frac{4r_1}{L} \quad \frac{\Delta p}{\rho_f v_m^2}$$

Model Component 3 - Conductive Heat Transfer Resistance: The conductive heat transfer resistance due to biofilm, U_{cond}^{-1}, and biofilm thermal conductivity, k_B, were determined by Characklis et. al. (1981).

$$U_{cond}^{-1} = \frac{r_I}{k_B} \ln \frac{r_1}{r_I}$$

Model Component 4 - Convective Heat Transfer Resistance: Colburn (1933) proposed a relationship to predict convective heat transfer coefficient from friction factor:

$$h = 0.125\ f\ c_p^{0.33} \eta^{-0.67}\ k^{0.67}\ \rho_f\ v_m$$

Then convective heat transfer resistance, $U_{conv}^{-1} = h^{-1}$.

A flow diagram for the model describing biofilm development in a tube and its influence on overall heat transfer resistance is presented in Figure 47. This model has been tested experimentally.

PUBLICATIONS

Publications related to our ONR research are contained in the appendix.

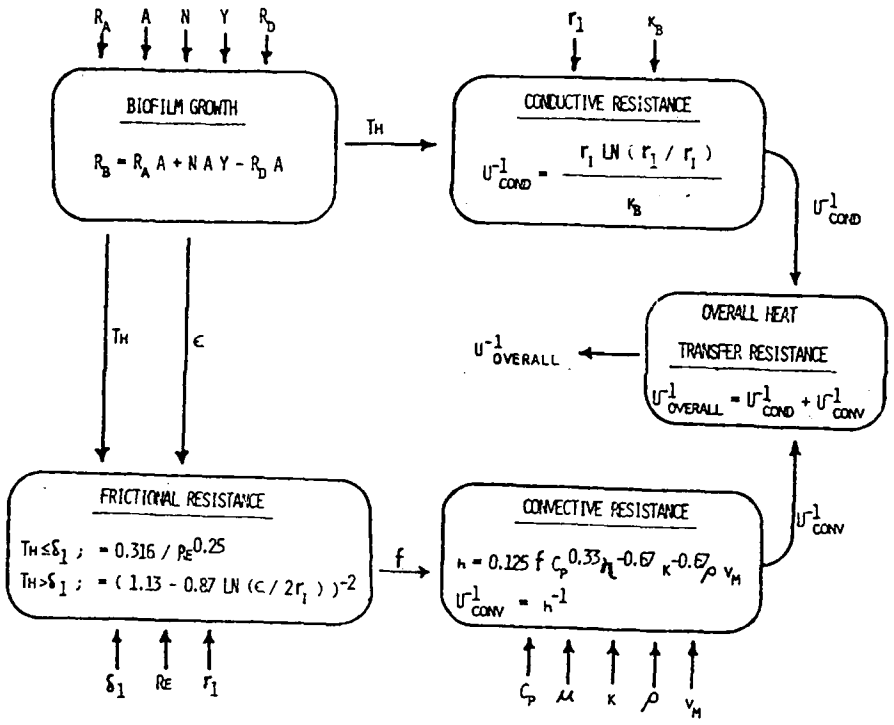

Figure 47. Mathematical Model Which Predicts Neat Transfer and Frictional Resistances Due to Biofilm Accumulation.

REFERENCES

Arnold, G.E. 1936. Crenothrix Chokes Conduits. Engrg. News Rec. 116:774-775.

Bryers, J.D. 1979. Rates of Initial Biofouling in Turbulent Flow Systems. Ph.D. Thesis, Rice University, Houston, Texas.

Characklis, W.G. 1980. Biofilm Development and Destruction. Final Report. Electric Power Research Inst., RP 902-1, Palo Alto, CA., 160 pp.

Characklis, W.G., Nimmons, M.J., and Picologlou, B.F., "Biofilm Development and Heat Transfer," accepted by Heat Transfer Engineering, 1981.

Colburn, A.P. 1933. A Method of Correlating Forced Convection Heat Transfer Data and a Comparison with Fluid Friction. Trans. AIChE, 29:174.

Corpe, W.A. 1970. An Acid Polysaccharide Produced by a Primary Film-Forming Marine Bacterium. Dev. Ind. Microbiol. 11:402-412.

Davies, J.T., Turbulence Phenomena, Academic Press, New York, 1972.

Dehart, R. 1979. Marine Research, Inc., Sandwich, MA. Personal communication.

Dexter, S.C. 1976. Influence of Substrate Wettability on the Formation of Bacterial Slime Films on Solid Surfaces Immersed in Natural Sea Water. Proc. 4th Int'l. Cong. on Marine Corr. and Fouling, Juan-Les-Pins, Antibes, France.

Dias, F.F., Dondero, N.C., and Finstein, M.S., "Attached Growth of Sphaerotilus and Mixed Populations in a Continuous-flow Apparatus." Applied Microbiology, 16, 1191 (1968).

Fetkovich, J.G., Granneman, G.N., Mahalingam, L.M., and Meier, D.L. 1978. Measurements of Biofouling in OTEC Heat Exchangers. Presented at 5th OTEC Conference.

Fletcher, M. 1977. The Effects of Culture Concentration and Age, Time, And Temperature on Bacterial Attachment to Polystyrene. Can. J. Microbiol. 23:1-6.

Fletcher, M. and Loeb, G.I. 1979. Influence of Substratum Characteristics on the Attachment of a Marine Pseudomonad to Solid Surfaces. Appl. Env. Microbiol. 37:67-72.

Hobbie, J.E., R.F. Daley, S. Jasper, 1977. Use of Nucleopore Filters for Counting Bacteria by Fluoresence Microscopy. Applied and Environmental Microbiology, 33(5), pp 1225-1228.

Kirkpatrick, J.P., McIntire, L.B. and Characklis, W.G. 1980. Mass and Heat Transfer in a Circular Tube with Biofouling. Wat. Res., 14: 117-12[illegible].

AD-A107 566 MONTANA STATE UNIV BOZEMAN DEPT OF CIVIL ENGINEERING--ETC F/G 13/10
MICROBIAL FOULING AND ITS EFFECT ON POWER GENERATION.(U)
SEP 81 W G CHARACKLIS, F L ROE, N ZELVER N00014-80-C-0475

UNCLASSIFIED NL

2 OF 2
AD A
107 566

END
DATE FILMED
1 -82
DTIC

Kornegay, B.H., and Andrews, J.F. 1967. Characteristics and Kinetics of Biological Film Reactors. Final Report, FWPCA, Research Grant No. WP-01181, U.S. GPO, Washington, D.C.

LaMotta, E.J. 1974. Evaluation of Diffusional Resistances in Substrate Utilization by Biological Films. Ph.D. Thesis, Univ. of North Carolina, Chapel Hill, NC.

LaPage, S.P., J.E. Shelton, T.G. Mitchell, and A.R. Mackenzie, 1970. Culture Colledions and the Preservation of Bacteria. pp. 135-228. In J.R. Novns and D.W. Ribbons (ed.), Methods in Microbiology. Vol. 3A. Academic Press, London.

Marshall, K.C. 1976. Interfaces in Microbial Ecology. Harvard University Press, Cambridge, Mass.

Marshall, K.C., Stout, R., and Mitchell, R. 1971. Mechanism of the Initial Events in the Sorption of Marine Bacteria to Surfaces. J. General Microbiol. 68:337-348.

Minkers, A.J., 1954. Determination of the Hydraulic Capa ity of Pipelines. J. New Engl. Wat. Wks. Assoc. 68:1-10.

Moody, L.G. 1944. Friction Factors for Pipe Flow. Trans. Amer. Soc. Mech. Eng. 66:671.

Nimmons, M.F. 1979. Heat Transfer Effects in Turbulent Flow Due to Biofilm Development. M.S. Thesis, Rice University, Houston, Texas. 100 pp.

Picologlou, B.F., Zelver, N., and Characklis, W.G., 1980. Biofilm Growth and Hydraulic Performance. J. Hydraulics Div., ASCE. 106 HY5: 733-746.

Pollard, A.L. and House H.E. 1959. An Unusual Deposit in a Hydraulic Tunnel. J. Pwr. Div., A.S.C.E. 85(POG): 163-171.

Ritter, R.B., Suitor, J.W., and Cypher, G.A. 1977. Thermal Fouling Rates of 90-10 Copper-Nickel and Titanium in Seawater Service. Report to INCRA, HTRI, Alhambra, CA.

Sanders, W.M., 3rd, 1964. Relationship Between the Oxygen Utilization of Heterotrophic Slime Organisms and the Wetted Perimeter. Ph.D. Dissertation, the Johns Hopkins University, Baltimore, MD.

Schlichting, H. 1968. Boundary Layer Theory. McGraw-Hill Book Co., New York.

Standard Methods for the Examinations of Water and Wastewater 12th Ed., 1971. pp 84-86. Michael J. Taras, Editor. American Public Health Assoc., Washington, DC.

Stathopoulos, N.A. 1981. Influence of Temperature on Biofilm processes. M.S. Thesis, Rice University, Houston, Texas.

Trulear, M.G. 1979. Rate of Biofilm Development in a Turbulent Flow Field. M.S. Thesis, Rice University, Houston, Texas.

Trulear, M.G., and Characklis, W.G. 1979. Dynamics of Biofilm Processes. Presented at 34th Annual Purdue Industrial Waste Conference, W. Lafayette, Indiana, May 8-10. 58 pp.

Trulear, M.G. and Characklis, W.G. 1980. Dynamics of Biofilm Processes. Presented at 53rd Annual Conference of the WPCF, Las Vegas, Nevada.

Trulear, M.G., Characklis, W.G., "Dynamics of Biofilm Processes," accepted for publication, Journal Water Pollution Control Federation, 1981.

Zelver, N. 1979. Biofilm Development and Associated Energy Losses in Water Conduits. M.S. Thesis, Rice University, Houston, Texas.

Zelver, N., W.G. Characklis, F.L. Roe, Discriminating Between Biofouling and Scaling in a Deposition Monitor. Presented at the 1981 Annual Meeting of the Cooling Tower Institute, Houston, Texas.

Zobell, C.E. 1943. The Effect of Solid Surfaces Upon Bacterial Activity. J. Bact. 46:39-59.

Nomenclature

A = wetted surface area	(L^2)
A_I = inside surface area of biofilm, $2\pi r_I L$	(L^2)
B = biofilm mass	(M)
C_p = specific heat	$(L^2t^{-2}{}_T{}^{-1})$
d = tube diameter	(L)
f = friction factor, $2d\Delta p/L\rho_f v_m^2$	(dimensionless)
F = volumetric flow rate	(L^3t^{-1})
F_D = dilution flow rate	(l^3t^{-1})
F_R = recycle flow rate	(L^3t^1)
h = convective heat transfer coefficient at r_I	$(Mt^{-3}{}_T{}^{-1})$
k = fluid thermal conductivity	$(MLt^{-3}{}_T{}^{-1})$
k_A = adsorption rate coefficient	(Lt^{-1})
k_A = saturation coefficient	(ML^{-2})
k_B = apparant thermal conductivity of biofilm	$(MLt^{-3}{}_T{}^{-1})$
k_D = detachment rate coefficient	(t^{-1})
k_D' = coefficient	$(lt^2{}_M{}^{-1})$
k_p = specific biofilm production rate	(t^{-1})
k_p' = saturation coefficient	(ML^{-3})
k_s = equivalent sand roughness	(L)
k_{tube} = thermal conductivity of tube wall material	$(MLt^{-3}{}_T{}^{-1})$
L = length of heat exchanger tube	(L)
m = maintainance coefficient	(t^{-1})
M_t = total reactor biomass	(M)
N = rate of nutrient consumption by biofilm	$(ML^{-2}t^{-1})$
p_b = biofilm polymer carbon concentration	$(M\ L^3)$
Δp = pressure drop across length L	(ML^1t^2)
q_r = heat flux in -r direction	(Mt^3)

q_2	= heat flux at r_2	(Mt^{-3})
Q	= heat transfer rate into the bulk fluid	(ML^2t^{-3})
r	= radial distance	(L)
r_1	= inner radius of tube	(L)
r_2	= outside radius of tube	(L)
r_i	= radial distance to inner thermistor of TWHE	(L)
r_{ii}	= radial distance to outer thermistor of TWHE	(L)
r_I	= radial distance to the biofilm	(L)
r_p	= specific production rate of polymer carbon	(t^{-1})
R_A	= net rate of transport and adsorption of cells, organic and inorganics to the surface	$(ML^{-2}t^{-1})$
R_B	= net biofilm accumulation rate	(Mt^{-1})
R_D	= rate of detachment of biofilm	$(ML^{-2}t^{-1})$
R_{d_p}	= biofilm polymer detachment rate	$(M\ L^{-2}t^{-1})$
R_{d_x}	= biofilm cellular detachment rate	$(M\ L^{-2}t^{-1})$
R_E	= rate of biofilm decay	(t^{-1})
Re	= Reynolds Number	(dimensionless)
R_f	= fouling factor	(t^3TM^{-1})
R_g	= glucose removal rate	$(ML^{-2}t^{-1})$
s	= limiting nutrient concentration in bulk water	(ML^{-3})
s_i	= input substrate concentration	(ML^{-3})
T_1	= temperature at r_1	(T)
T_i	= temperauture in TWHE at r_i	(T)
T_{ii}	= temperature in TWHE at r_{ii}	(T)
T_b	= bulk fluid temperautre	(T)
Th	= biofilm thickness, r_1-r_I	(L)
T_I	= temperatureat r_I	(T)
U	= overall heat transfer coefficient	$(Mt^{-3}T^{-1})$

N_{calc}^{-1} = conductive heat transfer	$(M^{-1}t^3T)$
U_{cond}^{-1} = conductive heat transfer	$(M^{-1}t^3T)$
U_{conv}^{-1} = convective heat transfer resistance	$(M^{-1}t^3T)$
$U_{meas}^{-1} = U_{overall}^{-1}$ measured in TWHE	$(M^{-1}t^3T)$
$U_o^{-1} = U_{conv}^{-1}$ in clean tube	$(M^{-1}t^3T)$
$U_{overall}^{-1}$ = overall heat transfer resistance	$(M^{-1}t^3T)$
V = reactor volume	(L^3)
v_m = mean fluid velocity	(Lt^{-1})
X = cellular carbon concentration	(ML^{-3})
x = biomass concentration in bulk water	(ML^{-3})
x_i = input biomass concentration in bulk	(ML^{-3})
X_b = biofilm cellular carbon concentration	$(M\ L^{-3})$
Y, Y_B = mass of biofilm produced per unit nutrient mass consumed.	(dimensionless)
Y_{bio} = total biofilm carbon yield coefficient	$(M\ M^{-1})$
Y_p = polymer yield coefficient	(dimensionless)
Y_{pb} = biofilm polymer yield coefficient	(dimensionless)
Y_x = suspended biomass produced per unit nutrient mass consumed	(dimensionless)
Y_{x_b} = biofilm cellular carbon yield coefficient	$(M\ M^{-1})$
z = length	(L)
α = glucose removal coefficient for cellular reproduction (mg glucose removed for cellular reproduction/total mg biofilm glucose removed)	$(M\ M^{-1})$
$(1-\alpha)$ = glucose removal coefficient for polymer production (mg glucose removed for polymer production/total mg biofilm glucose removed)	$(M\ M^{-1})$
ν = fluid viscosity	$(ML^{-1}t^{-1})$
μ = specific growth rate of suspended biomass	(t^{-1})
ρ_f = fluid density	(ML^{-3})

ρ	= biofilm density	(ML^{-3})
τ_w	= fluid shear stress at biofilm surface	$(ML^{-1}t^{-2})$
δ_l	= viscous sublayer thickness	(L)
ε	= effective height of roughness element	(L)
t	= time	(t)

PUBLICATIONS AND PRESENTATIONS

Publications:

Kirkpatrick, J.P., McIntire, L.V. and Characklis, W.G. "Mass and Heat Transfer in a Circular Tube with Biofouling," Water Research, 14, 117-127 (1980).

Picologlou, B.F., Zelver, N. and Characklis, W.G. "Effect of Biofilm Growth on Hydraulic Performance," J. of Hydraulics Div., ASCE, 106, HY5, 733-746 (1980).

Bryers, J.D. and Characklis, W.G. "Initial Biofouling in a Turbulent Flow System: Overall Kinetics," Water Research, 15, pp. 483-491 (1981).

Characklis, W.G. "Fouling Biofilm Development: A Process Analysis," accepted by Biotechnology and Bioengineering.

Characklis, W.G., Nimmons, M.J. and Picologlou, B.F. "Influence of Fouling Biofilm on Heat Transfer", accepted by Heat Transfer Engineering.

Trulear, M.G. and Characklis, W.G. "Dynamics of Biofilm Processes", accepted by Journal Water Pollution Control Federation.

Characklis, W.G., Bryers, J.D., Trulear, M.G. and Zelver, N. "Dynamics of Biofilm Processes: Methods," accepted by Water Research.

Characklis, W. G., Zelver, N. and Turakhia, M., "Fouling and Heat Transfer", In Fouling in Heat Exchange Equipment, ASME (1981).

Chapters in books:

Bryers, J.D. and Characklis, W.G. "Measurement of Primary Biofilm Formation," Chap. 11, pp. 169-183 in Condenser Biofouling Control, Garey, J.F. (ed), Ann Arbor Science, Ann Arbor, MI (1980).

Characklis, W.G., Trulear, M.G., Stathopoulos, N. and Chang, L.C., "Oxidation and Destruction of Microbial Films," Chap. 32, pp. 349-368 in Water Chlorination: Environmental Impact and Health Effects, Vol. 3, Jolley, R.L. (ed), Ann Arbor Science, Ann Arbor, MI (1980).

Characklis, W. G., "Process Analysis in Microbial Systems: Biofilms as a Case Study" In Mathematical Techniques in Microbiology (Bazin, ed), Academic Press, London, in press.

Characklis, W. G., Zelver, N. and Turakhia, M. "Microbial Films and Energy Losses". In Marine Biodeterioration (Costlow and Tipper, eds), U. S. Naval Institute, Annapolis, MD (1981).

Proceedings:

Trulear, M.G. and Characklis, W.G. "Dynamics of Biofilm Processes," pp. 838-853 in Proc., Industrial Waste Conference, Purdue University, Ann Arbor Science, Ann Arbor, MI (1980).

Characklis, W.G., "Microbial Fouling: A Process Analysis," Proceedings, International Conference on The Fouling of Heat Transfer Equipment, Rensselear Polytechnic Institute, Troy, NY, August (1980).

Bryers, J.D. and Characklis, W.G., "Kinetics of Initial Biofilm Formation Within a Turbulent Flow System," Proceedings, International Conference on The Fouling of Heat Transfer Equipment, Rensselear Polytechnic Institute, Troy, NY, August (1980).

Characklis, W.G. and Trulear, M.G., "Dynamics of Microbial Film Processes," pp. 365-408 in Vol. I, Proceedings, 1st National Symposium on Rotating Biological Contactor Technology Smith, E.D., Miller, R.D. and Wu, Y.C. (eds), (1980).

Reports:

Characklis, W.G., "Engineering Aspects of Microbial Film Development and Its Prevention". Prepared for National Science Foundation, Chemical Process Program (November 1980).

Presentations at Technical Meetings (astericks denote invited presentations):

*Characklis, W.G. and Selver, N. "Biofilm Dynamics" Second International Symposium on Waste Treatment and Utilization, University of Waterloo, Waterloo, Ontario, Canada, (June, 1980).

Characklis, W.G. and Brown, R.L. "Microbial Adhesion: Transport Considerations", at Microbial Adhesion to Surfaces, University of Reading, Reading, England, (Sept. 1980).

Characklis, W.G. "The Dynamics of Microbial Film Processes" Second International Symposium on Microbial Ecology, University of Warwick, Warwick, England, (Sept. 1980).

Trulear, M.J. and Characklis, W.G. "Dynamics of Biofilm Processes" presented at WPCF Conference, Las Vegas, NV (Oct. 1980).

Selver, N., Characklis, W. G. and Roe, F. L., "Discriminating between Biofouling and Scaling in a Deposition Monitor", presented at the Cooling Tower Institute Annual Meeting, Houston, TX, January 1981.

*Characklis, W. G., "Chemical and Physical Factors Affecting Biofilm Formation and Water Quality", Am. Soc. Microbiol Annual Mtg., Dallas, TX, Mar. 1981.

*Characklis, W. G., "Microbial Films and Energy Losses", Marine Biodeterioration, Office of Naval Research, Wash. D. C., Apr. 1981.

Invited Lectures:

Program in Social Ecology, University of California, Irvine, (May, 1980).
Dept. of Civil Engineering, University of California, Davis, (May, 1980).
Dept. of Civil Engineering, University of California, Berkeley, (May, 1980).
College of Marine Studies, University of Delaware, Lewes, DE (Nov. 1980).
Dept. of Chemistry, University of Wisconsin-Milwaukee, Milwaukee, WI (Nov. 1980).
Great Lakes Chemical Corp., W. Lafayette, IN, (March, 1981).
SOHIO, Cleveland, OH (March, 1981)
Drew Chemical Corp., Boonton, N.J. (April, 1981).

Continuing Education

"Biofilms", a short course (W. G. Characklis, Director), August 1980 at MSU.

DISTRIBUTION LIST

HEAT TRANSFER/BIOLOGICAL FOULING

	One copy except as noted
Mr. M. Keith Ellingsworth Power Program Office of Naval Research 800 N. Quincy Street Arlington, VA 22217	5
CDR Ronald C. Tipper Director, Ocean Biology Program Office of Naval Research NSTL Station, Mississippi 39529	5
Defense Documentation Center Building 5, Cameron Station Alexandria, VA 22314	12
Technical Information Division Naval Research Laboratory 4555 Overlook Avenue SW Washington, DC 20375	6
Professor Paul Marto Chairman, Mechanical Engineering Department U.S. Naval Post Graduate School Monterey, CA 93940	
Professor Eugene C. Haderlie Department of Oceanography U.S. Naval Post Graduate School Monterey, CA 93940	
Professor Bruce Pankin Naval Systems Engineering U.S. Naval Academy Annapolis, MD 21402	
Office of Naval Research Eastern/ Central Regional Office Bldg. 114, Section D 666 Summer Street Boston, Massachusetts 02210	
Office of Naval Research Branch Office 536 South Clark Street Chicago, Illinois 60605	

Office of Naval Research
Western Regional Office
1030 East Green Street
Pasadena, CA 91106

Dr. George I. Loeb
Marine Biology Branch
Ocean Sciences Division
Naval Research Laboratory
4555 Overlook Avenue
Washington, DC 20375

CDR Bill Marsh
Code 05DC3
Naval Sea Systems Command
Washington, DC 20362

Mr. Charles Miller, Code 05R13
Crystal Plaza #6
Naval Sea Systems Command
Washington, DC 20362

Heat Exchanger Branch, Code 5223
National Center #3
Naval Sea Systems Command
Washington, DC 20362

Mr. Ed Ruggiero, NAVSEA 08
National Center #2
Washington, DC 20362

Dr. Eugene Fischer, Code 2853
David Taylor Ship R&D Center
Annapolis, MD 21402

Mr. Wayne Adamson, Code 2722
David Taylor Ship R&D Center
Annapolis, MD 21402

Mrs. Brenda J. Little
Naval Oceanographic R&D Activity
NSTL
Bay St. Louis, Mississippi 39522

Mr. John Depalma
Bldg. 1105
Naval Oceanographic Office
NSTL
Bay St. Louis, Mississippi 39520

Mr. Daniel F. Lott
Code 793
Naval Coastal Systems Laboratory
Panama City, Florida 32407

Dr. Win Aung
Heat Transfer Program
National Science Foundation
Washington, DC 20550

Mr. Michael Perlsweig
Department of Energy
Mail Station E-178
Washington, DC 20545

Dr. W.H. Theilbahr
Chief, Energy Conservation Branch
Dept. of Energy, Idaho Operations Office
550 Second Street
Idaho Falls, Idaho 83401

Professor Ephriam M. Sparrow
Department of Mechanical Engineering
University of Minnesota
Minneapolis, Minnesota 55455

Professor J.A.C. Humphrey
Department of Mechanical Engineering
University of California, Berkeley
Berkeley, CA 94720

Professor Brian Launder
Thermodynamics and Fluid Mechanics Division
University of Manchester
Institute of Science & Technology
P088 Sackville Street
Manchester M601QD England

Professor Shi-Chune Yao
Deartment of Mechanical Engineering
Carnegie-Mellon University
Pittsburgh, PA 15213

Professor K.E. Cooksey
Rosential School of Marine and Atmospheric Science
University of Miami
Miami, Florida 33149

Professor Stephen C. Dexter
College of Marine Studies
University of Delaware
Lewes, Delaware 19958

Professor Sol M. Gerchakov
School of Medicine
University of Miami
Miami, Florida 33152

Professor Arthur E. Bergles
Mechanical Engineering Department
Iowa State University
Ames, Iowa 50011

Professor Kenneth J. Bell
School of Chemical Engineering
Oklahoma State University
Stillwater, Oklahoma 74074

Dr. James Lorenz
Component Technology Division
Argonne National Laboratory
9700 South Cass Avenue
Argonne, Illinois 60439

Dr. David M. Eissenberg
Oak Ridge National Laboratory
P.O. Box Y, Bldg. 9204-1, MS-0
Oak Ridge, Tennessee 37830

Dr. Jerry Taborek
Technical Director
Heat Transfer Research Institute
1000 South Fremont Avenue
Alhambra, CA 91802

Dr. Simion Kuo
Chief, Energy Systems
Energy Research Laboratory
United Technology Research Center
East Hartford, Connecticut 06108

Mr. Jack Yampolsky
General Atomic Company
P.O. Box 81608
San Diego, CA 92138

Mr. Ted Carnavos
Noranda Metal Industries, Inc.
Prospect Drive
Newtown, Connecticut 06470

Dr. Ramesh K. Shah
Harrison Radiator Division
General Motors Corporation
Lockport, New York 14094

Dr. Ravi K. Sakhuja
Manager, Advanced Programs
Thermo Electron Corporation
101 First Avenue
Waltham, Massachusetts 02154

Professor Charles B. Watkins
Chairman, Mechanical Engineering Department
Howard University
Washington, DC 20059

Professor Adrian Bejan
Department of Mechanical Engineering
University of Colorado
Boulder, Colorado 80309

Professor Donald M. McEligot
Department of Aerospace and Mechanical Engineering
Engineering Experiment Station
University of Arizona 85721

Professor Paul A. Libby
Department of Applied Mechanics and Engineering Sciences
University of California San Diego
Post Office Box 109
La Jolla, CA 92037

Professor C. Forbes Dewey Jr.
Fluid Mechanics Laboratory
Massachusetts Institute of Technology
Cambridge, Massachusetts 02139

Professor William G. Characklis
Dept. of Civil Engineering and Engineering Mechanics
Montana State University
Bozeman, Montana 59717

Professor Ralph Webb
Department of Mechanical Engineering
Pennsylvania State University
208 Mechanical Engineering Bldg.
University Park, PA 16802

Professor Warren Rohsenow
Mechanical Engineering Department
Massachusetts Institute of Technology
77 Massachusetts Avenue
Cambridge, Massachusetts 02139

Professor A. Louis London
Mechanical Engineering Department
Bldg. 500, Room 501B
Stanford University
Stanford, CA 94305

Professor James G. Knudsen
Associate Dean, School of Engineering
Oregon State University
219 Covell Hall
Corvallis, Oregon 97331

Mr. Robert W. Perkins
Turbotec Products, Inc.
533 Downey Drive
New Britain, Connecticut 06051

Dr. Keith E. Starner
York Division, Borg-Warner Corp.
P.O. Box 1592
York, PA 17405

Mr. Peter Wishart
C-E Power Systems
Combustion Engineering, Inc.
Windsor, Connecticut 06095

Mr. Henry W. Braum
Manager, Condenser Engineering Department
Delaval
Front Street
Florence, New Jersey 08518

Dr. Thomas Rabas
Steam Turbine-Generator Technical Operations Division
Westinghouse Electric Corporation
Lester Branch
P.O. Box 9175 N2
Philadelphia, PA 19113

Professor Daryl Metzger
Chairman, Mechanical and Energy
Systems Engineering
Arizona State University
Tempe, Arizona 85281